1
The Solar Wind

Alexis P. Rouillard[1], Nicholeen Viall[2], Viviane Pierrard[3], Christian Vocks[4], Lorenzo Matteini[5], Olga Alexandrova[6], Aleida K. Higginson[2], Benoit Lavraud[7], Michael Lavarra[1], Yihong Wu[4], Rui Pinto[1,8], Alessandro Bemporad[9], and Eduardo Sanchez-Diaz[1]

[1] *Institut de Recherche en Astrophysique et Planétologie, Toulouse, France*

[2] *NASA Goddard Space Flight Center, Greenbelt, Maryland, USA*

[3] *Belgian Institute for Space Aeronomy, Brussels, Belgium*

[4] *Leibniz Institute for Astrophysics Potsdam, Potsdam, Germany*

[5] *Department of Physics, Imperial College London, London, UK*

[6] *Laboratoire d'Etudes Spatiales et d'Instrumentation en Astrophysique, Observatoire de Paris, Université PSL, CNRS Sorbonne Université, Université de Paris, Meudon, France*

[7] *Laboratoire d'Astrophysique de Bordeaux, Université de Bordeaux, CNRS, B18N, Pessac, France*

[8] *Laboratoire Dynamique des Etoiles, des (Exo)planètes et de leur Environnement (LDE3), Astrophysics Division (DAp/ AIM), Saclay Nuclear Research Centre (CEA Saclay), Gif-sur-Yvette, France*

[9] *INAF Osservatorio Astrofisico di Torino, Turin, Italy*

1.1. INTRODUCTION

One of the current mysteries in heliophysics is the heating of the solar atmosphere to temperatures that are orders of magnitude hotter than the solar surface. As a result of this heating, the Sun cannot contain its atmosphere, and a continual outflow of plasma streams out from the solar corona to interplanetary space and beyond. For the debate surrounding the exact physical mechanisms of the heating of the corona, we direct the reader to Chapter 2. We here discuss the physical mechanisms behind the formation and propagation of the solar wind that are not yet well understood.

The whole volume of space influenced by the solar wind is called the heliosphere, and its size is in part modulated by the solar wind ram pressure. The solar wind extends from the corona to well beyond a hundred astronomical units (AU) to a termination shock. Beyond that shock, the solar wind slows down abruptly in response to the pressure of the interstellar medium, and the plasma becomes compressed and more turbulent until it reaches a zone where it can no longer push back the interstellar plasma. In situ measurements of these outer regions are sparse, and our exploration of this boundary layer has only just begun with the *Voyager* spacecraft. In particular, the global shape of the heliosphere is still not known because the *Voyager* has only measured a very small region of the heliospheric boundary.

Birkeland (1908) argued very early that a corpuscular emission from sunspots consisting of relativistic electrons must impact Earth's magnetic field and be deflected to the polar regions to create the aurora. For several decades, it was realized that particles could be emitted from the Sun during flares, but it was generally thought that the space around Earth was mostly empty or perhaps traversed by occasional streams of particles from the Sun (Chapman & Ferraro, 1931). The prevailing view was that the solar corona consists of a hot gas (possibly extending to 1 AU), in thermal and hydrostatic equilibrium, pulled back by the solar gravitational field (Chapman & Zirin, 1957). Detailed observational studies of comets by Biermann (1951) showed that a subset of their tails cannot be accelerated by radiation pressure alone but may also respond to material flowing out from the Sun's atmosphere. He suggested that the passage of solar particles at the comet formed an ion tail and that these particles must have a very high speed relative to the comet in order to align the tail in the Sun's direction. Parker (1958) built on these observations and realized that the high temperature of the corona can provide enough energy to force coronal plasma to accelerate from subsonic to supersonic speeds. He demonstrated that the hydrostatic approach predicted too high kinetic pressure at infinity and that a continuous radial expansion of solar gas must act to reduce the coronal pressure. This was the first theory describing the continual expansion of what we now call the *solar wind*.

In this model, a dominant force affecting coronal particles and pushing them outward is induced by the thermal pressure gradient in the corona. Parker's original model assumed an isothermal corona, but subsequent models allowing for a varying temperature with radial distance confirmed that a supersonic wind can also form under such conditions. The presence of an outflowing supersonic wind ranging from 300 to 800 km/s was confirmed by plasma measurements from the *Luna* 1, 2, 3; *Venera* 1; and *Mariner 2* (e.g., Neugebauer & Snyder, 1962) and the numerous subsequent solar wind dedicated missions (e.g., Hundhausen & Gosling, 1976; Marsch et al., 1982). The Parker model provided an acceleration from subsonic speed in the coronal region to supersonic speeds of around 300–400 km/s typical of the slow solar wind. His model was unable, however, to explain fast solar wind speeds of 700–800 km/s without assuming unrealistic coronal hole temperatures in excess of 2×10^6K. As we shall show in this chapter, coronal and solar wind measurements suggest that additional physical mechanisms must be accounted for to produce a fast solar wind.

The solar wind has been measured in situ for several decades near 1 AU. Typical solar wind speeds near 1 AU range from 300 to 800 km/s, proton temperatures take values between 10^5 K in the slow wind to about 2×10^5 in the fast wind. There is now no doubt that the fast solar wind measured in situ originates near the center of coronal holes at

the Sun (see Chapters 2 and 3). Coronal holes are cooler regions of the solar atmosphere that exhibit drops in Extreme UltraViolet (EUV) emissions. The cooler temperatures result from the significant escape of heat out in the solar wind. The fast solar wind streams out along open magnetic fields connecting regions deep inside coronal holes to the interplanetary medium. The origin of the slow wind is more complex and likely consists of multiple source components: these include transient releases from helmet streamers, plasma accelerating on rapidly expanding magnetic fields rooted at the boundary of coronal holes (through processes likely similar to that of the fast wind), and/or continual plasma exchanges between loops and open magnetic fields. We will describe these different components in the following sections.

1.2. OBSERVATIONS OF THE NASCENT SOLAR WIND

1.2.1. Remote-Sensing Observations of Coronal Heating and the Solar Wind

We begin our story on the solar wind with its formation in the solar corona; we first present remote-sensing observations that have provided important information on the conditions in which the winds are produced.

It is hard to observe the coronal source regions of the fast and slow solar winds in white-light images obtained routinely by coronagraphs. This is because the fast solar wind originates in very tenuous coronal holes, whereas the slow solar wind emerges from the vicinity of dense streamer loops that completely dominate coronal brightness. In contrast, spectroscopic observations provide more detailed information about the temperatures, flow velocities, and wave properties during the formation of the winds near their sources.

The *Solar and Heliospheric Observatory* (*SoHO*; Domingo et al., 1995) revolutionized how we observe the corona and the nascent solar wind. In particular, the Ultraviolet Coronagraph Spectrometer (UVCS/SoHO; Kohl et al., 1995) revealed that heavy ions such as O^{5+} and Mg^{9+} are heated hundreds of times more strongly than protons and electrons, and have very anisotropic kinetic temperatures (Antonucci et al., 2000; Kohl et al., 1997, 1998), meaning that temperatures measured in the direction perpendicular to the magnetic field are often much larger than those parallel to the field (see Chapter 2). A comparison between different ion and electron temperatures derived from coronal observations and solar wind measurements are shown in Figure 1.1. The measured temperatures provide support to coronal heating mechanisms involving collisionless wave–particle resonances with frequencies of 10 Hz to 10 kHz. These waves could be damped to heat preferentially heavy ions (Cranmer et al., 1999; Tu & Marsch, 1997). It is not clear yet how such hypothetical waves can be generated from lower-frequency Alfvén waves typically emitted at minute periods. Some proposed mechanisms involve the turbulent cascade of magneto-plasma fluctuations from low to high frequencies (Hollweg, 2002). Then kinetic processes must occur to damp the small-scale fluctuations that have spectrally cascaded to oblique wavevectors. Proposed mechanisms include ion-cyclotron and Landau damping (Leamon et al., 1998). Nonlinear processes such as beam instabilities or mode conversion and damping have also been proposed.

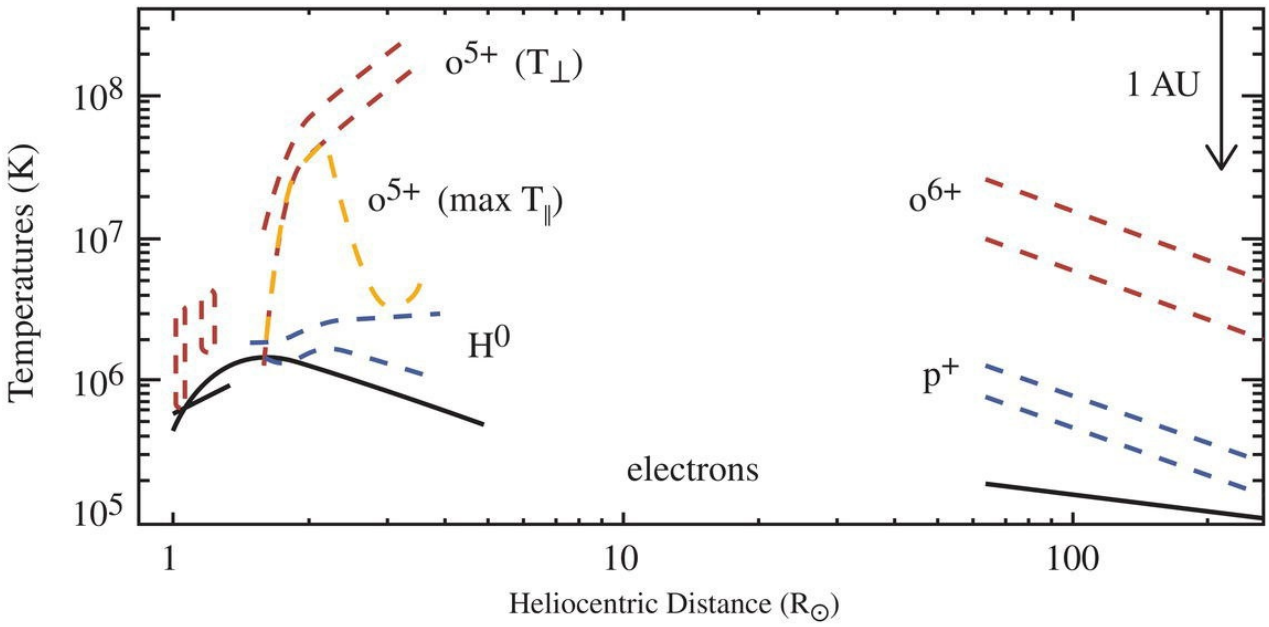

Figure 1.1 Radial evolution of solar wind temperatures from the corona to 1 AU. Indirect estimates of coronal temperatures are derived for three species (electrons, oxygen, and hydrogen) from an "empirical coronal model" that exploits SUMER (1–1.2$R_\odot$) and UVCS (1.5–4$R_\odot$) line widths compared with direct in situ measurements at distances greater than 60$R_\odot$) in the high-speed wind (Cranmer et al., 1999). The in situ data were assembled from *Helios*, *IMP*, *Ulysses*, and *Voyager* particle data, and double sets of curves denote rough lower and upper bounds on representative fast-wind values. The upper and lower limits correspond to extreme values of an assumed non-thermal component to the line broadening that is attributed to unresolved MHD wave motions along the line of sight. Temperatures of electrons (solid black), hydrogen (dotted), and oxygen (dashed) are shown. Oxygen ions correspond to O5+ in the corona but O6+ in the far solar wind, and coronal temperatures of neutral hydrogen are here compared with proton temperatures in the solar wind. Figure taken with permission from (Cranmer et al., 1999).

Emission lines, and more specifically the dimming of certain lines measured via coronal spectroscopy, have been used to infer the outflow speed and density of the forming fast solar wind. This effect is most important for spectral lines in the UV range that have a significant component due to ion excitation via resonant scattering of chromospheric emission (followed by spontaneous emission). For some lines, such as O VI doublet 103.2 nm and 103.8 nm lines, and of the HI Lyman- α 121.6 nm and Lyman- β 102.5 nm lines, the collisional and radiative components can be separated (Marocchi et al., 2001). This separation can be used to investigate the dimming of the radiative component, which is due to the radial expansion of the emitting coronal atoms. This Doppler shifts the (narrow) exciting chromospheric profile with respect to the (broad) atomic absorption profile. As a result, the UV intensity of the resonantly scattered component of the line emission decreases with increasing outflow velocities (Hyder & Lites, 1970; Noci et al., 1987; Withbroe et al., 1982). These observations applied to the O VI doublet lines have shown that the fast solar wind becomes supersonic much closer to the Sun than the slow solar wind. The fast O^{5+} ions reach speeds in excess of 600 km/s within 4 solar radii from the solar surface (Antonucci et al., 2000). Identical techniques were also used to study flows in the vicinity of streamers, adjacent but not above the helmet, and found that the slow solar wind accelerates more slowly, with its outflow speed remaining below 200 km/s at least until 4 solar radii (Abbo et al., 2010; Strachan et al., 2000). Figure 1.2 presents a summary of these results.

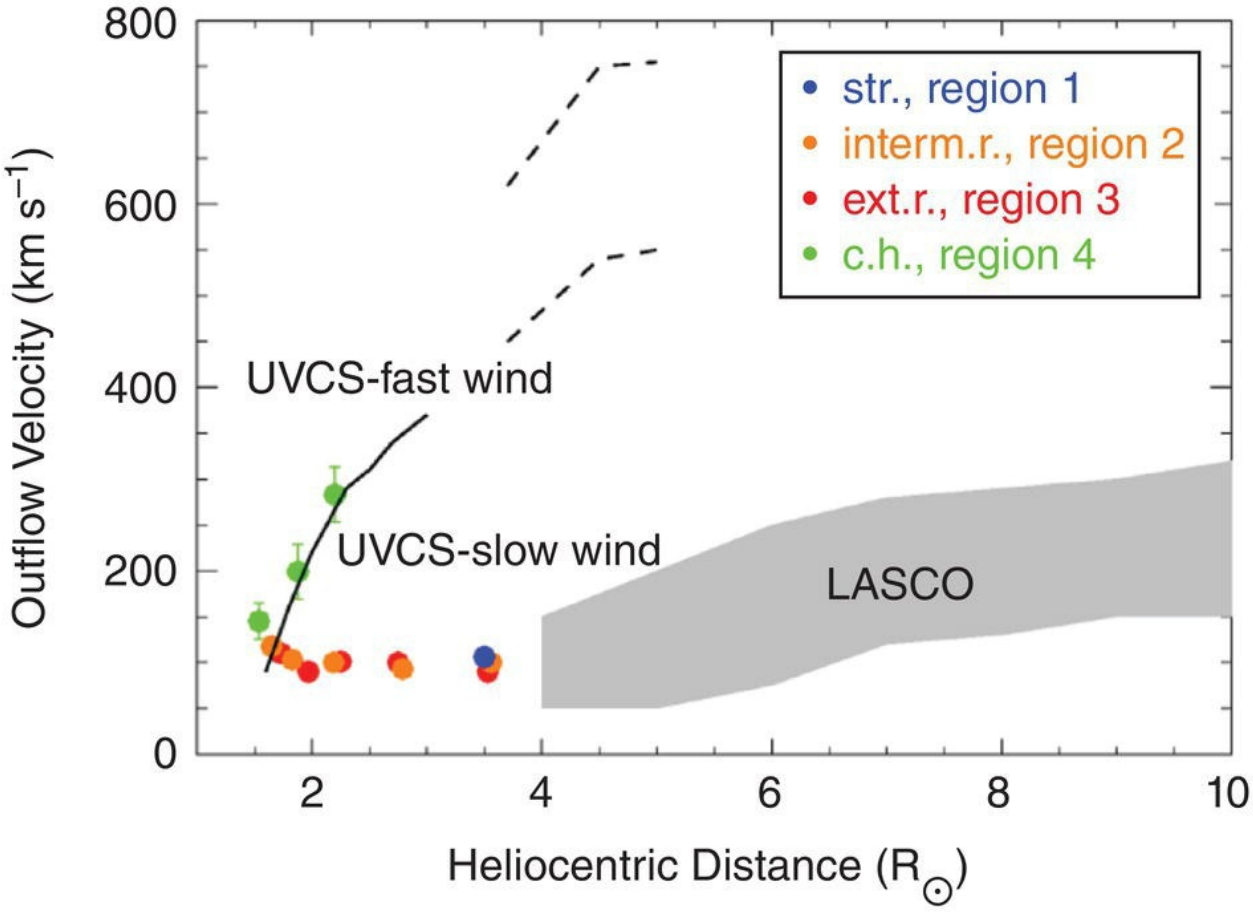

Figure 1.2 Outflow velocity (km/s) of the solar wind for the considered four regions as a function of the heliocentric distance (in solar radii). The gray band from 4 to 10 $R_\odot$ shows the range of outflow velocities for the slow wind obtained with LASCO (Sheeley et al., 1997). The solid curve up to 3 $R_\odot$ represents the values of the fast wind obtained from the UVCS data (Antonucci et al., 2000), and the dashed curves show the results by Telloni et al. (2007) of the fast wind velocity. The error bars (small in many cases) have been estimated based on the propagation of the statistical uncertainties of the observed OVI 1032 and 1037 line intensities.

(*Source*: Reproduced from Abbo et al., 2010. © 2010, Elsevier.)

A similar analysis of the Doppler dimming technique has been applied to the Lyman- α (121.6 nm) emission of neutral hydrogen. The latter moves outward in response to rapid charge-exchange coupling with the heated protons that eventually form the bulk of the solar wind. Neutral hydrogen therefore acts as a proxy for protons at heights up to 2.5 solar radii in coronal holes, and higher heights in more dense structures. In some coronal structures, He^+ can act as a proxy for alpha particles, which are also an important component of the solar corona. The UVCS/SoHO instrument has provided H I Lyman- α spectral line data over 18 years. This makes it possible to study proton outflow speeds throughout the solar cycle, focusing on the coronal region sampled by the spectrometer field of view, such as coronal streamers (Susino et al., 2008; Zangrilli & Poletto, 2016) and coronal holes (Antonucci et al., 2000; Strachan et al., 1993; Teriaca et al., 2003).

In a recent analysis (Bemporad, 2017), UVCS daily Lyman- α synoptic data were combined to provide the first 2D images of coronal Lyman- α emission, representative of future data that will be acquired by the Metis coronagraph onboard Solar Orbiter (Antonucci et al., 2017). These have been directly combined with classical 2D coronagraphic images acquired in white light with LASCO to derive 2D maps of HI outflow speeds, with a technique originally described by Withbroe et al. (1982) that neglects line-of-sight integration effects. As pointed out by Bemporad (2017), because both the radiative component of Lyman- α emission and the white-light polarized emission depend on the electron density distribution integrated along the line of sight, this latter quantity can be simplified by directly taking the ratio between the two UV and white-light intensities.

Figure 1.3 shows an example of a 2D outflow velocity map, ranging between 1.5 and 4.0 $R_\odot$, that was obtained this way (Bemporad, 2017). The map shows an increasing speed with altitude from about 150–200 km/s in the equatorial regions to 400 km/s in the polar regions. As we shall see, these values are in agreement with the expected latitudinal distribution of slow and fast solar wind components during solar minimum, corresponding to equatorial regions, and mid-latitude and polar regions, respectively. Alternatively, as shown more recently by Dolei et al. (2018), line-of-sight integration effects can be fully taken into account (under some assumptions) by deriving electron densities from white-light coronagraphic images. From this, one can derive HI outflow speed maps by again exploiting the Doppler dimming technique discussed above.

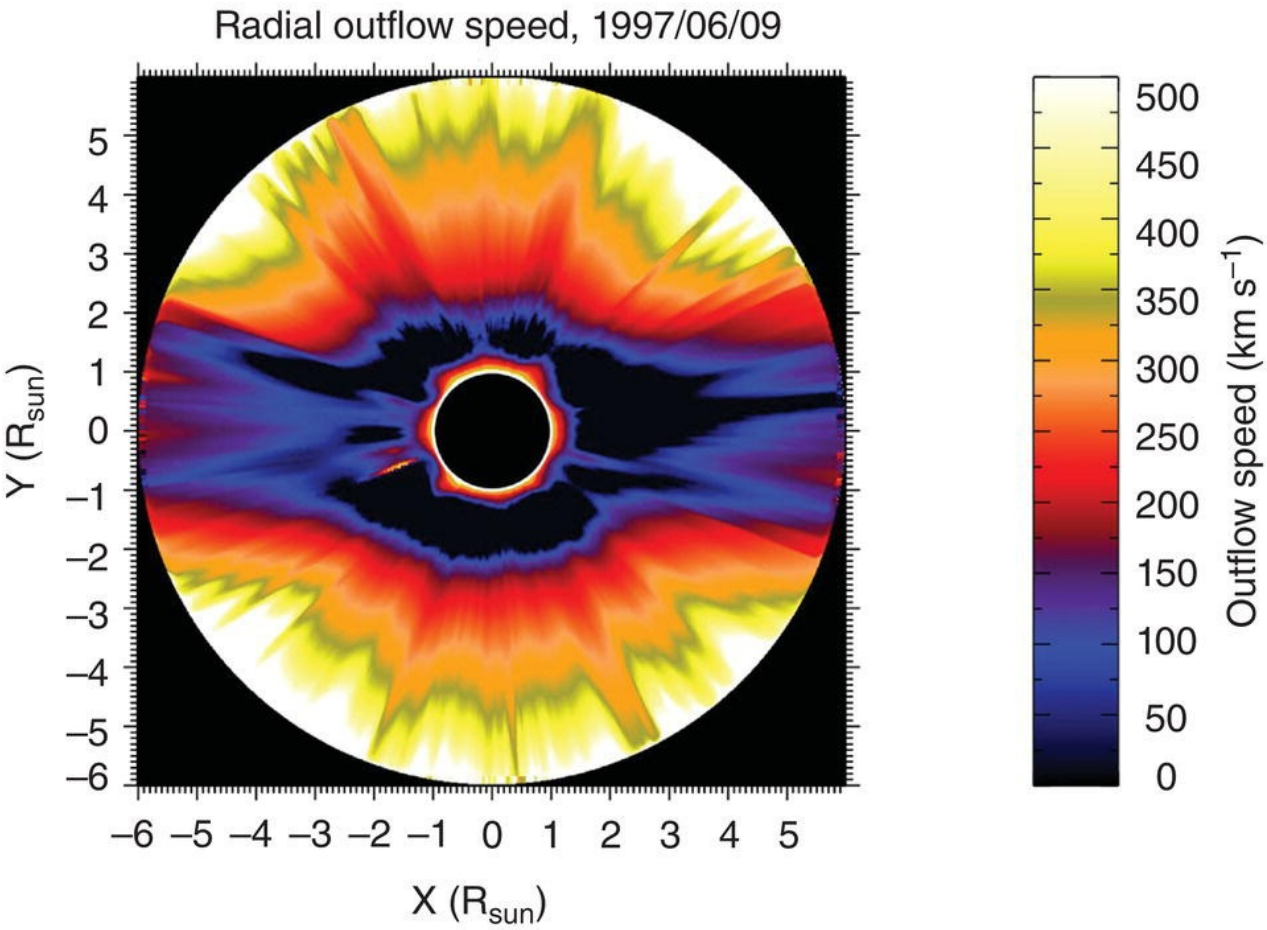

Figure 1.3 2D map of radial outflow velocity in the plane of the sky derived from the ratio between white-light and UV coronal emissions. The outer white region corresponds to altitudes where the Doppler dimming technique with the Ly spectral line cannot be applied anymore.

(*Source*: Taken from Bemporad, 2017. © 2017, IOP Publishing.)

The solar wind acceleration has also been measured via oscillations of the coronal plasma, identified as Alfvén waves in coronagraphic observations. Alfvén waves transverse to the plane-of-sky have been observed to be omnipresent in coronal holes within the first $0.3R_{\odot}$ of the solar atmosphere by the Coronal Multichannel Polarimeter (Tomczyk et al., 2016). Detailed analysis of off-limb Doppler shifts (Fe XIII) at high time cadence has furthermore revealed the presence of upward- and downward-propagating waves and, by comparing their respective phase speeds, allowed for the determination of the bulk flow speed profile of nascent fast wind flows (Morton et al., 2015, 2016). These observations have furthermore shown that the spectra of the oscillations show a predominant 1/f slope, reminiscent of solar wind measurements made beyond 0.3 AU by past space probes (e.g., Bavassano, Dobrowolny, Fanfoni et al., 1982; M. L. Goldstein et al., 1995). This supports the idea that the 1/f component of the oscillation spectra observed in the solar wind are already set in the low solar atmosphere and are advected outward (see, for example, Verdini et al., 2012). The statistical properties of fluctuations at magnetohydrodynamic (MHD) and kinetic scales are discussed further in Section 1.4.

1.2.2. Transient Coronal Outflows in the Nascent Solar Wind

The formation of the background solar wind, introduced in the previous section, is continually perturbed by the ejection of jets and small transients that form in the corona. Direct observations of these transient outflows in EUV and white-light images by the *STEREO* and *SoHO* spacecraft have provided new insights on the origin of mesoscale structures measured in situ in the solar wind.

Variable solar wind outflows in the form of plasmoids are continually released from helmet streamers in white-light (i.e., electron density) observations (e.g., Harrison et al., 2009; Rouillard, Davies, et al., 2010; Rouillard, Lavraud, et al., 2010; Rouillard et al., 2009; Sheeley et al., 1997; Sheeley et al., 2007; Wang et al., 1998; Wang et al., 2000). These plasmoids have been tracked from the corona, through the inner heliosphere, and in some cases out to 1 AU using heliospheric imagers (Rouillard, Davies, et al., 2010; Rouillard et al., 2011; Sheeley & Rouillard, 2010), showing in a direct way that some of the helmet streamer structures produced in the corona result in density structures measured in the inner heliosphere. Plasmoids (or "blobs") have been tracked from the tip of streamers where they typically form to several tens of solar radii, and analysis of their kinematic properties has confirmed that they are advected in the slow wind (Sheeley et al., 1997). In fact, this type of analysis has provided one of the rare kinematic measurements of the forming slow wind. It has revealed that a subset of the slow solar wind is released right above helmet streamers and accelerates over 20–30 solar radii to reach its terminal speed of about 300 km/s (this acceleration is shown as the gray area in Figure 1.2).

Helmet streamers form in the corona where magnetic fields of opposite polarity meet, and therefore a complex reconfiguration of the solar magnetic field is likely to occur due to magnetic reconnection. Magnetic reconnection can occur high up in the solar atmosphere (4–6 solar radii), and the collapse of newly formed magnetic loops can force the downward motion of coronal plasma. When densities are high enough, these plasma "inflows" are detected in coronagraphs in the vicinity of streamers and the coronal neutral line where the heliospheric current sheet (described next) forms (Wang et al., 2000). Multispacecraft studies using *SoHO* and *STEREO* images have recently shown that these inflows are associated with the release of density blobs in the slow solar wind (Sanchez-Diaz et al., 2017).

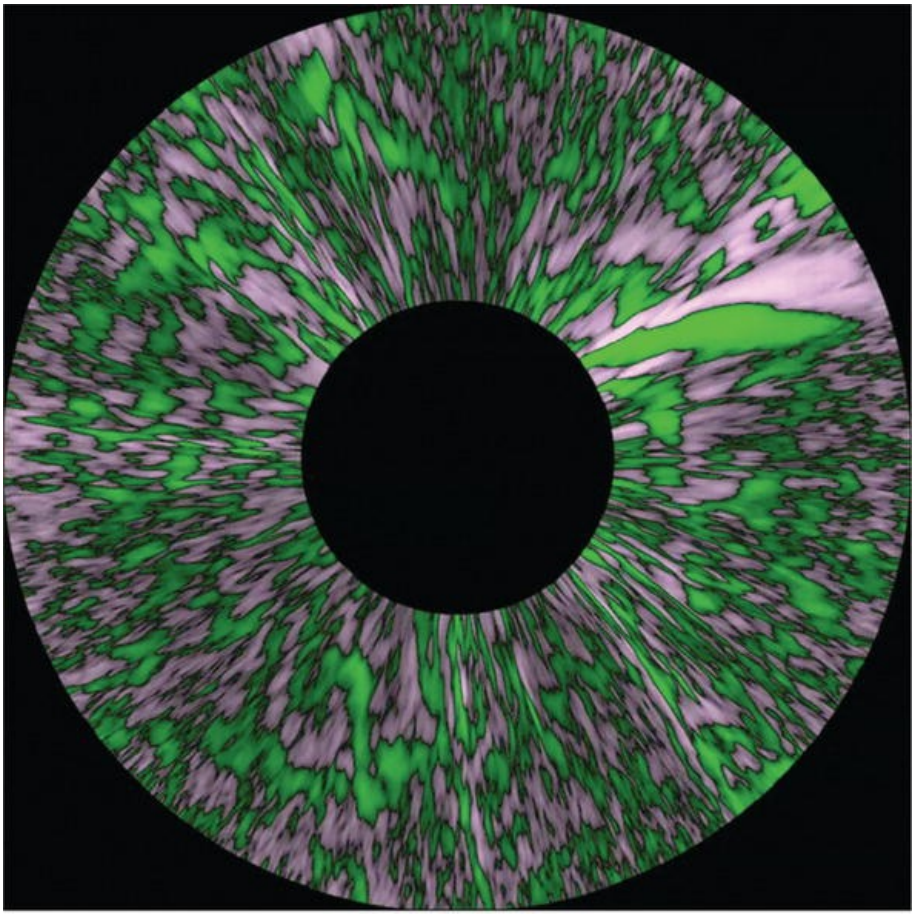

Figure 1.4 Propagating brightness fluctuations (green/black) derived from COR-2 observations during a dedicated deep-field campaign. The fluctuations are present at all azimuths and times, with a wide range of brightnesses and lateral sizes. The fluctuations appear with smaller scales than the Sheeley blobs (discussed in the text); such a blob is observed off the north-western limb in this image as the larger bright green feature.

(*Source*: Taken from DeForest et al., 2018.)

An important property of density blobs and plasmoids released in the solar wind is their multi-scale and cyclic nature. Fourier analysis of brightness variations released from a highly tilted current sheet near solar maximum has shown that the large plasmoids are released from the Sun with characteristic time scales of about 19–20 hr (Sanchez-Diaz et al., 2017). Similar spectral analysis has revealed characteristic 90 min timescales embedded within the larger plasmoids (Kepko et al., 2016; Viall et al., 2010; Viall & Vourlidas, 2015). DeForest et al. (2018) used deep-field, high-cadence coronagraph observations to show that there is still more substructure (shown in Figure 1.4)—both time dynamic on scales smaller than 90 min, and time stationary, filamentary streamer structures down to the resolution limit. The time-dynamic characteristic scale sizes likely have different formation causes, such as inherent time scales due to the characteristics of coronal heating (Endeve et al., 2004), or waves (Pylaev et al., 2017).

Observations of the corona therefore show that highly dynamic streamers host transient processes associated with the likely continual emergence, redistribution, and removal of solar magnetic flux directly influencing the properties of the magnetic fields and particles of the solar wind (Owens et al., 2013; Sanchez-Diaz et al., 2016). Magnetic reconnection occurring at the boundary of coronal holes was suggested to occur in the 1980s to explain the rigid rotation of coronal holes (Wang et al., 1988). Theoretical considerations (Fisk, 1996) and sophisticated numerical MHD simulations have highlighted the inevitable, complex evolution that takes place all along the corona's open-closed field boundaries (Antiochos et al., 2007; Linker et al., 2011; Lionello et al., 2005; Titov et al., 2009; Titov et al., 2011). The activity hosted by helmet streamers are the clearest example, with many different scales of plasma and magnetic field signatures generated by magnetic reconnection (Higginson et al., 2017; Higginson & Lynch, 2018; Lionello et al., 2005; Török et al., 2009).

Heliospheric imaging has also shown that not all structures at MHD scales measured in the solar wind form in the corona. DeForest, Matthaeus, Viall, and Cranmer (2016) showed turbulent density fluctuations setting in around 30 solar radii away from the Sun. These fluctuations coexist with outflowing helmet streamer plasmoids and are

advected with the solar wind.

1.3. MEASUREMENTS OF THE SOLAR WIND IN THE INNER HELIOSPHERE

1.3.1. Bulk Properties and Large-Scale Structures

The properties of the solar wind escaping the corona change throughout the solar cycle. This results from the evolving coronal magnetic topology that responds to the emergence and evolution of photospheric magnetic fields. This evolution alters both the magnetization and the bulk properties of the wind at different heliocentric latitudes. Spacecraft have measured in situ the properties of solar wind magnetic fields and particles at different locations in the heliosphere and over several decades. Figure 1.5 displays three dial plots showing the distribution of solar wind speeds with latitude measured by the *Ulysses* spacecraft during its three polar orbits. The sunspot number plotted below the dial plots is low in the left-hand and right-hand plots, marking the occurrence of solar minima (McComas et al., 2008). At these times, the Sun's magnetic field is quasi-dipolar, and the ambient solar wind is very clearly structured in at least two types of plasma flows. A fast wind is measured at high latitudes above coronal holes, and a more complex slow wind is measured at the low latitudes of solar streamers. As the solar cycle advances toward the activity maximum (middle panel), the polar coronal holes can disappear temporarily and the magnetic field evolves toward a non-dipolar structure. In response to this process, the bulk speed loses the ordered latitudinal structure shown in Figure 1.5 (left). At solar maximum, the large-scale spatial separation between the slow and fast solar wind is less clear as shown in the middle dial plot. Global numerical models of the solar wind show the clear link between these changes in the coronal magnetic topology and wind streams (Linker et al., 2011; Oran et al., 2013; Pinto et al., 2011; Pinto et al., 2016; van der Holst et al., 2014).

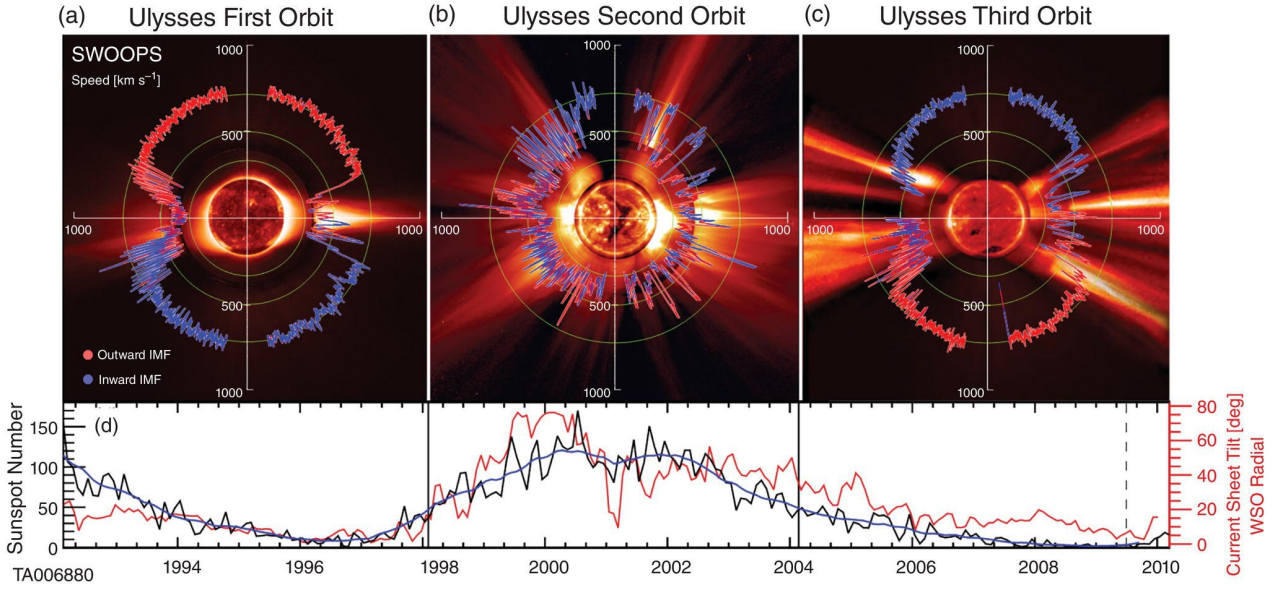

Figure 1.5 (a–c) Polar plots of the solar wind speed, colored by IMF polarity for Ulysses' three polar orbits to indicate measured magnetic polarity. (d) Contemporaneous values for the smoothed sunspot number (black) and heliospheric current sheet tilt (red), lined up to match Figures 1.1a–c. In Figures 1.1a–c, the solar wind speed is plotted over characteristic solar images for solar minimum for cycle 22 (17 August 1996), solar maximum for cycle 23 (7 December 2000), and solar minimum for cycle 23 (28 March 2006). From the center out, we blend images from the *Solar and Heliospheric Observatory* (*SoHO*) Extreme ultraviolet Imaging Telescope (Fe XII at 1950 nm), the Mauna Loa K coronagraph (700–950 nm), and the SoHO C2 white-light coronagraph.

(*Source*: Image reproduced with permission from McComas et al., 2008, © 2013 John Wiley & Sons.)

The first models capable of describing the general properties of the solar wind assumed a thermally driven flow. These include Parker's original (1958) theory that assumed a constant coronal temperature as well as subsequent fluid models that allowed for thermal stratification and inhomogeneities. The latest fluid models account for more detailed energy injection and transport mechanisms (Linker et al., 2011; Lionello et al., 2014; Oran et al., 2013; Pinto & Rouillard, 2017; van der Holst et al., 2014). Fluid models are not able, for known coronal temperatures, to explain the high speeds of the fast solar wind without including additional physical processes than just the effect of the thermal pressure gradient. These processes could involve Alfvén waves with their induced turbulent wave pressure and Reynolds stresses that would contribute to further accelerate the solar wind (Chandran, 2018; Cranmer et al., 1999; Lionello et al., 2014; Oran et al., 2013). Kinetic solar wind models suggest that heated particles such as suprathermal electrons, ubiquitous in the solar wind, could also contribute to the acceleration of the wind by imposing an electric field on the ions, extracting them out of the corona to high speeds (Pierrard & Pieters, 2014). It is, however, very challenging to deal with these different types of processes altogether in a unified view, as they work on very different scales.

At solar minimum, the quasi-dipolar distribution of coronal magnetic field lines extends into two magnetic hemispheres of opposite polarities in the interplanetary medium. These hemispheres are separated by a neutral line

called the heliospheric current sheet (HCS). A schematic of the global structure of the HCS is shown in Figure 1.6. The HCS is typically identified in situ as an abrupt change in the magnetic field direction and a 180° switch in the pitch angle of suprathermal electrons (above tens of eV). It is also commonly called a sector boundary (Liu et al., 2014). The HCS is usually surrounded by a high-density region called the Heliospheric Plasma Sheet (HPS) that may correspond to the heliospheric extension of coronal streamer rays (Winterhalter et al., 1994). The sector boundary and the magnetic field reversal are, at times, not collocated in situ (Owens et al., 2013). This is likely indicative of the dynamic effects, already mentioned, occurring in the solar corona near the source of sector boundaries leading to a local folding of the magnetic field that is not necessarily associated with the large-scale HCS (Owens et al., 2013). The HCS exerts only small latitudinal displacements during solar minimum, but can extend over a broad latitudinal range at solar maximum when solar active regions are more numerous at low latitudes. For weak to moderate solar activity, the topological shape of the HCS resembles that of a ballerina skirt, as illustrated in Figure 1.6.

The expansion of the solar wind plasma combined with the effect of solar rotation shapes the interplanetary magnetic field into Archimedean spirals rooted at the Sun with a radial position $r(\theta)=k\theta/(2\pi)$, where r is the radial coordinate, θ the azimuthal angle, and k is the product of synoptic period of the Sun and the solar wind speed (Parker, 1958). These spirals are known as Parker spirals and, according to Maxwell's equations, plasma elements situated on a same Parker spiral share a common source region at the Sun. The measured dependence between the magnetic field angle with respect to the radial direction and solar wind speed agrees very well with the simple Parker spiral model. This is true in the Helios spacecraft measurements of the inner heliosphere (Bruno & Bavassano, 1997), of near 1 AU measurements taken over several decades (Borovsky, 2010), and further out along the *Pioneer* and *Voyager* orbits in the more distant outer heliosphere (Burlaga & Ness, 1993). Measurements of magnetic fields at high latitudes have been limited to those made by the *Ulysses* spacecraft. These measurements also confirm that the angle of the interplanetary magnetic field to the radial direction also agrees well with the Parker spiral model (Forsyth et al., 2002). Deviation from the average spiral orientations can be due to dynamic processes that occur near the source region of the solar wind or the onset and development of turbulent flows (Fisk, 1996). Both of these are discussed at length in the later sections of this chapter; they are likely important to place constraints on theories of coronal heating and solar wind formation.

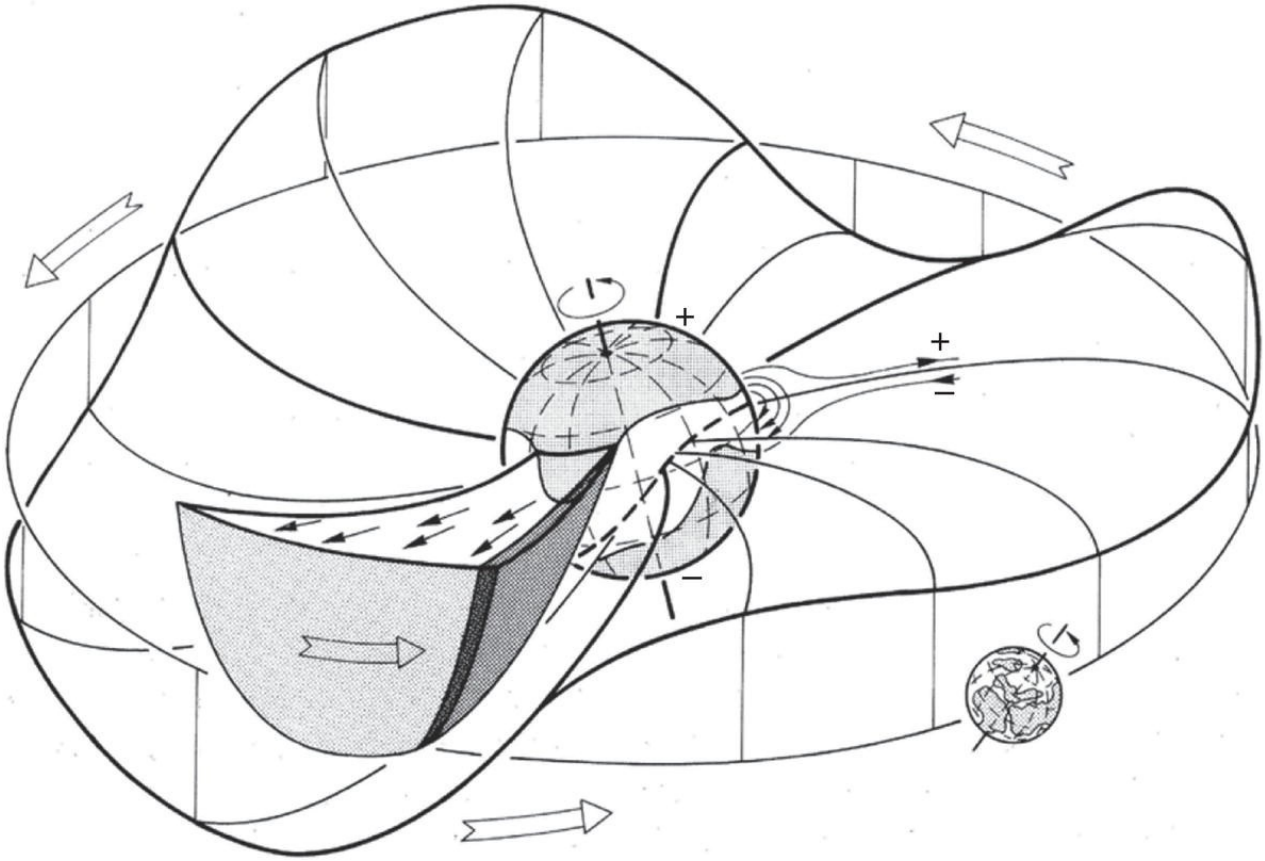

Figure 1.6 Configuration in the inner heliosphere of a "ballerina skirt" heliospheric current sheet extending above the streamer belt near solar minimum (for A > 0 solar magnetic field polarity, that is, outward field at the north pole), which lies ahead of a high-speed stream (drawn truncated at high latitudes) from an equatorward extension of a northern polar coronal hole. The dark shaded region is the interaction region.

(*Source*: Image reproduced with permission from Schwenn, 1990, © 1990, Springer.)

1.3.2. Composition of the Solar Winds

Figure 1.7 presents solar wind parameters during the passage of a high-speed stream bound by two intervals of the slow wind. In situ measurements at 1 AU and beyond are not ideal to study the origin of the solar winds because the latter evolve greatly between the Sun and 1 AU. For example, the fast and slow winds interact during transit to 1 AU, and the distribution functions are strongly affected by a number of processes during transport from the Sun as

discussed later in this chapter. In essence, the solar wind undergoes a number of processes that irreversibly erase information on their source regions during transit. Wind properties that remain unchanged during transit to 1AU are the abundance and ionization state of minor ions. They provide crucial information on the origins of these winds.

As an element rises in the solar atmosphere from the chromosphere to the hot corona, its ionization level increases due to radiative and collisional processes. This carries on until it reaches a height where radiative ionization is too weak and collisions are rare. Beyond that height, the charge state is said to be “frozen” and remains unchanged until it is measured in situ in the interplanetary medium. A measure of the charge state of heavy ions therefore provides unique information on the temperature at the source regions of the solar winds (Geiss et al., 1995). The charge state of an ion species will increase with temperature at the collisional coronal base of a solar wind flux tube. Solar wind measurements have shown that the carbon and oxygen ions have lower charge states (O7+/O6+ or C5+/C6+) in the fast than in the slow wind (Geiss et al., 1995; Kasper et al., 2012). This is clearly seen in Figure 1.7 for the O7+/O6+ ratio.

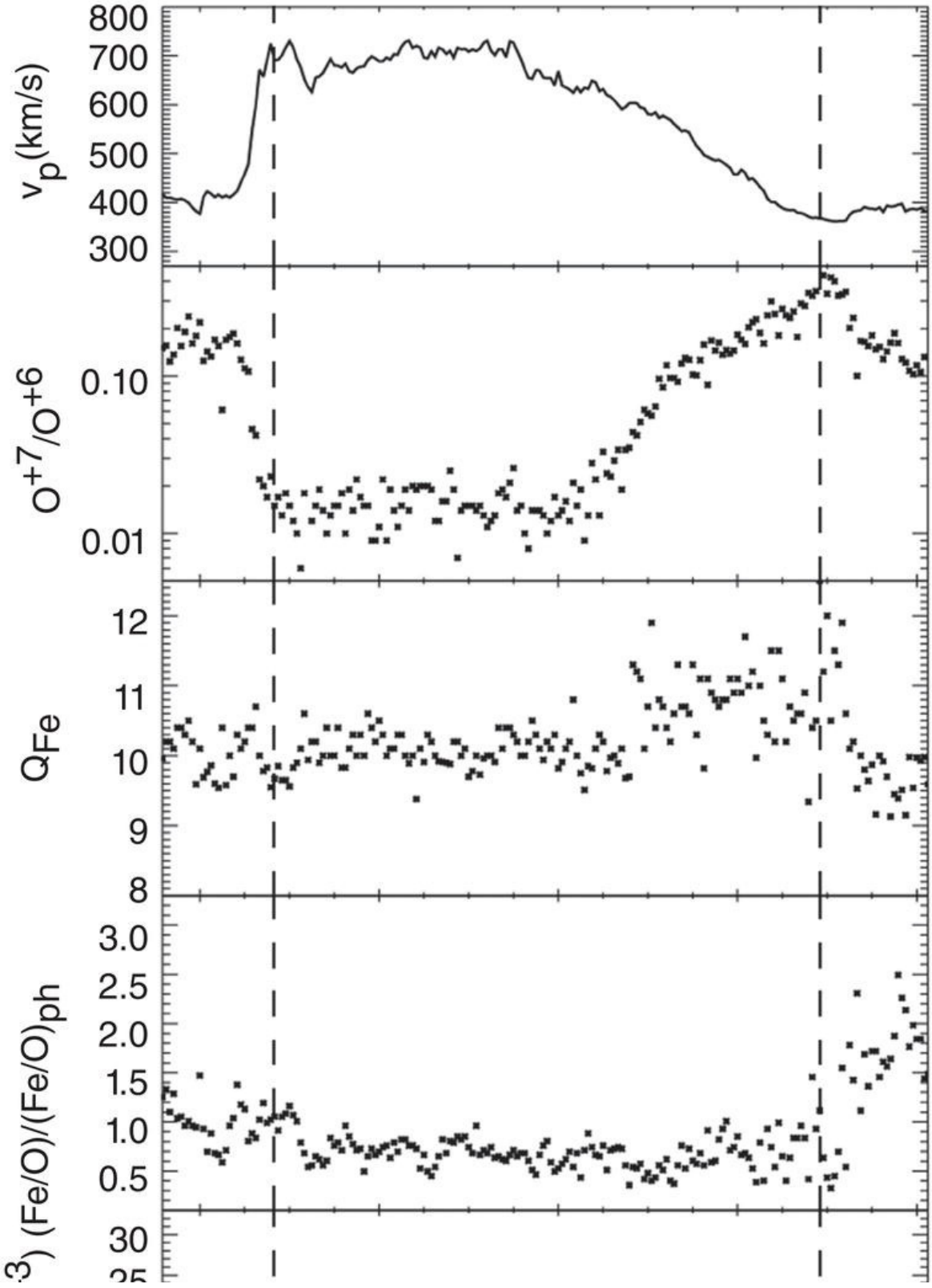

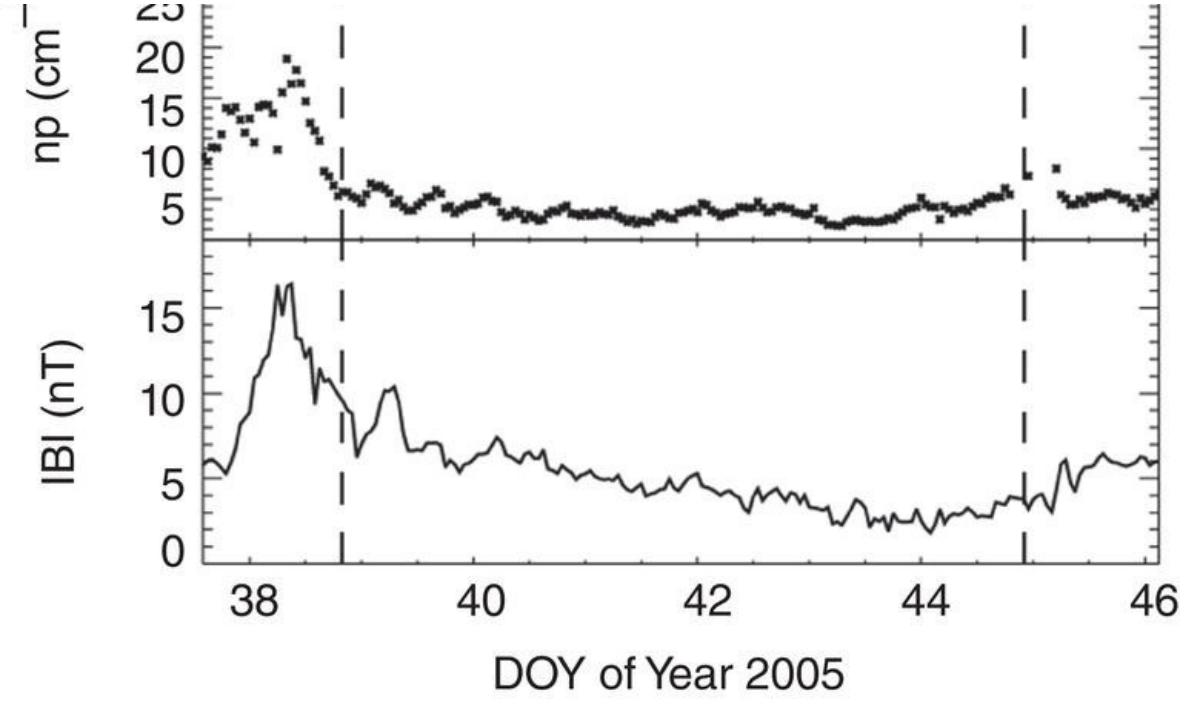

Figure 1.7 Typical time profiles of solar wind parameters for a selected solar wind interval. The SW parameters are (from top down) proton speed (vp), O+7/O+6 density ratio, average charge of Fe (QFe), Fe/O relative to its photospheric value (0.0646; Asplund et al., 2009, related to the first ionization potential, FIP, bias), proton density (np), and the magnitude of the associated interplanetary magnetic field (—B—). The selected SW interval is between the two vertical dashed lines.

(*Source*: Image taken with permission from Ko et al., 2014. © 2014, IOP Publishing.)

Electron temperatures prevailing in the source region of the fast solar wind are therefore lower than temperatures near the source region of the slow wind (temperature smaller than 1.2 MK). Near 1 AU, where ion temperatures of the fast and slow solar winds are higher than temperatures estimated from charge state ratios. This suggests that sustained heating processes occur in the fast and slow solar wind in the corona well above the heights where ionization states are frozen (Lopez et al., 1986).

Sharp O7+/O6+ boundaries occur at both leading and trailing edges of high-speed streams, suggesting rapid transitions between different coronal sources (Borovsky & Denton, 2016; Burton et al., 1999). High-cadence measurements of the ionization state of heavy ions in the slow wind have recently revealed a high degree of variability, changing by an order of magnitude inside density structures (Kepko et al., 2016). This will be discussed later in the chapter.

The higher charge state of heavy ions measured in the slow wind necessarily results from higher temperatures and densities at the coronal base of open field lines channeling the slow wind. Numerical models of the solar coronal plasma and magnetic field have been used to study the origin(s) of the slow wind. They reveal that magnetic fields are generally stronger at the base of flux tubes channeling the slow wind (Wang et al., 2009). There is a clear statistical correlation between coronal regions threaded by strong magnetic fields in the form of loops or open magnetic fields and high-plasma temperatures (Schrijver et al., 2004). Therefore, one possible interpretation for the high charge-state ratios measured in the slow wind resides in strong local heating near its source region due to the strong magnetic fields (Wang et al., 2009). Such a strong heating at the coronal base would lead to a strong heat flux conducted down to the chromosphere and enhanced densities in the slow wind. In contrast, less evaporation is likely to occur near the cooler source region of the fast wind, leading to a more tenuous fast wind. This interpretation can explain the fairly constant mass flux measured in situ in the fast and slow solar winds.

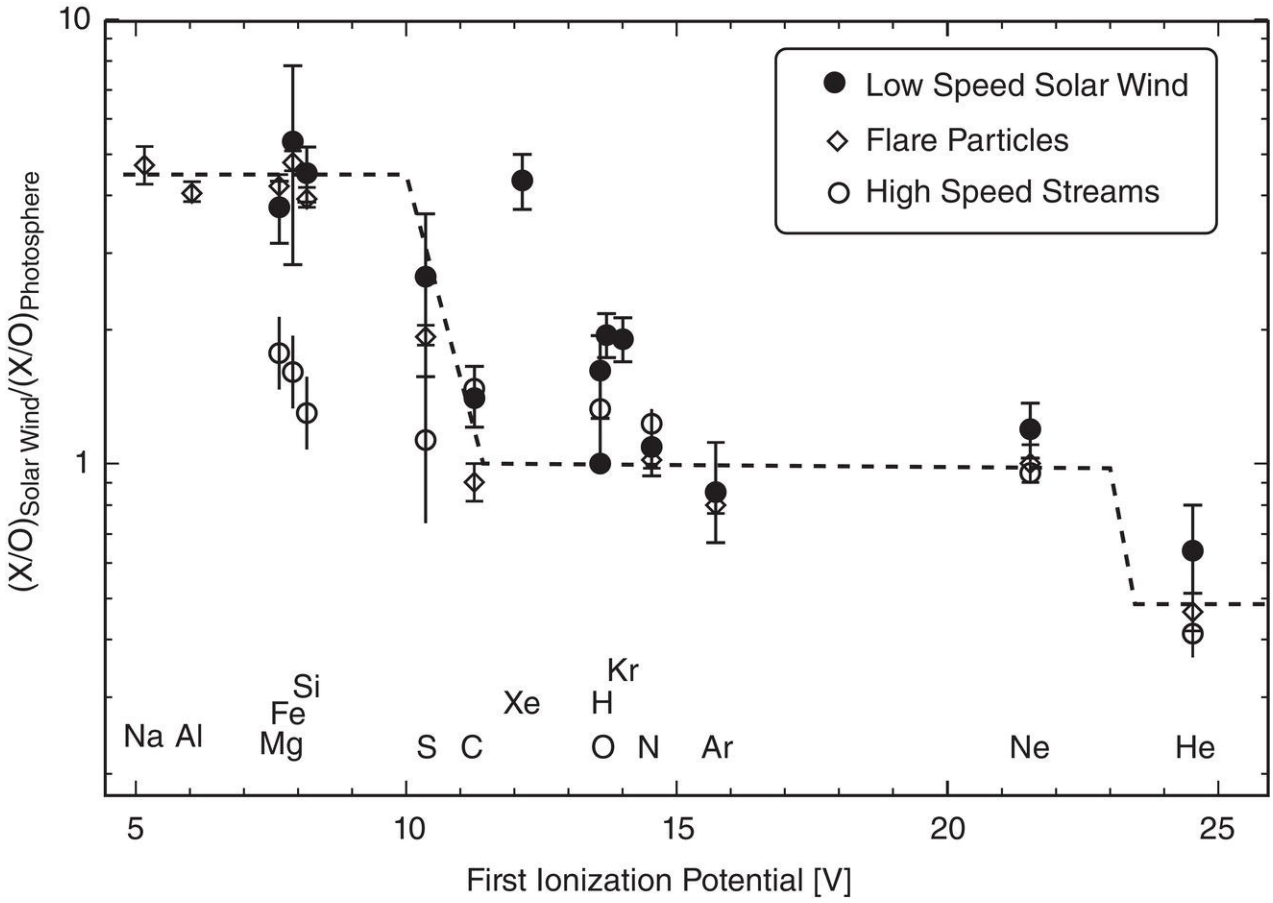

Figure 1.8 Element abundances as a function of the first ionization potential (FIP) in the average slow solar wind, fast solar wind. Abundances are given relative to oxygen and are normalized to photospheric abundances.

(*Source*: This figure was taken from Geiss, 1998 with permission from SSR. © 1998, Springer Nature.)

An alternative theory for the origin of the high charge states measured in the slow wind suggests that plasma initially confined to coronal loops is released along open magnetic field lines (Fisk et al., 1998; Schwadron et al., 1999). Loop plasma would naturally be pushed to higher ionization states because loops host typically hotter and denser plasma than open fields of coronal holes (Schwadron et al., 1999). For this mechanism to work, loop plasma must find a way to be transferred to the open field, which would require magnetic reconnection to occur continually.

The fast and slow solar winds also differ in their abundance of elements with low First Ionisation Potential (FIP), that is, the minimal energy required to ionize an atom. This first ionization occurs in the chromosphere for most elements. Overall, the corona and the solar winds exhibit higher abundances of elements with low FIP than known photospheric abundances. The slow wind exhibits even greater abundances of low-FIP elements such as Si, Fe, and Mg than the fast solar wind (von Steiger et al., 2000; Zurbuchen et al., 1999) as seen in the fourth panel of Figure 1.7 and in Figure 1.8. Such high abundances of low-FIP elements are not measured remotely in coronal holes but are more typical of closed coronal loops (Widing & Feldman, 2001). This supports the idea that the slow wind is supplied by plasma initially trapped on coronal loops and that are subsequently released in the wind (Fisk et al., 1998). In contrast, the fast wind carries fewer elements with low FIP (von Steiger et al., 2000). The composition of the fast solar wind agrees roughly with that measured in coronal holes.

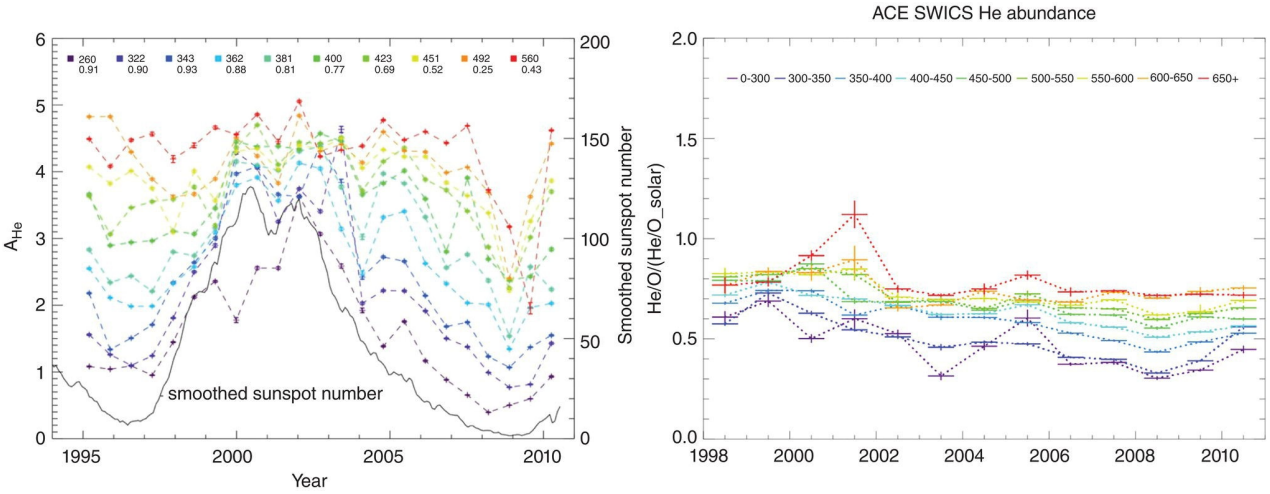

Figure 1.9 Left: The abundance of helium (computed as 100 times the density ratio of hydrogen) during 17 years of solar wind measurements by the Advanced Composition Explorer (ACE). The color coding indicates the solar wind speed. The monthly smoothed sunspot number is plotted as a black curve. Right: The abundance of helium relative to oxygen, measured by ACE/SWICS. The same trend of depletion with wind speed as for He/H is seen, but the solar cycle dependence is less pronounced.

(*Source*: Images reproduced with permission from Kasper et al., 2012 and Rakowski & Laming, 2012. © 2012, IOP Publishing.)

The fast and slow winds can also differ in their abundance of elements with higher FIP such as helium. As shown in the left-hand panel of Figure 1.9 taken from Kasper et al. (2012), the helium abundance of the fast wind remains steady (4–6%) throughout the solar cycle. In contrast, the helium abundance in the slow wind varies from around 1% at solar minima to around 4–6% at solar maxima (Aellig et al., 2001; Kasper et al., 2012). Therefore, the slow wind carries less helium than the fast wind at solar minima, but both present similar abundances at solar maxima.

There is currently no accepted mechanism for the regulation of heavy ion abundances in the solar wind. All proposed mechanisms must necessarily occur where elements are first ionized in the chromosphere and fractionate elements in a mass-independent manner. Several mechanisms have been invoked in this region to modulate the transfer of heavy ions from the chromosphere to the corona. They include, for example, the effect of Coulomb collisions in high-temperature gradients (Bø et al., 2013) and the effect of MHD waves via a ponderomotive force (Laming, 2009, 2015). The latter mechanism, in particular, is able to explain a broad range of composition measurements in the fast and slow solar winds for reasonable conditions in the solar atmosphere.

1.3.3. Solar Wind Interaction Regions

The rotation of the Sun and its associated solar wind sources such as coronal holes can result in the radial alignment of the fast and slow solar wind. A kinematic gathering of the interplanetary plasma when the fast wind catches up the slow stream, inducing an increase in plasma density near the stream interface. When the solar wind behind is much faster than the solar wind ahead, it can compress the slow wind before it reaches 1AU (as seen in Figure 1.7). When a compression region is measured over at least two consecutive solar rotations it is called a Corotating Interaction Region (CIR), otherwise one refers to simply a Stream Interaction Region (SIR; L. Jian et al., 2006). The interaction between fast and slow solar wind that creates a CIR is illustrated in Figure 1.10. Detailed descriptions of CIRs can be found in Gosling and Pizzo, 1999, and in Pizzo, 1982. As seen in the left-hand schematic of Figure 1.10, the interaction region forms, like the background solar wind, an Archimedian spiral rooted at the Sun. In three dimensions, the stream interface can be titled as it responds to the tilt of the solar magnetic dipole. Figure 1.10 illustrates how plasma flows are typically deflected inside CIRs in latitude as well as in longitude (Pizzo, 1982).

CIRs and SIRs can be more complex structures than spirals; they are composed of a multitude of smaller interaction regions that merge during the wind propagation to 1 AU. This is a consequence of the variability of the slow wind released by helmet streamers (as discussed in Section 1.2.2). Strong dynamic effects associated with the rise in total pressure inside the SIRs and CIRs are most apparent beyond 1 AU, where forward/reverse shock pairs (Lee, 2000) can bound the interaction region.

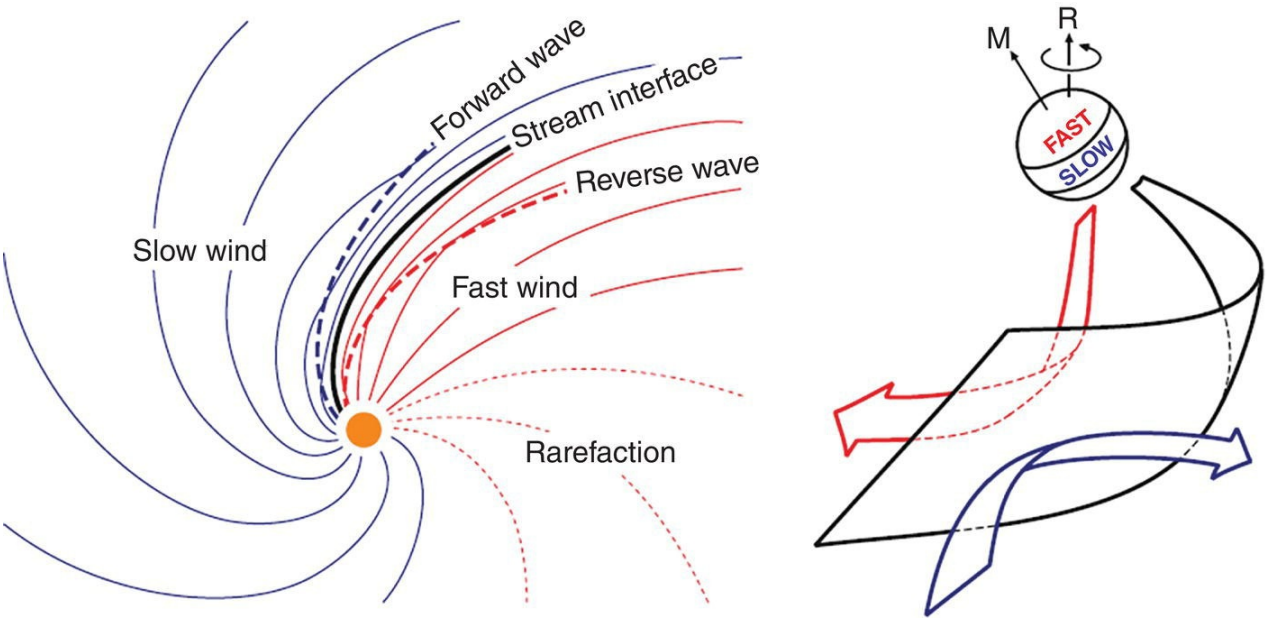

Figure 1.10 Two schematics illustrating CIRs where the fast solar wind catches up and compresses the slow solar wind. The left-hand schematic is a view from solar north, and the right-hand schematic illustrates the 3D interaction between flows when the stream interface is inclined relative to the north-south direction.

(*Source*: Figure taken from Owens & Forsyth, 2013. © 2013, Springer Nature.)

The interaction of the fast and slow solar winds, particularly in SIRs and CIRs, reduces the range of velocities of the solar wind. The slow solar wind has typical slow speeds between 300 km/s and 450 km/s. Between 0.3 and 0.4 AU, where interaction regions have not yet formed to accelerate the slowest plasma, the slow solar wind exhibits speeds less than 300 km/s nearly 10% of the time. This very slow solar wind can have speeds as low as 200 km/s inside 0.7 AU, a speed never measured at 1 AU. Wind speeds less than 300 km/s are very seldom measured in situ at 1 AU but have been extensively observed in white-light images (Rouillard, Davies, et al., 2010). This very slow wind typically has lower temperatures and higher densities than the regular slow solar wind. The properties and the source of this VSSW as well as its solar cycle variability were analyzed by Sanchez-Diaz et al. (2016).

1.3.4. Mesoscale Structures

There is an abundance of structures in the solar wind that are above the kinetic scales, but well below the global scales of the heliosphere. These so-called mesoscale structures abound in the solar wind that fills the inner heliosphere and their in situ measurements provide insights on the formation mechanisms of the solar wind.

As we saw in section 1.2.2, evidence that at least some in situ mesoscale density structures originate within the solar corona, as the solar wind forms, is found in the remote imaging of the corona. The images recorded by *SoHO* and *STEREO* have provided a tracking of density fluctuations continuously at mesoscales (several 100 Mm) from the Sun to the interplanetary medium, where it is measured in situ. As we describe below, composition, electron strahl, velocity, magnetic field, plasma temperature, and plasma density measured in situ have also been used to begin to piece together a picture where time dynamics, such as reconnection, and spatial structure at the Sun combine to create mesoscale structure in the solar wind. In essence, the solar wind measured in situ is far from homogeneous and is most likely formed that way.

The solar wind measured near the HCS is one region where myriad mesoscale structures are found. Crooker et al. (1996, 1993) showed that the highly structured solar wind measurements associated with the HCS at 1 AU were not simply due to multiple crossings of a single wavy current sheet, but rather the sampling of a HCS comprising intertwined flux ropes. They suggested that some were formed in the solar corona as the result of transient activity. In a statistical survey of mesoscale flux ropes found in the solar wind, Cartwright and Moldwin (2010a) found them to by highly concentrated near the heliospheric current sheet. As previously discussed, *STEREO* has tracked structures of sufficient density variations from the Sun to the spacecraft making in situ measurements (Rouillard, Davies, et al., 2010; Rouillard, Lavraud, et al., 2010; Rouillard et al., 2011). This unequivocally confirms the association of many of the mesoscale structures as magnetic flux ropes measured at 1 AU at the HCS and “blobs” released from helmet streamers. We now discuss mesoscale structures measured in situ that have not yet been associated with specific coronal features because they could not be tracked *from the Sun* continuously in *remote imaging*. For these, only likely associations have been made with coronal structures observed separately near the Sun by using numerical simulations of the solar corona and wind.

As already shown in Figure 1.5, the slow solar wind and the HCS are generally associated with the helmet streamer structure in the solar corona (McComas et al., 1998). Gosling et al. (1981) showed helium abundance variations associated with the crossing of the HCS, confirming that variations associated with the HCS are of solar origin. Kilpua et al. (2009) identified in *STEREO* in situ data 17 different transient structures at the HCS, which they linked to time dynamics in helmet streamers, 7 of which had counter-streaming electrons, indicating that the structures were still connected at both ends back to the Sun. Kepko et al. (2016) identified a cyclic train of mesoscale structures

around the HCS. They exhibited cyclic compositional changes, confirming a solar source. One of the structures was a flux rope with counter-streaming electrons, followed by a strahl dropout; the compositional changes indicate that magnetic reconnection in the corona created these structures.

Mesoscale structures are not restricted to the HCS. The slow solar wind includes the HCS, but can be observed as far as 30° away from the HCS (Burlaga et al., 1982), and is more generally associated with the boundary between field lines that are open to the heliosphere (coronal holes) and those that are close in the corona (streamers). Numerical modeling shows that open-closed boundaries can be a complex web of separatrices (the so-called S-web; Antiochos et al., 2011) where reconnection is likely to occur. During solar maximum, these separatrices can form a complex web, mapping to many locations away from the HCS in the heliosphere (Crooker et al., 2012; Crooker et al., 2014). Mesoscale structures in the slow solar wind outside of the HCS are observed in density as seen in Figure 1.11 taken from Viall et al. (2008), but thye are also observed in magnetic field (Borovsky, 2008), and composition (Viall et al., 2009).

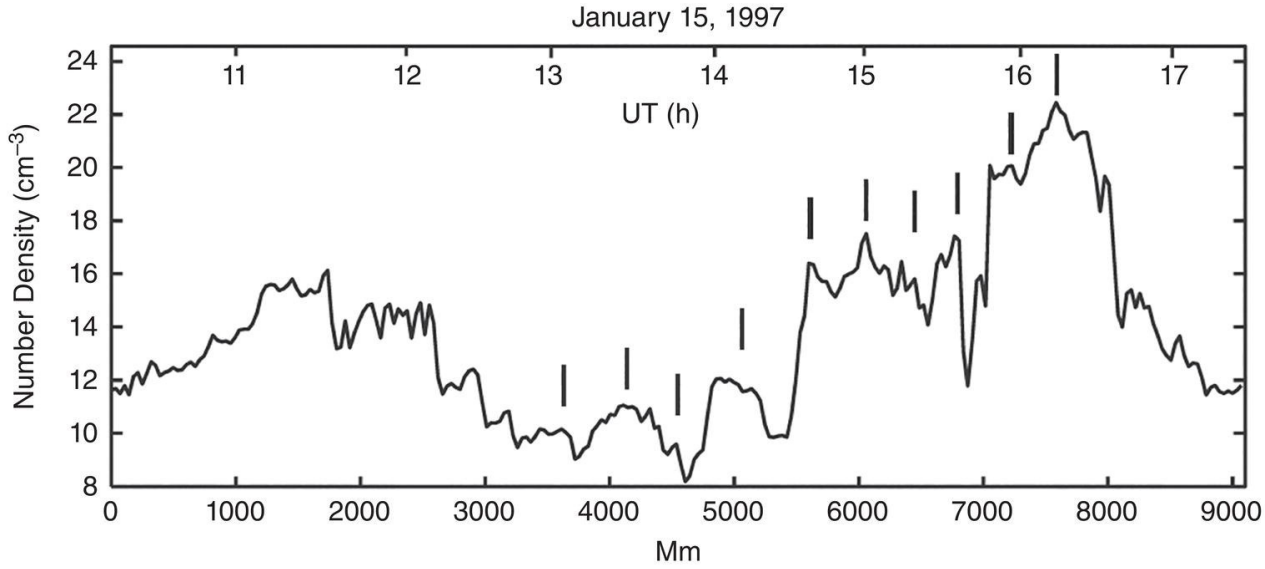

Figure 1.11 Solar wind number density data for 15 January 1997. Bottom *x*-axis is in radial-length scale steps, top *x*-axis shows the corresponding UT. Tick marks indicate a clear 400 Mm periodicity.

(*Source*: Taken from Viall et al., 2008. © 2008, John Wiley and Sons.)

It is thought that interchange reconnection could be a source of mesoscale structures perhaps forming at these modeled separatrices (Higginson et al., 2017). One signature expected when interchange reconnection occurs is that the electron strahl—which always flows away from the Sun—is observed to be in the opposite sense expected from the magnetic field direction (Crooker et al., 1996; Crooker et al., 2004; S. Kahler & Lin, 1994; S. W. Kahler et al., 1996), indicating that the magnetic field is locally folded back on itself. Owens et al. (2013) shows these inverted strahl signatures in the slow, dense solar wind at 1 AU associated both with helmet streamers, and with pseudostreamers, also associated with separatrices. Stansby and Horbury (2018) and Di Matteo et al. (2019) argue that signatures of interchange reconnection away from the HCS can be identified in *Helios* data inside of 1 AU. They identified mesoscale structures using density and showed concurrent temperature signatures, which are retained close to the Sun, strongly suggesting a solar source.

Mesoscale structures also occur in the fast wind. One prominent example is that of microstreams (Neugebauer, 2012; Neugebauer et al., 1995; Neugebauer et al., 1997). Microstreams are observed in the fast, polar solar wind with velocity fluctuations of ±35 km/s, last 6 hr or longer, have higher kinetic temperatures, higher proton flux, and slightly FIP enhanced compared to the rest of the fast solar wind. They are associated with large angle magnetic discontinuities and compositional changes that are consistent with a solar origin. Neugebauer (2012) showed that X-ray jets and the reconnection that causes them are the most likely sources of microstreams, though they could also be related to polar plumes (Neugebauer et al., 1997; Poletto, 2015). The distinction is difficult, because jets and plumes are themselves related (Raouafi et al., 2016). Simulations support the plume–microstream connection (Velli et al., 2011), and the jet–microstream/Alfvén wave connection (Karpen et al., 2017).

Horbury et al. (2018) found even smaller structures in *Helios* data at 0.3 AU, lasting tens of seconds to minutes, and reaching up to 1000 km/s. They are Alfvénic in nature, exhibiting large magnetic field deflections. These structures may form during jets from the chromosphere and/or low corona. Borovsky (2016) showed hours-long structures in the fast solar wind with large variations in number density, temperature, magnetic field strength, composition, electron strahl, and proton specific entropy, and also argue these mesoscale structures map to features in the solar corona. In contrast to the dynamic sources described above, Borovsky (2016) argues that these mesoscale structures are the result of relatively time stationary coronal flux tubes.

Pressure balances structures where the magnetic pressure balances the thermal pressure (Burlaga & Ogilvie, 1970) are also prevalent in the fast solar wind (Bavassano et al., 2004; Reisenfeld et al., 1999; Thieme et al., 1990). Unlike microstreams, McComas et al. (1996) showed that PBSs were not distinguishable from the rest of the fast solar wind, and may not be relics of transient coronal structure.

Mesoscale structures in the solar wind are an important part of the solar terrestrial connection, because they can drive magnetospheric dynamics. Often, mesoscale structures are cyclic, identified as discrete frequencies in plasma density (Di Matteo & Villante, 2017; Sanchez-Diaz et al., 2017; Viall et al., 2008) and dynamic pressure (Kepko & Spence, 2003; Kepko et al., 2002) Sometimes the structures exhibit periodicities in all plasma components (Stephenson & Walker, 2002). They are observed to directly drive global oscillations of the magnetosphere at the exact same frequencies (Kepko & Spence, 2003; Kepko et al., 2002; Viall et al., 2009; Villante et al., 2013), even by ground-based magnetometer on Earth (Villante et al., 2016) in radar oscillations in the high latitude ionosphere (Fenrich & Waters, 2008), polar UV imaging data (Liou et al., 2008), and even the equatorial ionosphere (Dyrud et al., 2008). MHD simulations have confirmed that cyclic solar wind dynamic pressure structures directly drive magnetospheric oscillations, and locations of field line resonance will even amplify the waves (Claudepierre et al., 2010; Hartinger et al., 2014).

The variations in the magnetic field of mesoscale structures in the ambient solar wind are important for an understanding of both their creation and their effect on the heliosphere and, in particular, on energetic particles. One fundamental scale size in the magnetic field on mesoscales is the correlation scale length perpendicular to the mean field. Crooker et al. (1982) measured this quantity at 1 AU and found it to have a characteristic size of 130 Mm during low magnetic field variance, and a characteristic length scale of 320 Mm during high variance. Collier, Slavin, and Lepping (2000) extended this analysis of magnetic field characteristic size scales at 1 AU and found that there is an additional scale size—the radius of curvature of the magnetic field—equal to 640 Mm.

The magnetic field changes that produce mesoscale length scales are either in the form of flux ropes (e.g., Feng et al., 2007; Moldwin et al., 1995; Moldwin et al., 2000) or flux tubes with magnetic field discontinuities at their boundaries (e.g., Bruno et al., 2001; Thieme et al., 1989). Magnetic flux ropes have a characteristic core magnetic field and magnetic rotation, and are often consistent with a force-free equilibrium (Burlaga, 1988; H. Goldstein, 1983). Flux ropes in large-scale ICMEs are a common, well-known example. There is a population of flux ropes lasting tens of minutes to hours, which are not associated with ICMEs, and instead occur with the ambient solar wind. Unlike ICMEs, the mesoscale flux ropes are not observed to be expanding due to overpressure, they do not exhibit ICME temperature depletion, they occur more often during solar minimum, and they occur in conjunction with the heliospheric current sheet. These observations make it clear that they are a slow wind feature, and not a continuation of a distribution of ICMEs to smaller scales (Cartwright & Moldwin, 2008, 2010b; Crooker et al., 1996; Moldwin et al., 1995, 2000).

Though flux ropes occur often in the slow solar wind, statistical measurements indicate that they do not make up a large portion, with occurrence rates of only six per year. There is considerable uncertainty about this rate, however, as different identification criteria can lead to vastly different event lists, and compressive Alfvén waves can be mistaken for flux ropes (Cartwright & Moldwin, 2008, 2010b; Feng et al., 2007; Higginson & Lynch, 2018).

Flux tube structures take the form of a discontinuous, planar change in the magnetic field and plasma parameters at the boundaries of the mesoscale structures. These are typically described as tangential and rotational discontinuities (Hudson, 1970), and are abundant throughout the solar wind, occurring even in the slow wind away from the HCS and in the fast wind (Neugebauer et al., 1984).

Mesoscale structures ahead of energetic particle events can influence energetic particle transport. *STEREO* observations of energetic particles have shown that variations appear to be linked to flux tubes with diameters of 6000 Mm (von Rosenvinge et al., 2009). Furthermore, even shorter fluctuations in the particle properties suggest that these flux tubes have sizes that extend down to 500 Mm. These intensity changes are similar to particle “dropouts” (Chollet et al., 2007; Mazur et al., 2000). Dropouts have been attributed to changes in the magnetic connectivity between the particle detector and the particle accelerator at the Sun due to flux tubes (at scales of 10–100 Mm) that meander or mix through the interplanetary medium (Chollet & Giacalone, 2011; Giacalone et al., 2000). Particle dropouts and heat flux loss often indicate changes within the underlying magnetic topology occurring with HCS crossings or local kinks in magnetic flux tubes (Borovsky, 2008; Crooker et al., 1982). We note that the majority of sharp changes in energetic particle populations during ambient solar wind conditions occur with changes in plasma and magnetic fields at tangential discontinuities (Neugebauer & Giacalone, 2015).

Whether the smaller flux tubes and flux ropes are created at the Sun and advected with the solar wind, or whether they are created in transit is still an open question. For example, Cartwright and Moldwin (2008) argued that flux ropes are generated by reconnection across the HCS in transit, and indeed plenty of reconnection is known to occur locally in the solar wind (Gosling, 2012), though not in direct association with a mesoscale flux rope. Magnetic reconnection in the solar wind is discussed in Section 1.3.5. On the other hand, Crooker et al. (1996) argued the flux ropes were formed at the Sun as the solar wind is created. Measurements of the flux ropes as a function of radial distance from the Sun shows that there are fewer at greater distances, and that they are larger with distance (Cartwright & Moldwin, 2010b), indicating merging or expansion rather than local creation.

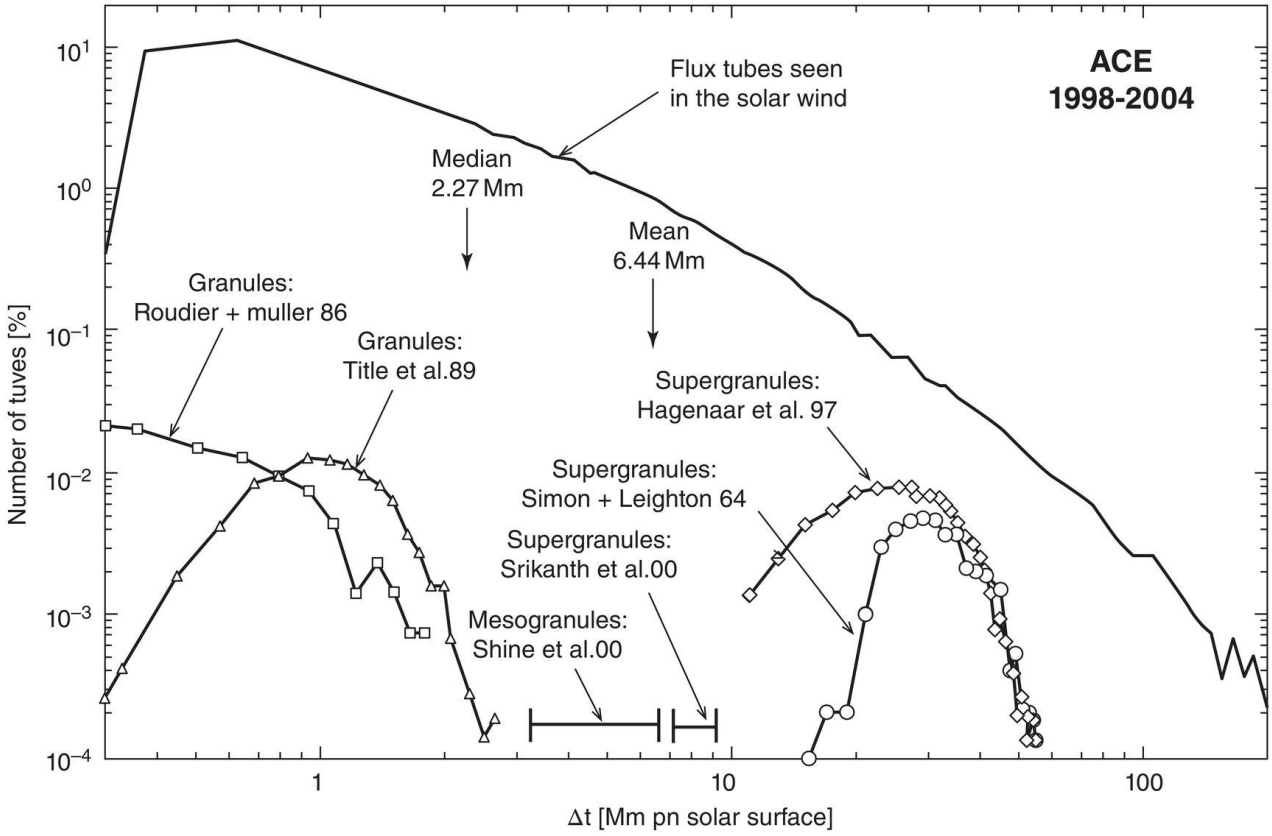

Figure 1.12 Occurrence distribution of flux tube sizes mapped to the solar surface is plotted as the black curve. Also plotted are distributions of solar granules and supergranules, and supergranule sizes obtained with high-resolution measurements are indicated with horizontal bars.

(*Source*: Taken with permission from Borovsky, 2008. © 2008, John Wiley and Sons.)

One idea is that the solar wind is filled with coherent "fossil structure" flux tubes from the solar corona that advect with the solar wind (Bruno et al., 2001; Marsch & Tu, 1993; Thieme et al., 1989). Borovsky (2008) and Collier et al. (2000) both used geometric arguments (e.g., solar rotation rate, radial expansion of the solar wind) to relate the mesoscale flux tube structure observed at 1 AU to granules. A comparison of the occurrence distribution of flux tube sizes between in situ and observed solar features is shown in Figure 1.12. Neugebauer and Giacalone (2015) argued that tangential discontinuities were preexisting flux tube boundaries formed at the Sun based on the corresponding plasma parameters, and were not consistent with in-transit turbulence. However, it is unclear if a direct connection with granules in the photosphere is possible, and simulations show that the boundaries of flux tubes created from granulation would not survive to 1 AU (Cranmer et al., 2013).

Some of the mesoscale structures, such as the characteristic magnetic field correlation lengths, may be related to turbulence. In general, it is known that the spectra of fluctuations in the solar wind have an inertial range at smaller scales, and at larger scales, follow a 1/f form that is a condition of low-frequency Alfvénic turbulence. The origin of the 1/f turbulent fluctuations is still debated but may itself originate from the corona (e.g., Matthaeus & Goldstein, 1986; Nicol et al., 2009) and footpoint stirring in the solar photosphere, with the inertial range being the transit turbulent decay. When compositional changes are associated with discontinuities and flux ropes, that is uncontroversial evidence that those structures were formed at the Sun (Borovsky, 2012; Borovsky & Denton, 2016; Kepko et al., 2016; Neugebauer, 2012; Viall et al., 2009). Structures without compositional change are ambiguous and could be formed either at the Sun or in transit (Owens et al., 2011).

We should point out the impact of mesoscale structures on global heliospheric structures. The variable coronal outflows imaged by coronagraphs and discussed in Section 1.2.2 indeed have repercussions on the structure of the solar wind. The standard picture of a CIR (Burlaga & Barouch, 1976; Lee, 2000; Pizzo, 1982) considers them as recurrent, uniform, and stable structures. In situ measurements made during the maximum phase of cycle 23 have revealed that interaction regions do not necessarily recur, a result of coronal hole reconfigurations and of the single-point nature of in situ measurements (L. Jian et al., 2006). Heliospheric imaging further reveals that individual CIRs or SIRs are by no means smooth compression regions distributed along a spiral but exhibit strong variability along the interaction region in response to several dynamic processes occurring at the Sun (Rouillard, Davies, et al., 2010). First, coronal holes can rapidly form and disappear during a solar rotation period, which leads to the appearance and disappearance of interaction regions in the interplanetary medium. Second, the density variations induced by the release of the small and large-scale streamer events discussed in the previous paragraph modifies the global structure of CIRs. In this regard, heliospheric imagery has provided new insights into the global structure of CIRs. It has been shown that in the inner heliosphere, CIRs are made up of compressed density structures (Rouillard, Lavraud, et al., 2010). The presence of strong pressure variations along the CIR surface suggests that shock formation will also be nonuniform with heliospheric location and time. Strong pressure enhancements would develop due to the compression by high-speed streams of small-scale transients. The shape of the CIR shock may

therefore become a highly irregular surface beyond 1 AU. This could have implications for the formation of MIRs by the interaction of CIRs toward the outer regions of the heliosphere.

1.3.5. Magnetic Reconnection in the Solar Wind

Over the last couple of decades, magnetic reconnection has become a widely studied plasma process, ubiquitous in most if not all astrophysical contexts. Although it has long been known to occur at the Sun and in Earth's magnetosphere, only a few studies proposed that it should be occurring frequently in the solar wind and at the interfaces of CMEs during propagation (McComas et al., 1988; Moldwin et al., 1995, 2000; Riley et al., 2004; Wei et al., 2003). Despite these suggestions, it was only later that the first in situ observational evidence for magnetic reconnection in the solar wind was provided by Gosling et al. (2005). The evidence consisted in the observation of a velocity change (or jet) bounded by two discontinuities (cf. Figure 1.13) where the flow and field properties where consistent with the Walén relation (Hudson, 1970; Phan et al., 2006) but with opposite signs. The relation is of opposite sign at each discontinuity because the Alfvénic perturbation is propagating parallel to the magnetic field at one discontinuity (A1 in Figure 1.13) but anti-parallel at the other (A2).

Since then, a number of observational studies have shown that magnetic reconnection is indeed frequent in the solar wind. It has in particular been shown that (a) the magnetic reconnection exhausts may contain two oppositely streaming proton beams resulting from the mixing of the two populations from the inflow media (Gosling et al., 2005); (b) it often occurs at the HCS, where spacecraft typically observe counter-streaming electron populations resulting from the mixing of either strahl or halo electrons (Gosling, 2005; Lavraud et al., 2009), signaling field lines either closed or disconnected from the Sun; (c) it occurs also well inside of 1 AU; (d) reconnection X lines in the solar wind may extend over very large distances and be active for long periods of time (from multiple spacecraft observations), suggesting that the reconnection process is not inherently intermittent (Gosling et al., 2006; Lavraud et al., 2009; Phan et al., 2006); (e) reconnection occurs for a wide range of guide fields and plasma beta properties, but is more frequent for low plasma beta (Eriksson et al., 2009; Gosling & Phan, 2013); and (f) magnetic reconnection may be driven within or at the interfaces of CMEs (Gosling et al., 2005; Ruffenach et al., 2015; Wang et al., 2012), as well as at small flux ropes in the solar wind (Feng et al., 2011; Tian et al., 2010). Many other studies, in particular based on theory and simulations, have been conducted to understand the structure of the exhaust, its boundaries, and its evolution, but these are not summarized here. It is important to note, however, that the occurrence of reconnection at CME boundaries was early perceived as broadly important (McComas et al., 1988). Indeed, its occurrence implies that the magnetic structure of the CME will change over time during propagation, so that the outer magnetic shells of the structure are peeled off, or in other words, the CME is eroded (Dasso et al., 2007; Möstl et al., 2008; Ruffenach et al., 2012; Tian et al., 2010). Direct evidence for this process was studied in detail through both case and statistical studies in Ruffenach et al. (2012, 2015), demonstrating the frequent occurrence of CME erosion during propagation. The process was also studied through global simulations by Manchester et al. (2014) and Manchester, van der Holst, and Lavraud (2014). The importance of CME erosion by magnetic reconnection also comes from its potential effect on CME geoeffectiveness (Lavraud et al., 2014).

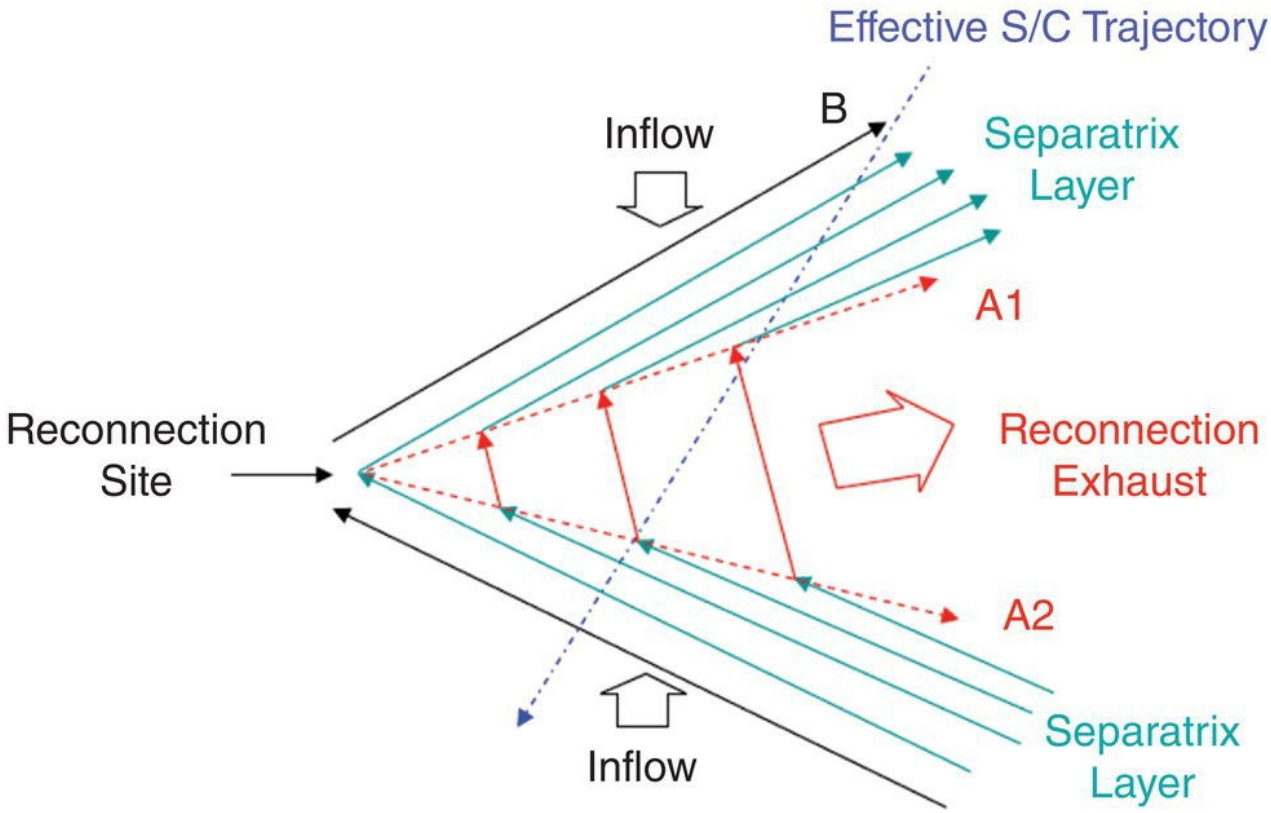

Figure 1.13 Highly idealized planar projection of a slightly asymmetric reconnection exhaust, not to scale, convecting with the nearly radial (from the Sun) solar wind flow. The dash-dot arrow shows an effective spacecraft trajectory through the exhaust. For simplicity, the oppositely directed exhaust is not shown.

(*Source*: From Gosling & Szabo, 2008. © 2008 John Wiley and Sons.)

Other broader impacts of the frequent occurrence of magnetic reconnection in the solar wind come from the fact that it may affect solar wind heating, in particular near the Sun, as well as the generation of turbulence and associated intermittency, topics that are reviewed in the next sections.

1.4. WAVES AND TURBULENCE

1.4.1. Spectra of Solar Wind Fluctuations at All Scales

In situ measurements allow us to make detailed analysis of electromagnetic fluctuations in the solar wind plasma over a wide range of scales. Figure 1.14 (left) shows an example of a composite magnetic spectrum taken at 1 AU using the *ACE* and *Cluster* spacecraft (Kiyani et al., 2015). Fluctuations are organized in different frequency ranges, each with a different power law. The main central part (10^{-3}Hz < f < 10^{-1}Hz) is characterized by a Kolmogorov −5/3 spectral slope; this corresponds to the inertial range of an MHD turbulent cascade that transports energy from large to small scales, as in hydrodynamics turbulence (Bruno & Carbone, 2013).

It should be recalled here that due to the high speed of the solar wind flow compared to the typical velocities associated to the motion of the plasma fluctuations (Taylor hypothesis), time frequencies measured in the spacecraft frame can be interpreted as spatial k-vectors in the plasma frame. It is then possible to study the 3D distribution of k-vectors in the inertial range using measurements at different angles with respect to the main field (Horbury et al., 2008; Saur & Bieber, 1999; Wicks et al., 2010); this suggests a quasi-2D distribution of the power, constituted by very elongated turbulent eddies along the magnetic field and a turbulent cascade that occurs preferentially for k-vectors perpendicular with respect to the magnetic field.

At larger scales, the spectrum of magnetic fluctuations is often characterized by a shallower slope, close to −1 (Bavassano, Dobrowolny, Mariani et al., 1982; Denskat & Neubauer, 1982); this range, called 1/f, is sometimes considered as the energy reservoir for the turbulent cascade, in analogy with hydrodynamics, although this analogy is not necessarily straightforward (Tu & Marsch, 1995) and more generally, the origin of the 1/f range is still under debate in the community (Chandran, 2018; Matteini et al., 2018; Matthaeus & Goldstein, 1986; Velli et al., 1989; Verdini et al., 2012).

At higher frequencies, around scales corresponding to the typical ion characteristic lengths (ion gyroradius ρ_i and inertial length d_i), the spectrum becomes steeper. This is expected when MHD breaks down, and kinetic physics starts to play a role. Moreover, fluctuations become more compressible at these scales, as a result of the transition from a regime where the electric field is controlled by ideal-MHD to a Hall-MHD regime (e.g., Alexandrova et al., 2008; Kiyani et al., 2013; Lacombe et al., 2017). As a consequence, the spectrum of the electric field, which follows that of the magnetic field at large MHD fluid scales, starts to depart at ion scales and display a shallower spectral slope at sub-ion scale, such that the ratio of electric-to-magnetic fluctuations increases linearly with f (Matteini et al.,

2017).

At even higher frequencies, approaching electron plasma scales (f: 50–100Hz, corresponding to a few km at 1 AU), the magnetic spectrum of the background turbulence steepens further; see Figure 1.14 (right). We will discuss the background turbulence at electron scales in more detail below. Note that at these frequencies whistler wave activity is also sometimes observed, characterized by right-handed circular polarization very distinct from that of the background turbulence (Kajdič et al., 2016a; Lacombe et al., 2014; O. W. Roberts et al., 2017; Stansby et al., 2016)

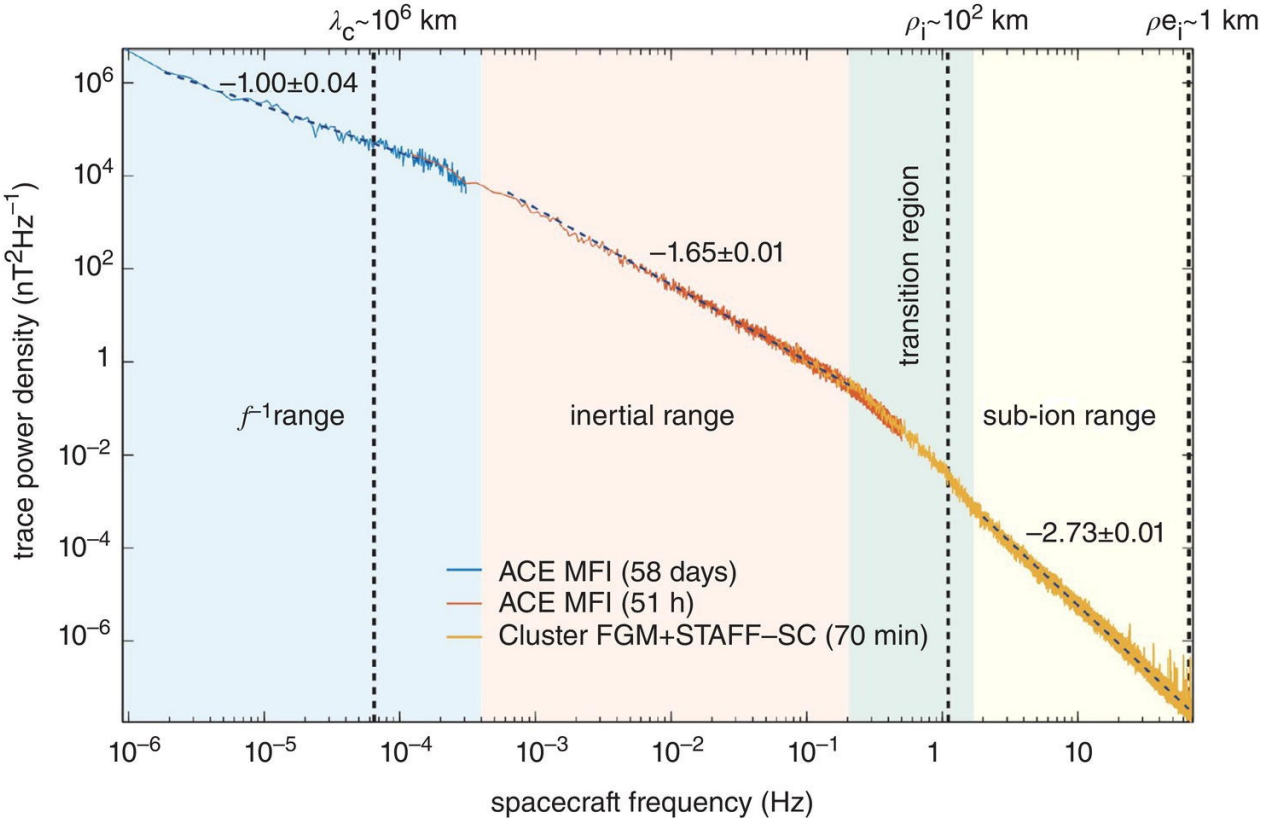

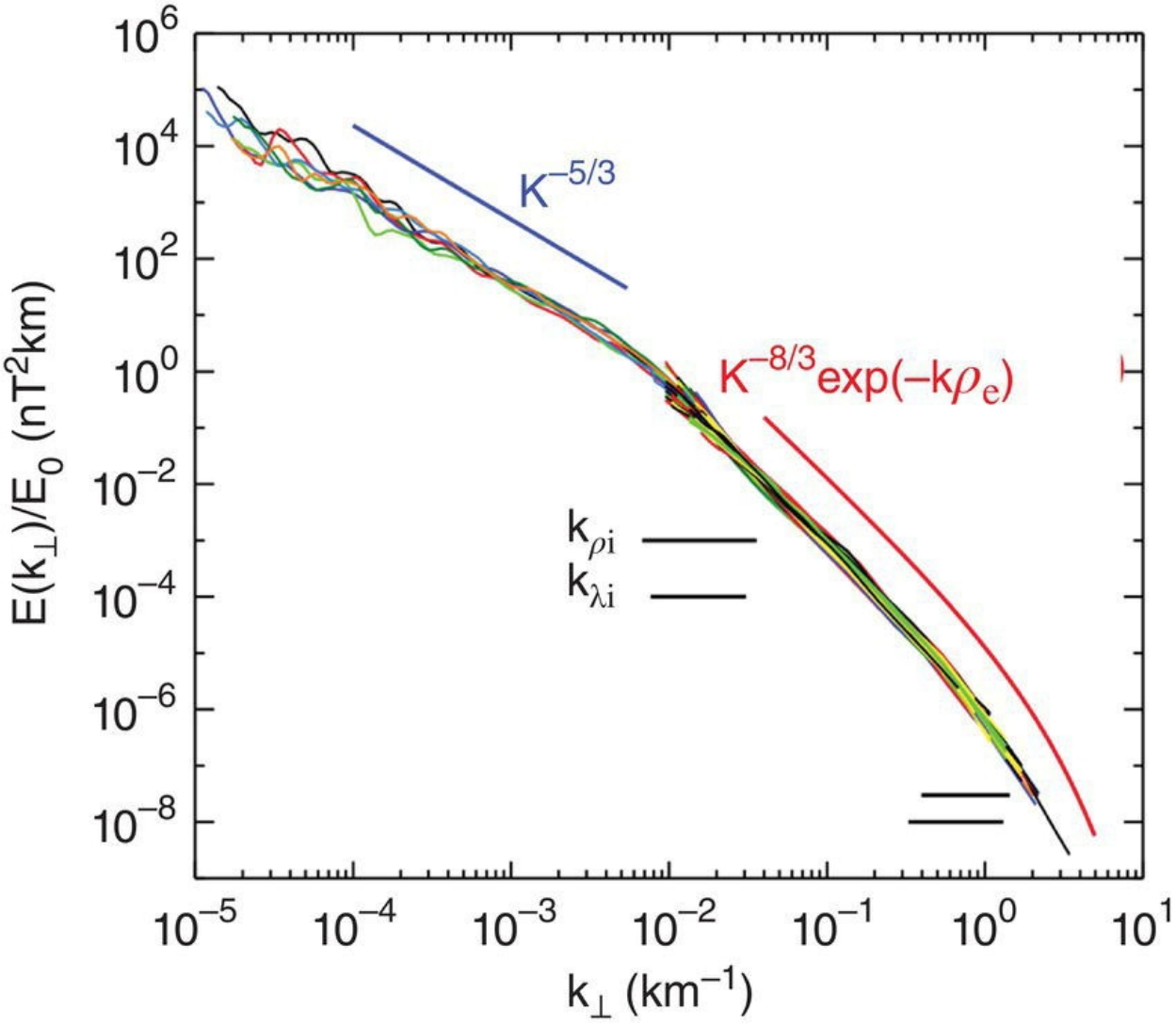

Figure 1.14 Top: Typical spectrum of magnetic field fluctuations in the solar wind from Kiyani et al. (2015). Measurements of ACE and Cluster at 1 AU from MHD to electron scales are shown. Doppler-shifted characteristic scales, such as the correlation length λ_c and the ion and electron Larmor radii $\rho_{i,\,e}$ are indicated by vertical dashed lines. Bottom: Superposed (more then 100) turbulent spectra of magnetic fluctuations under different plasma conditions from inertial to sub-electron scales as measured by Cluster (Alexandrova et al., 2012).

(*Source*: Kiyani et al., 2015.)

1.4.2. Alfvén Waves in the Fast and Slow Winds

At large scales, one of the most distinctive feature is the high degree of correlation between magnetic and velocity fluctuations, suggesting an Alfvénic origin and corresponding to a flux of waves moving away from the Sun (Belcher & Davis, 1971). Even though the spectrum of velocity fluctuations within the inertial range follows a shallower power law, $f^{-3/2}$, than the one governing magnetic fluctuations (Podesta et al., 2006; C. Salem et al., 2009). Alfvénic fluctuations are ubiquitous in the fast solar wind, where the correlation between velocity and magnetic field is typically very high, especially closer to the Sun. This is not the case in the slow wind, which is more irregular and compressible, and in general it does not display a high level of Alfvénic correlation. However, there are also periods of slow wind that appear highly Alfvénic, suggesting then a common origin as the main fast wind coming from coronal holes (D'Amicis & Bruno, 2015). Consistent with that, all the properties of this Alfvénic slow wind match those of the fast wind, thus reinforcing the idea of a common origin of the plasma (D'Amicis et al., 2018). Interestingly, in situ measurements suggest that a higher fraction of slow solar wind is also Alfvénic closer to the Sun (Stansby et al., 2019); this is an aspect that will benefit from the future explorations of *Solar Orbiter* and *Parker Solar Probe*.

Alfvénic streams (fast and slow) always display a $1/f$ range at large scales (Bavassano, Dobrowolny, Mariani et al., 1982; Denskat & Neubauer, 1982). It has been suggested that these fluctuations originate in the corona (Matthaeus & Goldstein, 1986), could be generated by Alfvén wave reflection in the acceleration region due to strong density gradients (Velli et al., 1989; Verdini et al., 2012), by parametric instability (Chandran, 2018), or be a consequence of a saturation of the wave amplitude (Matteini et al., 2018).

Alfvénic periods in the solar wind are also characterized by a remarkably low plasma and magnetic field compressibility (Matteini et al., 2015). This means that fluctuations in the 1/f range, although large and comparable

to the background magnetic field intensity, act mostly like directional changes rather than compressing the field. How this state is achieved is today not fully understood, but it is very well maintained by the plasma during expansion, as confirmed by observations by *Ulysses* beyond 1 AU. Another consequence of this state is that modulation of the magnetic field also implies (anti-correlated) local variations of the flow speed. This results in a spiky velocity profile in the fast solar wind (Matteini et al., 2014); the amplitude of the velocity enhancements tracks the Alfvén speed and is then largest close to the Sun. As mentioned earlier, Horbury et al. (2018) have suggested that the Alfvénic spikes observed in fast streams could be signatures of Alfvénic pulses injected by coronal jets surviving in interplanetary space (Karpen et al., 2017; M. A. Roberts et al., 2018). It has been argued that the effect of jets and velocity shears that may develop in the corona could significantly increase the strength of the radial component of the interplanetary magnetic field with radial distance away from the Sun (Lockwood et al., 2009a, 2009b). These kinematic effects could be the source of discrepancy between the open magnetic flux derived from numerical models of the solar corona and the magnetic field measured in situ (Lockwood et al., 2009a).

Below the $1/f$ range, and at scales smaller than a few hours, a turbulent inertial range is observed in all main fields (magnetic, electric, velocity and density); for example, see the review paper by Alexandrova et al. (2013). In the fast/Alfvénic wind, this corresponds to an almost incompressible MHD cascade, where fluctuations in density are small compared to magnetic and velocity fluctuations. The slow wind typically has a higher level of compressibility, suggesting a mixture of Alfvénic fluctuations and compressible structures, whose weight in the power spectrum also varies as a function of distance. Estimations of the turbulent cascade rate (Coburn et al., 2014; Sorriso-Valvo et al., 2007) confirm the existence of an energy flux through MHD scales, whose amplitude roughly matches the external energy input needed to explain ion temperature profiles in interplanetary space (Hellinger et al., 2011)

1.4.3. Solar Wind Fluctuations at Kinetic Scales

We now discuss the turbulent fluctuations at the end of the Kolmogorov inertial range and at smaller scales, that is, the *kinetic range* of the solar wind turbulence, sometimes called the *dissipation range* by analogy with the usual hydrodynamic (HD) turbulence.

Approaching ion scales (100 km at 1 AU), the MHD approximation is no more valid, and ions and electrons cannot be considered as one fluid. As protons are much heavier than electrons, in the vicinity of the ion inertial length λ_i, there is a separation into two fluids (Hall-MHD description). Arriving at the ion Larmor radius scale, ρ_i, ions should be considered as particles and not a fluid. The corresponding time scale is the ion cyclotron frequency f_{ci}. In the vicinity of f_{ci}, Alfvén waves become dispersive. In plasma with anisotropic ions, the Alfvén ion cyclotron (AIC) instability generates quasi-parallel AIC waves, visible in turbulent spectra as bumps or breaks at the vicinity of f_{ci} (e.g., L. K. Jian et al., 2014; Lion et al., 2016). The intermittent structures present in the inertial range, have their smallest spatial scales with the strongest gradients. For example, the thickness of the current sheets is observed to be several λ_i, or the cross section of magnetic vortices is about a few ρ_i (Perrone et al., 2016, 2017). These small-scale discontinuities have a distinct Fourier spectrum, f^{-2}, for current sheets and shocks, and f^{-4} for magnetic vortices (Alexandrova, 2008). Thus, the presence of different phenomena, like ion temperature instabilities (Bale et al., 2009; Hellinger et al., 2006) and the strongest gradients of the intermittent structures, is at the origin of the spectral variability observed in the frequency range covering ion scales~[0.1,3] Hz (C. W. Smith et al., 2006).

Between ion and electron scales, ~[3, 30] Hz at 1 AU, one observes another general power-law behavior of the magnetic spectrum (Alexandrova et al., 2009, 2012; Sahraoui et al., 2013). This suggests a small-scale turbulent cascade of the electron fluid (e.g., Alexandrova et al., 2008; Schekochihin et al., 2009). This cascade is more compressible than the MHD inertial range (Alexandrova et al., 2008; Hamilton et al., 2008; Kiyani et al., 2013; Leamon et al., 1998; C. S. Salem et al., 2012; Turner et al., 2011). The observed compressibility can be explained by the β -dependent compressibility of oblique kinetic Alfvén waves (KAWs; Cerri et al., 2017; Lacombe et al., 2017; C. S. Salem et al., 2012).

In the vicinity of the electron scales (1 km at 1 AU), ions are fully kinetic and electrons start to become kinetic, so no magneto-fluid motions are expected anymore. At these scales, the magnetic spectrum has an exponential shape similar to the dissipation range spectrum of the usual HD turbulence; see Figure 1.1 (right). This spectrum can be explained by the dissipation of KAWs via Landau damping (Howes et al., 2006, 2011; Schreiner & Saur, 2017).

In fact, the statistical properties described above, such as spectral shape and compressibility, are just averaged characteristics of the turbulent flow. The nature of turbulence at kinetic scales remains an open question. Even if KAWs can explain the observed compressibility and the exponential spectral shape, it is not clear if turbulence at these small scales is a mixture of such linear waves. To address the question of the nature of turbulent fluctuations, one should consider time-domain measurements and not only spectral properties. Few observations at sub-ion scales show the presence of intermittent coherent structures in the form of current sheets (Greco et al., 2016; Perri et al., 2012) and magnetic vortices (Jovanic et al., 2020 submitted). These observations suggest a non-homogeneous dissipation of the electromagnetic turbulent cascade in space that contradicts the homogeneous dissipation of KAWs via Landau damping.

It is possible that both phenomena, that is, a mixture of quasi-linear waves and coherent structures, coexist within the kinetic range of scales. This can be at the origin of a balance between linear and nonlinear effects (the so-called *critical balance*). To verify this point, one needs to find a way to estimate characteristic times at different scales of the kinetic range.

1.5. KINETIC PROCESSES AND HEATING IN THE SOLAR WIND

1.5.1. Evolution of Anisotropies of the Solar Wind Distribution Function

Particle distributions in interplanetary space have been studied over many decades with *Helios*, *Ulysses*, *Wind*, *Cluster*, and various other spacecraft, mainly near 1 AU, but with also some observations from 0.3 to 4 AU up to now. The observed particle distributions are not Maxwellian, but show distinguishable structures. The physical processes that regulate the shape of particle distribution functions in the super-Alfvénic solar wind include plasma heating/instabilities, particle collisions and adiabatic particle motion. The main constituents of the solar wind, protons, electrons and alpha particles, can develop highly anisotropic velocity distribution functions. In this chapter, we illustrate these effects by considering electrons only and refer the reader to other reviews of the field of 'ion kinetics' that is not discussed here (e.g. Matteini et al. 2012). Electron distributions usually consist of a thermal core, an extended suprathermal halo, and an anti-sunward beam or "strahl" (Lin, 1974; Pilipp et al., 1987). Core and halo distributions often show temperature anisotropies, that is, different temperatures $T_\parallel$ parallel to the background magnetic field, and $T_\perp$ perpendicular to it. The temperatures of electron distributions can be determined by fits with bi-Maxwellian or bi-kappa distributions to core and halo components, the latter after subtraction of the asymmetric strahl component (Ogilvie et al., 2000). The different components of the electron distributions are illustrated in Figure 1.16.

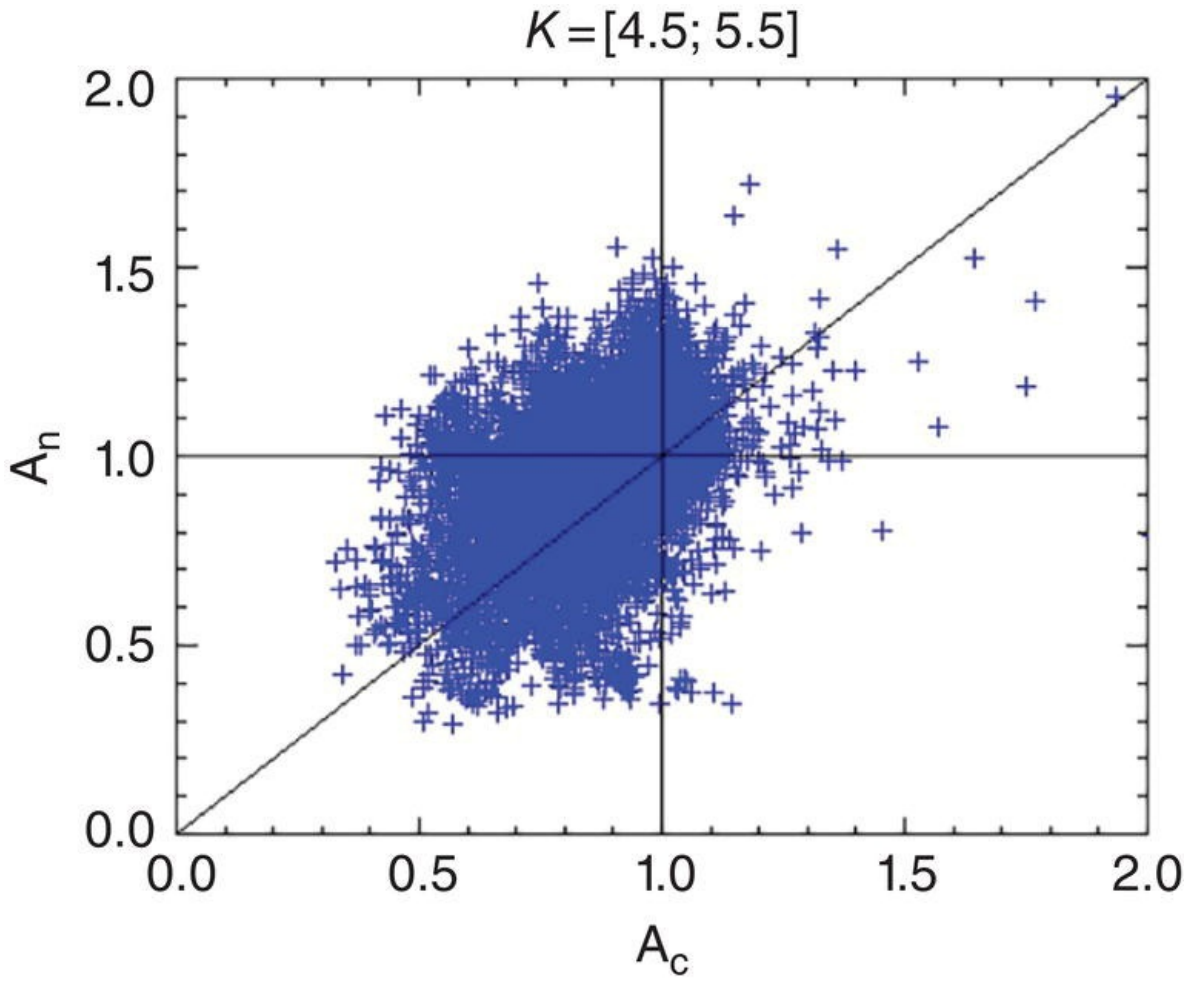

Figure 1.15 Electron temperature anisotropy of the halo ($A_h = T_{h\perp}/T_{h\parallel}$) as a function of the temperature anisotropy of the electron core ($A_c = T_{c\perp}/T_{c\parallel}$) observed in the solar wind with *Helios*, *Cluster*, and *Ulysses* from 0.7 to 1.5 AU for kappa values ranging between 4.5 and 5.5.

(*Source*: From Pierrard et al., 2016. © 2016, Springer Nature.)

A naive expectation for an electron distribution in the expanding solar wind would be focusing into the magnetic field direction, caused by the mirror force in the expanding magnetic field geometry of the Parker spiral. This would lead to a pronounced temperature anisotropy $T_\parallel > T_\perp$. However, this is not observed, Figure 1.15 displays temperature anisotropies measured in the inner heliosphere and shows that even $T\perp > T\parallel$ is frequently measured in situ in the inner heliosphere. This observation alone already indicates that processes must be active in the solar wind that are capable of increasing $T_\perp$ relative to $T_\parallel$.

Early observations (Pilipp et al., 1990) have revealed that $T_\parallel > T_\perp$ is dominant in the fast solar wind, whereas $T_\perp > T_\parallel$ is more commonly found in slow solar wind streams. An extensive review of solar wind electron temperature anisotropies for solar distances between 0.3 AU and 4 AU has been provided by Pierrard et al. (2016). Core and halo electron temperature anisotropies, A_c and A_h , with $A = T_\perp/T_\parallel$, are generally correlated, but their values are widely scattered between 0.5 and 2 (see Figure 1.15). Generally, $A_c < 1$ and $A_h < 1$, but instances with $A_c > 1$ and $A_h < 1$,

and vice versa, are observed. The latter case, $A_c < 1$ and $A_h > 1$, then is much more common.

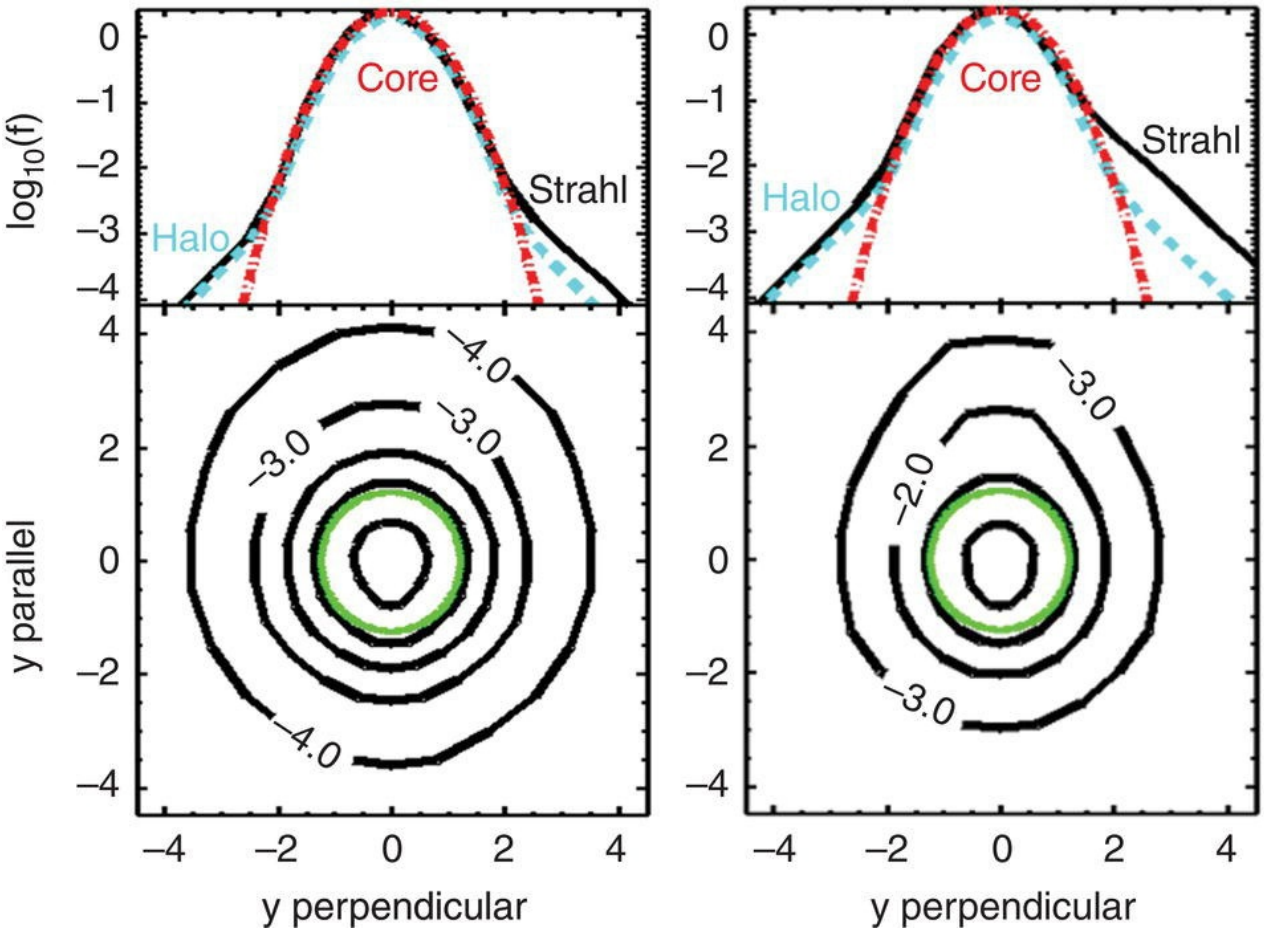

Figure 1.16 Typical electron velocity distribution function (VDF) observed by *WIND* at 1 AU in the low-speed (left) and in the high-speed (right) solar wind. Bottom panels: The plane of velocities (normalized to the thermal velocity) parallel and perpendicular to the interplanetary magnetic field. Top panels: Parallel (solid black line) and perpendicular (dashed blue line) cross section of the observed VDF. The dashed-dotted red line represents the Maxwellian distribution that well fits the core of observed VDF.

(*Source*: From Pierrard, 2011. © 2011, Springer Nature.)

The maximum range of values for temperature anisotropies is constrained by the onset of plasma instabilities. $A > > 1$ values are unstable toward the generation of whistler waves, and $A < < 1$ values are subject to the firehose instability (Gary 1993). $A > > 1$

This picture is similar for solar wind proton distributions. They frequently show temperature anisotropies $T_\perp > T_\parallel$ plus an anti-sunward beam (see Marsch, 2012, for a review based on *Helios* data covering solar distances between 0.3 AU and 1 AU). The temperature anisotropy, A, shows a strong correlation with the observed ion cyclotron wave power, which indicates that the distributions are shaped by wave–particle interactions. As for electrons, the temperature anisotropies are constrained by thresholds for firehose and mirror instabilities, but are hardly observed near these limits. Observations suggest that temperature anisotropy instabilities may play a role in controlling the level of temperature anisotropy.

1.5.2. Wave–Particle Interactions, Kinetic Instabilities, and Collisions

The low density of the solar wind plasma could lead to the expectation that it could be described as collisionless; that is, Coulomb collisions are negligible. Nevertheless, Coulomb collisions do play a role in constraining temperature anisotropies (Pierrard et al., 2016; Pierrard et al., 2011; C. Salem et al., 2003; Štverák et al., 2008)

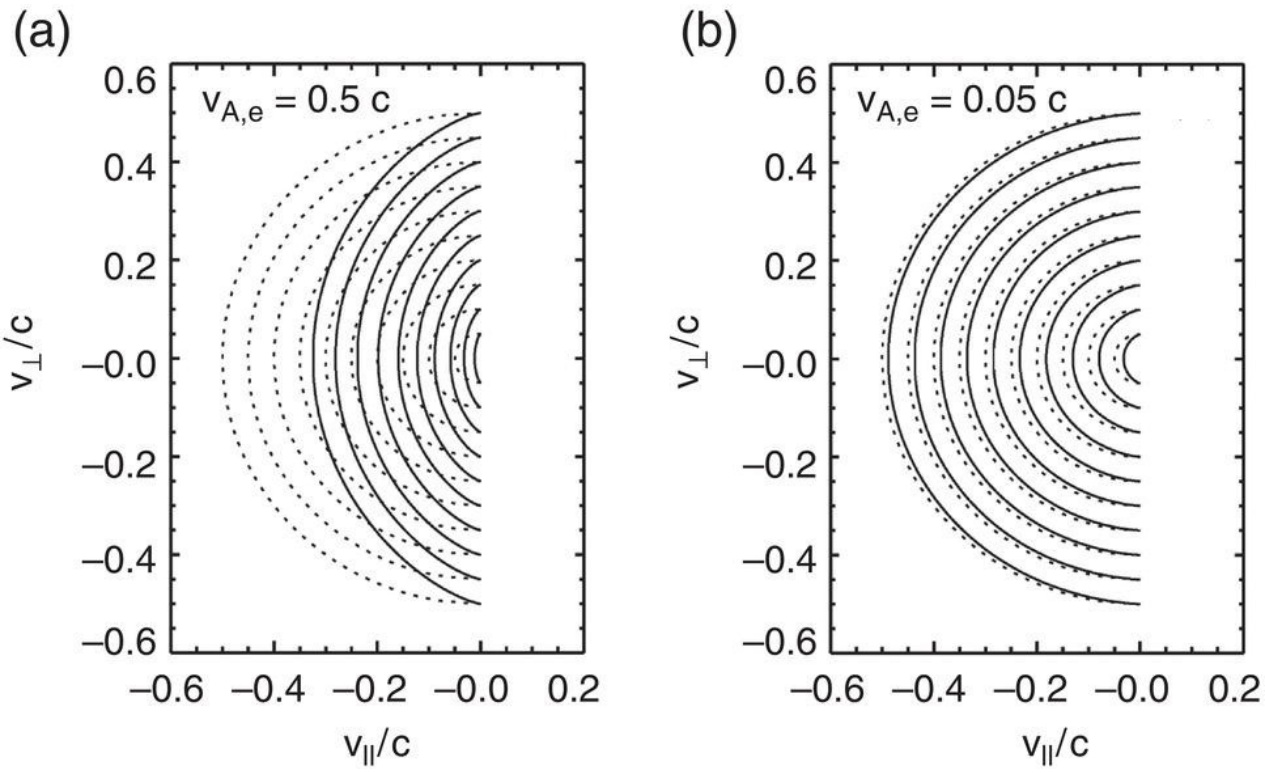

Figure 1.17 Kinetic shells formed in the electron VDF by resonant electron–whistler interaction (solid lines), and isolines of an undisturbed Maxwellian VDF (dotted lines). Shown are two plots for different values of the electron Alfvén speed, $v_{A,e}$ = 0.5 c (left, (a)), and $v_{A,e}$ = 0.05 c (right, (b)).

(*Source*: From Vocks & Mann, 2003. © 2003, IOP Publishing.)

Non-Maxwellian particle distributions can become unstable toward numerous plasma instabilities (Štverák et al., 2008). Quasi-linear theory (Kennel & Engelmann, 1966) is a useful tool to study the effect of whistler waves on the evolution of solar wind electron distributions. It considers nonlinear effects between plasma waves and the fluctuations they cause in the plasma, and therefore diffusion terms are included in the Boltzmann–Vlasov equation. Solar wind models including the effects of whistler wave turbulence are capable of reproducing the observed characteristics of solar wind electrons (Pierrard et al., 2011; Vocks, 2012).

While whistler wave turbulence leads to waves propagating in all directions relative to the background magnetic field (Chen et al., 2010; Gary & Smith, 2009), even solar wind models that consider only the interaction between electrons and whistlers propagating parallel to the magnetic field result in electron distributions with a core, halo, and strahl (Vocks et al., 2005).

The quasi-linear interaction between parallel propagating whistlers and electrons leads to pitch-angle scattering in the reference frame of the waves, which leads to the formation of "kinetic shells" (Isenberg et al., 2001); see Figure 1.17. In interplanetary space, whistler wave phase speeds are not larger than electron thermal speeds, so there is little difference between the wave frame and the plasma rest frame. So whistler turbulence tends to lead to more pitch-angle diffusion. The observation of finite strahl widths already implies that some pitch-angle scattering mechanism must be active in the solar wind, because otherwise the conservation of magnetic momentum in the expanding magnetic field geometry of the solar corona and wind would focus the electrons into an extremely narrow beam.

If the whistler wave phase speed is much higher than electron thermal speeds, as is the case in the solar corona, then the kinetic shell formation not only leads to pitch-angle diffusion, but also deforms the distribution toward higher temperature anisotropies, $T_\perp > T_\parallel$. The diffusion process brings electrons from a phase-space location with low $v_\parallel$, $v_\perp = 0$ to a position with high $v_\perp$, $v_\parallel = 0$. In the plasma frame, this corresponds to a gain of kinetic energy. Therefore, this mechanism is capable of producing a suprathermal population out of an initially Maxwellian electron distribution (Vocks et al., 2008), thus forming a halo component with a power-law distribution.

1.5.3. Suprathermal Particles

Kinetic effects induce strong distortions of the VDFs in the thermal regime, but also by forming suprathermal populations that include electron strahl, non-thermal ion beams, and heavy ion differential streaming. In this chapter, we focus on the origin and important effects of suprathermal electrons and direct the reader to the review by Marsch et al. (2009) for a discussion of suprathermal ions.

As already mentioned, solar wind electron distributions show distinct particle populations; a thermal core; an extended suprathermal halo; the asymmetric, anti-sunward strahl; and an isotropic super-halo at higher energies (Lin, 1998). The thermal core can be described by a bi-Maxwellian distribution, but this does not work so well for the halo (Pilipp et al., 1987) component. Core and halo can be much better fitted by kappa distributions (Maksimovic et

al., 1997), that show power-law suprathermal tails $\propto v^{-2(\kappa+1)}$. The κ parameter can reach values as low as 2. Note that $\kappa \to \infty$ corresponds to a Maxwellian, and for $\kappa \to 1.5$, the thermal energy, that is, the temperature, diverges.

An even better fit to observed electron data can be achieved if the core is additionally fitted by a (bi-)Maxwellian (Pierrard et al., 2016). The density of the halo is less than that of the core, but due to the higher halo temperature, their thermal energies are comparable (Maksimovic et al., 2000). A coronal origin of these suprathermal electrons is possible (Pierrard et al., 1999; Vocks et al., 2005), but whistler wave turbulence in the solar wind also plays a role in shaping these distributions (Yoon et al., 2015).

Pierrard et al. (2016) have studied the evolution of the suprathermal halo through the heliosphere between 0.3 AU and 4 AU. Temperature anisotropies were considered by applying bi-kappa fits to the electron halo population. As already found in earlier works (Maksimovic et al., 1997), the kappa value, and thus the strength of the suprathermal population, is not constant but varies in time with solar wind conditions.

Throughout the heliosphere, the kappa of the halo population generally decreases with increasing solar distance. Values of $\kappa = 7$ are frequently found closer than 1 AU, but rarely beyond 1 AU. A similar trend is found for kappa values around 5, and $\kappa = 3$ is hardly found below 1.5 AU, and more frequently beyond 1.5 AU. The strahl population can follow a different trend.

This reduction of kappa corresponds to an increase in kinetic temperature. Therefore, some mechanism for energizing these electrons has to be present in the solar wind.

The presence of non-thermal populations in many space plasmas suggests a universal mechanism for their creation. This concerns mainly electrons, but also the ions in the solar wind. Observations of electron suprathermal tails in the solar wind suggest their existence in the solar corona, because the electron mean free path in the solar wind is around 1 AU. The ion-charge measurements also confirm that suprathermal electrons can already be present in the corona. In any case, measurements made by Helios a radial distances as low as 0.3 AU confirm the presence of suprathermal electrons, even if they are characterized by a larger kappa index for the halo population at low radial distances (Pierrard et al., 2016). *Solar Orbiter* will have the advantage of measuring the distributions at low distances inside and outside the ecliptic plane. Up to now, the distributions at low distances have come from *Helios*, and those at large distances from *Ulysses*. Even if useful to study the average evolution with the radial distances, the observations were made at very different time periods (1970s for *Helios*, 1990s for *Ulysses*) and by different instruments measuring the distributions on different energy ranges.

Different scenarios have been suggested to generate the suprathermal particles (see Pierrard & Lazar, 2010, for a review). Turbulence associated with the long range of the Coulomb interactions has been proposed. Models including the generation of suprathermal electrons by resonant interaction with whistler waves in the solar corona and wind have been developed (Pierrard et al., 2011; Vocks & Mann, 2003). Recent scenarios use the kinetic theory to show that Kappa-like distributions could correspond to a particular thermodynamic equilibrium state. Kappa-like distributions can result as a consequence of the entropy generalization in nonextensive statistics (Leubner & Vörös, 2005), physically related to the long-range nature of the Coulomb potential, turbulence, and intermittency.

Suprathermal particles have important consequences for plasma fluctuations, resonant and nonresonant wave–particle acceleration, the heat flux, and plasma heating. These effects are well described by the kinetic approaches, where no closure requires the distributions to be nearly Maxwellian. The heating of the corona can be naturally explained by the velocity filtration, without depositing wave or magnetic field energy. Indeed, if suprathermal particles are present, their ratio over thermal ones increases as a function of altitude in an attraction field and automatically lead to an increase in temperature. This process works for electrons, but also protons and other ions if they are characterized by an enhanced population of suprathermal particles already in the low corona. The mass-to-charge ratio then determines the temperature of each ion species in good agreement with observations (Pierrard & Lamy, 2003). At larger radial distances (typically above 1.5 solar radii), the wind starts to blow, and the temperature reaches a maximum before starting to decrease. The presence of suprathermal electrons also increases the solar wind velocity as shown by Pierrard and Pieters (2014), in comparison to what is obtained with a simple thermal population characterized by a Maxwellian distribution.

1.6. THE EVOLUTION OF THE SOLAR WIND FROM THE INNER TO OUTER HELIOSPHERE

There are far fewer measurements of the solar wind in the outer heliosphere than in the inner heliosphere; however, measurements of the solar wind taken by the *Pioneer 10/11* and *Voyager 1/2* spacecraft showed that the heliosphere changes in two important ways. First, beyond 1 AU, solar wind interaction regions begin to dominate the heliosphere. Around 2–3 AU (Gosling et al., 1976; Hundhausen & Gosling, 1976; E. J. Smith & Wolfe, 1976), the dynamic compression of the slow wind by the fast wind creates a high-pressure region that expands in the reference frame of the solar wind, producing a forward fast shock and a reverse shock. The expansion of the compression region into the fast stream continually removes plasma from the high-speed stream to create larger, simpler structures. As the wind continues outward, the slower streams become more prominent, and the interaction regions broaden ahead of the fast wind.

At approximately 7 to 10 AU, by which time the fast and slow wind streams have given way to large interaction regions (Burlaga et al., 1995), successive interaction regions begin to interact themselves, forming “merged interaction regions.” On average, there exists a single merged interaction region per solar rotation near 10 AU (Hundhausen & Gosling, 1976). Around 20 AU, these merged interaction regions and their associated shocks are replaced by corotating pressure enhancements that slowly form large pressure rings concentric to the Sun (Whang &

Burlaga, 1990). These have been called “global merged interaction regions” and, together with merged interaction regions, play a significant role in the modulation of galactic cosmic rays (Burlaga et al., 1993; Wang et al., 2006).

The second important difference in the solar wind of the outer heliosphere is the existence of a new population of ions called “pick-up ions.” Beyond several tens of AUs, these pick-up ions actually modify the properties of the solar wind and must be accounted for. A pick-up ion is created when a neutral atom, streaming into the heliosphere from the local interstellar medium, becomes ionized (Vasyliunas & Siscoe, 1976; Isenberg, 1987). The ionization processes include charge exchange with solar wind ions, photoionization from solar photons, and impact ionization from solar wind electrons. Out of these, charge exchange is the dominant interaction process, whereby a singly charged ion passes close to the neutral atom and captures one of its electrons.

Once ionized, the new pick-up ion starts to gyrate around the magnetic field. The ion starts with a very small velocity as compared with the solar wind flow (about 23 km/s). Therefore, the ion experiences a motional electric field caused by the moving solar wind plasma. The pick-up ion gains energy from this electric field until its guiding center reaches a velocity that is equivalent to the solar wind flow velocity, at which point it becomes part of the bulk flow and is convected outward with the expanding solar wind. After the pick-up, the ions experience gyrotropization and isotropization by either ambient or self-generated, low-frequency electromagnetic fluctuations in the solar wind plasma. In the spacecraft frame, this process appears as if those new ions are “picked up” by the solar wind flow.

We have not thoroughly grasped the transport of pick-up ions in the solar wind due to the lack of measurements of keV-ions in the outer heliosphere. The production of the suprathermal tails on the velocity distribution functions, in particular, remains a puzzle (Chalov et al., 2003; Fahr & Fichtner, 2011). It is believed that during their propagation through the outer heliosphere, pick-up ions undergo pitch-angle scattering and stochastic acceleration by interactions with different kinds of solar wind turbulences (Chalov et al., 1997). Pick-up ions may also play a significant role in mediating the solar wind interaction with the interstellar medium, possibly changing the structure of the heliosheath through charge exchange (Zank, 1999), but more measurements are needed.

1.7. OUTSTANDING QUESTIONS AND FUTURE PROSPECTS

We have decades of in situ measurements of the solar wind plasma, composition, and magnetic field within 1 AU, and we have decades of remote imaging and spectroscopy of the solar corona and young solar wind. NASA’s *Parker Solar Probe* and ESA’s *Solar Orbiter* missions provide an amazing opportunity to finally unite these disparate data sets and make a direct connection between the remotely observed corona and the “ground truth” in situ solar wind observations.

These missions will enable highly detailed studies of the mysterious solar wind heating. Not only will these provide new constraints on kinetic models of solar wind ions and elections and their interaction with plasma waves, but also direction comparison of the data with kinetic model results will be possible. Additionally, because together *Solar Orbiter* and the *Parker Solar Probe* will cover such a wide range of solar distances, it will be possible to study (a) the radial evolution of plasma turbulence in the expanding solar wind, (b) temperature anisotropy evolution for different particle species, and (c) to distinguish whether power-law suprathermal tails are formed due to local turbulent processes in the solar wind or have their origin in the solar corona. Similarly, we will be able to investigate the nature of the formation of in situ mesoscale structures, weighing the importance of turbulent processing or magnetic reconnection that occurs during transit against time-dynamic magnetic reconnection in the corona or stationary coronal streamer substructure.

Despite the many unanswered questions surrounding the formation and propagation of the solar wind, it is obvious that heliophysics is poised on the threshold of an exciting era of discovery.

ACKNOWLEDGMENTS

OA is supported by the French Centre National d’Etude Spatiales (CNES). VP and CV thank ISSI for the project on kappa distributions. APR, YU, BL, RP, and ML acknowledge support from the French space agency (Centre National des Etudes Spatiales; CNES; https://cnes.fr/fr) that funds activity in plasma physics data center (Centre de Données de la Physique des Plasmas; CDPP; http://cdpp.eu/) and the Multi Experiment Data & Operation Center (MEDOC; https://idoc.ias.u-psud.fr/MEDOC), and the space weather team in Toulouse (Solar-Terrestrial Observations and Modelling Service; STORMS; http://storms-service.irap.omp.eu/). This includes funding for the data mining tools AMDA (http://amda.cdpp.eu/), CLWEB (clweb.cesr.fr/), and the propagation tool (http://propagationtool.cdpp.eu). APR, YW, BL, RP, and ML also acknowledge financial support from ERC for the project SLOW_SOURCE - DLV-819189 as well as ANR project COROSHOCK No *ANR* – 18 – *ERC*1 – 0006 – 01.

REFERENCES

Abbo, L., Antonucci, E., Mikić, Z. et al. (2010, December). Characterization of the slow wind in the outer corona. *Advances in Space Research 46*: 1400–1408. https://doi.org/10.1016/j.asr.2010.08.008.

Aellig, M.R., Lazarus, A.J., and Steinberg, J.T. (2001). The solar wind helium abundance: Variation with wind speed and the solar cycle. *Geophysical Research Letters 28*: 2767–2770. https://doi.org/10.1029/2000GL012771.

Alexandrova, O. (2008, February). Solar wind vs magnetosheath turbulence and Alfvén vortices. *Nonlinear Processes in Geophysics 15*: 95–108.

Alexandrova, O., Carbone, V., Veltri, P., and Sorriso-Valvo, L. (2008, February). Small-scale energy cascade of the solar wind turbulence. *The Astrophysical Journal 674*: 1153–1157. https://doi.org/10.1086/524056.

Alexandrova, O., Chen, C.H.K., Sorriso-Valvo, L. et al. (2013, October). Solar wind turbulence and the role of ion instabilities. *Space Science Reviews 178*: 101–139. https://doi.org/10.1007/s11214-013-0004-8.

Alexandrova, O., Lacombe, C., Mangeney, A. et al. (2012, December). Solar wind turbulent spectrum at plasma kinetic scales. *The Astrophysical Journal 760*: 121. https://doi.org/10.1088/0004-637X/760/2/121.

Alexandrova, O., Saur, J., Lacombe, C. et al. (2009, October). Universality of solar-wind turbulent spectrum from MHD to electron scales. *Physical Review Letters 103* (16): 165003. https://doi.org/10.1103/PhysRevLett.103.165003.

Antiochos, S.K., DeVore, C.R., Karpen, J.T., and Mikić, Z. (2007, December). Structure and dynamics of the sun's open magnetic field. *The Astrophysical Journal 671*: 936–946. https://doi.org/10.1086/522489.

Antiochos, S.K., Mikić, Z., Titov, V.S. et al. (2011, April). A model for the sources of the slow solar wind. *The Astrophysical Journal 731*: 112. https://doi.org/10.1088/0004-637X/731/2/112.

Antonucci, E., Andretta, V., Cesare, S., Ciaravella, A., Doschek, G., Fineschi, S., et al. (2017, November). METIS, the Multi Element Telescope for Imaging and Spectroscopy: an instrument proposed for the solar orbiter mission. In *Society of photo-optical instrumentation engineers (spie) conference series* (Vol. *10566*, p. 105660L). doi: https://doi.org/10.1117/12.2308225.

Antonucci, E., Dodero, M.A., and Giordano, S. (2000, November). Fast solar wind velocity in a polar coronal hole during solar minimum. *Solar Physics 197*: 115–134. https://doi.org/10.1023/A:1026568912809.

Bavassano, B., Dobrowolny, M., Fanfoni, G. et al. (1982, June). Statistical properties of MHD fluctuations associated with high-speed streams from Helios-2 observations. *Solar Physics 78*: 373–384. https://doi.org/10.1007/BF00151617.

Bavassano, B., Dobrowolny, M., Mariani, F., and Ness, N.F. (1982, May). Radial evolution of power spectra of interplanetary Alfvenic turbulence. *Journal of Geophysical Research 87*: 3617–3622.

Bavassano, B., Pietropaolo, E., & Bruno, R. (2004, February). Compressive fluctuations in high-latitude solar wind. *Annales Geophysicae*, *22*, 689–696. doi: 10 .5194/angeo-22-689-2004

Belcher, J.W. and Davis, L. Jr. (1971). Large-amplitude waves in the interplanetary medium, 2. *Journal of Geophysical Research Atmospheres 76*: 3534–3563.

Bemporad, A. (2017, September). Exploring the inner acceleration region of solar wind: A study based on coronagraphic UV and visible light data. *The Astrophysical Journal 846*: 86. https://doi.org/10.3847/1538-4357/aa7de4.

Biermann, L. (1951). Kometenschweife und solare Korpuskularstrahlung. *Zeitschrift für Astrophysik 29*: 274.

Birkeland, K. (1908). The Norwegian aurora polaris expedition, 1902–1903, Vol. I, Section 1, H Aschehoug, Oslo.

Bø, I.M.T., Esser, R., and Lie-Svendsen, Ø. (2013, May). Effect of Coulomb collisions on the gravitational settling of low and high first ionization potential elements. *The Astrophysical Journal 769*: 60. https://doi.org/10.1088/0004-637X/769/1/60.

Borovsky, J.E. (2008, August). Flux tube texture of the solar wind: Strands of the magnetic carpet at 1 AU? *Journal of Geophysical Research: Space Physics 113*: A08110. https://doi.org/10.1029/2007JA012684.

Borovsky, J.E. (2010, September). On the variations of the solar wind magnetic field about the Parker spiral direction. *Journal of Geophysical Research: Space Physics 115*: A09101. https://doi.org/10.1029/2009JA015040.

Borovsky, J. E. (2012, June). Looking for evidence of mixing in the solar wind from 0.31 to 0.98 AU. *Journal of Geophysical Research: Space Physics*, *117*, A06107. doi: 10.1029/2012JA017525.

Borovsky, J.E. (2016, June). The plasma structure of coronal hole solar wind: Origins and evolution. *Journal of Geophysical Research: Space Physics 121*: 5055–5087. https://doi.org/10.1002/2016JA022686.

Borovsky, J.E. and Denton, M.H. (2016, July). The trailing edges of high-speed streams at 1 AU. *Journal of Geophysical Research: Space Physics 121*: 6107–6140. https://doi.org/10.1002/2016JA022863.

Bruno, R. and Bavassano, B. (1997, September). On the winding of the IMF spiral for slow and fast wind within the inner heliosphere. *Geophysical Research Letters 24*: 2267. https://doi.org/10.1029/ 97GL02183.

Bruno, R., & Carbone, V. (2013, May). The solar wind as a turbulence laboratory. *Living Reviews in Solar Physics*, *10*, 2. doi: 10.12942/lrsp-2013-2.

Bruno, R., Carbone, V., Veltri, P. et al. (2001, October). Identifying intermittency events in the solar wind. *Planetary and Space Science 49*: 1201–1210. https://doi.org/10.1016/S0032-0633(01)00061-7.

Burlaga, L.F. (1988, July). Magnetic clouds and force-free fields with constant alpha. *Journal of Geophysical Research: Space Physics 93*: 7217–7224. https://doi.org/10.1029/JA093iA07p07217.

Burlaga, L.F. and Barouch, E. (1976, January). Interplanetary stream magnetism – Kinematic effects. *The Astrophysical Journal 203*: 257–267. https://doi.org/10.1086/154074.

Burlaga, L.F., Lepping, R.P., Behannon, K.W. et al. (1982, June). Large-scale variations of the interplanetary magnetic field – Voyager 1 and 2 observations between 1 and 5 AU. *Journal of Geophysical Research: Space Physics 87*: 4345–4353. https://doi.org/10.1029/JA087iA06p04345.

Burlaga, L.F., McDonald, F.B., and Ness, N.F. (1993, Jan). Cosmic ray modulation and the distant heliospheric magnetic field: Voyager 1 and 2 observations from 1986 to 1989. *Journal of Geophysical Research: Space Physics 98* (A1): 1–12. https://doi.org/10.1029/92JA01979.

Burlaga, L.F. and Ness, N.F. (1993, October). Large-scale distant heliospheric magnetic field: Voyager 1 and 2 observations from 1986 through 1989. *Journal of Geophysical Research: Space Physics 98*: 17451–17460. https://doi.org/10.1029/93JA01475.

Burlaga, L.F., Ness, N.F., and McDonald, F.B. (1995, August). Magnetic fields and cosmic rays in the distant heliosphere at solar maximum: Voyager 2 observations near 32 AU during 1990. *Journal of Geophysical Research: Space Physics 100*: 14763–14772. https://doi.org/10.1029/95JA01557.

Burlaga, L.F. and Ogilvie, K.W. (1970, November). Magnetic and thermal pressures in the solar wind. *Solar Physics 15*: 61–71. https://doi.org/10.1007/BF00149472.

Burton, M.E., Neugebauer, M., Crooker, N.U. et al. (1999, May). Identification of trailing edge solar wind stream interfaces: A comparison of Ulysses plasma and composition measurements. *Journal of Geophysical Research: Space Physics 104*: 9925–9932. https://doi.org/10.1029/JA104iA05p09925.

Cartwright, M.L. and Moldwin, M.B. (2008, September). Comparison of small-scale flux rope magnetic properties to large-scale magnetic clouds: Evidence for reconnection across the HCS? *Journal of Geophysical Research: Space Physics 113*: A09105. https://doi.org/10.1029/2008JA013389.

Cartwright, M.L. and Moldwin, M.B. (2010a, August). Heliospheric evolution of solar wind small-scale magnetic flux ropes. *Journal of Geophysical Research: Space Physics 115*: A08102. https://doi.org/10.1029/2009JA014271.

Cartwright, M.L. and Moldwin, M.B. (2010b, August). Heliospheric evolution of solar wind small-scale magnetic flux ropes. *Journal of Geophysical Research: Space Physics 115*: A08102. https://doi.org/10.1029/2009JA014271.

Cerri, S.S., Servidio, S., and Califano, F. (2017, September). Kinetic cascade in solar-wind turbulence: 3D3V Hybrid-kinetic simulations with electron inertia. *The Astrophysical Journal 846*: L18. https://doi.org/10.3847/2041-8213/aa87b0.

Chalov, S.V., Fahr, H.J., and Izmodenov, V. (1997, April). Spectra of energized pick-up ions upstream of the two-dimensional heliospheric termination shock. II. Acceleration by Alfvenic and by large-scale solar wind turbulences. *Astronomy and Astrophysics 320*: 659–671.

Chalov, S.V., Fahr, H.J., and Izmodenov, V.V. (2003, June). Evolution of pickup proton spectra in the inner heliosheath and their diagnostics by energetic neutral atom fluxes. *Journal of Geophysical Research: Space Physics 108*: 1266. https://doi.org/10.1029/2002JA009492.

Chandran, B.D.G. (2018, February). Parametric instability, inverse cascade and the range of solar-wind turbulence. *Journal of Plasma Physics 84* (1): 905840106. https://doi.org/10.1017/S0022377818000016.

Chapman, S. and Ferraro, V.C.A. (1931). A new theory of magnetic storms. *Terrestrial Magnetism and Atmospheric Electricity (Journal of Geophysical Research) 36*: 77. https://doi.org/10.1029/TE036i002p00077.

Chapman, S. and Zirin, H. (1957). Notes on the solar corona and the terrestrial ionosphere. *Smithsonian Contributions to Astrophysics 2*: 1.

Chen, C.H.K., Horbury, T.S., Schekochihin, A.A. et al. (2010, June). Anisotropy of solar wind turbulence between ion and electron scales. *Physical Review Letters 104* (25): 255002. https://doi.org/10.1103/PhysRevLett.104.255002.

Chollet, E. E., & Giacalone, J. (2011, February). Evidence of confinement of solar-energetic particles to interplanetary magnetic field lines. *The Astrophysical Journal*, *728*, 64. doi: 10 .1088/0004-637X/728/1/64.

Chollet, E.E., Giacalone, J., Mazur, J.E., and Al Dayeh, M. (2007, November). A new phenomenon in impulsive-flare-associated energetic particles. *The Astrophysical Journal 669*: 615–620. https://doi.org/10.1086/521670.

Claudepierre, S. G., Hudson, M. K., Lotko, W., Lyon, J. G., & Denton, R. E. (2010, November). Solar wind driving of magnetospheric ULF waves: Field line resonances driven by dynamic pressure fluctuations. *Journal of Geophysical Research: Space Physics*, *115*, A11202. doi: https://doi.org/10.1029/2010JA015399.

Coburn, J.T., Smith, C.W., Vasquez, B.J. et al. (2014, May). Variable cascade dynamics and intermittency in the solar wind at 1 AU. *The Astrophysical Journal 786*: 52. https://doi.org/10.1088/0004-637X/786/1/52.

Collier, M.R., Slavin, J.A., and Lepping, R.P. (2000, June). IMF length scales and predictability: The two length scale medium. *International Journal of Geomagnetism and Aeronomy 2*: 3–16. https://doi.org/10.1029/2012JA017525.

Cranmer, S.R., Field, G.B., and Kohl, J.L. (1999, June). Spectroscopic constraints on models of ion cyclotron resonance heating in the polar solar corona and high-speed solar wind. *The Astrophysical Journal 518*: 937–947. https://doi.org/10.1086/307330.

Cranmer, S.R., van Ballegooijen, A.A., and Woolsey, L.N. (2013, April). Connecting the Sun's high-resolution magnetic carpet to the turbulent heliosphere. *The Astrophysical Journal 767*: 125. https://doi.org/10.1088/0004-637X/767/2/125.

Crooker, N.U., Antiochos, S.K., Zhao, X., and Neugebauer, M. (2012, April). Global network of slow solar wind. *Journal of Geophysical Research: Space Physics 117*: A04104. https://doi.org/10.1029/2011JA017236.

Crooker, N.U., Burton, M.E., Siscoe, G.L. et al. (1996, November). Solar wind streamer belt structure. *Journal of Geophysical Research 101*: 24331–24342. https://doi.org/10.1029/96JA02412.

Crooker, N.U., Kahler, S.W., Larson, D.E., and Lin, R.P. (2004, March). Large- scale magnetic field inversions at sector boundaries. *Journal of Geophysical Research: Space Physics 109*: A03108. https://doi.org/10.1029/2003JA010278.

Crooker, N.U., McPherron, R.L., and Owens, M.J. (2014, June). Comparison of interplanetary signatures of streamers and pseudostreamers. *Journal of Geophysical Research: Space Physics 119*: 4157–4163. https://doi.org/10.1002/2014JA020079.

Crooker, N.U., Siscoe, G.L., Russell, C.T., and Smith, E.J. (1982, April). Factors controlling degree of correlation between ISEE 1 and ISEE 3 interplanetary magnetic field measurements. *Journal of Geophysical Research: Space Physics 87*: 2224–2230. https://doi.org/10.1029/JA087iA04p02224.

Crooker, N.U., Siscoe, G.L., Shodhan, S. et al. (1993, June). Multiple heliospheric current sheets and coronal streamer belt dynamics. *Journal of Geophysical Research: Space Physics 98*: 9371–9381. https://doi.org/10.1029/93JA00636.

D'Amicis, R. and Bruno, R. (2015, May). On the origin of highly Alfvénic slow solar wind. *The Astrophysical Journal 805*: 84. https://doi.org/10.1088/0004-637X/805/1/84.

D'Amicis, R., Matteini, L., & Bruno, R. (2018, December). On slow solar wind with high Alfv\'enicity: From composition and microphysics to spectral properties. *arXiv e-prints*.

Dasso, S., Nakwacki, M.S., Démoulin, P., and Mandrini, C.H. (2007, August). Progressive transformation of a flux rope to an ICME. Comparative analysis using the direct and fitted expansion methods. *Solar Physics 244*: 115–137. https://doi.org/10.1007/s11207-007-9034-2.

DeForest, C.E., Howard, R.A., Velli, M. et al. (2018, July). The highly structured outer solar corona. *The Astrophysical Journal 862*: 18. https://doi.org/10.3847/1538-4357/aac8e3.

DeForest, C.E., Matthaeus, W.H., Viall, N.M., and Cranmer, S.R. (2016, September). Fading coronal structure and the onset of turbulence in the young solar wind. *The Astrophysical Journal 828*: 66. https://doi.org/10.3847/0004-637X/828/2/66.

Denskat, K.U. and Neubauer, F.M. (1982, April). Statistical properties of low- frequency magnetic field fluctuations in the solar wind from 0.29 to 1.0 AU during solar minimum conditions – HELIOS 1 and HELIOS 2. *Journal of Geophysical Research: Space Physics 87*: 2215–2223. https://doi.org/10.1029/JA087iA04p02215.

Di Matteo, S., Viall, N.M., Kepko, L. et al. (2019). Helios observations of quasiperiodic density structures in the slow solar wind at 0.3, 0.4, and 0.6 AU. *Journal of Geophysical Research: Space Physics 124* (2): 837–860. https://doi.org/10.1029/2018JA026182.

Di Matteo, S. and Villante, U. (2017, May). The identification of solar wind waves at discrete frequencies and the role of the spectral analysis techniques. *Journal of Geophysical Research: Space Physics 122*: 4905–4920. https://doi.org/10.1002/2017JA023936.

Dolei, S., Susino, R., Sasso, C. et al. (2018, May). Mapping the solar wind HI outflow velocity in the inner heliosphere by coronagraphic ultraviolet and visible-light observations. *Astronomy & Astrophysics (A&A) 612*: A84. https://doi.org/10.1051/0004-6361/201732118.

Domingo, V., Fleck, B., and Poland, A.I. (1995, December). The SOHO mission: An overview. *Solar Physics 162*: 1–37. https://doi.org/10.1007/BF00733425.

Dyrud, L.P., Behnke, R., Kepko, E.L. et al. (2008, July). Ionospheric ULF oscillations driven from above Arecibo. *Geophysical Research Letters 35*: L14101. https://doi.org/10.1029/2008GL034073.

Endeve, E., Holzer, T.E., and Leer, E. (2004, March). Helmet streamers gone unstable: Two-fluid magnetohydrodynamic models of the solar corona. *The Astrophysical Journal 603*: 307–321. https://doi.org/10.1086/381239.

Eriksson, S., Gosling, J.T., Phan, T.D. et al. (2009). Asymmetric shear flow effects on magnetic field configuration within oppositely directed solar wind reconnection exhausts. *Journal of Geophysical Research: Space Physics 114* (A7) https://doi.org/10.1029/2008JA013990.

Fahr, H.J. and Fichtner, H. (2011, September). Pick-up ion transport under conservation of particle invariants: How important are velocity diffusion and cooling processes? *Astronomy and Astrophysics 533*: A92. https://doi.org/10.1051/0004-6361/201116880.

Feng, H.Q., Wu, D.J., and Chao, J.K. (2007, February). Size and energy distributions of interplanetary magnetic flux ropes. *Journal of Geophysical Research: Space Physics 112*: A02102. https://doi.org/10.1029/2006JA011962.

Feng, H.Q., Wu, D.J., Wang, J.M., and Chao, J.W. (2011, March). Magnetic reconnection exhausts at the boundaries of small interplanetary magnetic flux ropes. *Astronomy & Astrophysics 527*: A67. https://doi.org/10.1051/0004-6361/201014473.

Fenrich, F.R. and Waters, C.L. (2008, October). Phase coherence analysis of a field line resonance and solar wind oscillation. *Geophysical Research Letters 35*: L20102. https://doi.org/10.1029/2008GL035430.

Fisk, L.A. (1996, July). Motion of the footpoints of heliospheric magnetic field lines at the Sun: Implications for recurrent energetic particle events at high heliographic latitudes. *Journal of Geophysical Research: Space Physics 101*: 15547–15554. https://doi.org/10.1029/96JA01005.

Fisk, L.A., Schwadron, N.A., and Zurbuchen, T.H. (1998, July). On the slow solar wind. *Space Science Reviews 86*: 51–60. https://doi.org/10.1023/A:1005015527146.

Forsyth, R.J., Balogh, A., and Smith, E.J. (2002, November). The underlying direction of the heliospheric magnetic field through the Ulysses first orbit. *Journal of Geophysical Research: Space Physics 107*: 1405. https://doi.org/10.1029/2001JA005056.

Gary, S.P. and Smith, C.W. (2009, December). Short-wavelength turbulence in the solar wind: Linear theory of whistler and kinetic Alfvén fluctuations. *Journal of Geophysical Research: Space Physics 114*: A12105. https://doi.org/10.1029/2009JA014525.

Geiss, J. (1998). Constraints on the FIP mechanisms from solar wind abundance data. *Space Science Reviews 85*: 241–252.

Geiss, J., Gloeckler, G., and von Steiger, R. (1995, April). Origin of the solar wind from composition data. *Space Science Reviews 72*: 49–60. https://doi.org/10.1007/BF00768753.

Giacalone, J., Jokipii, J.R., and Mazur, J.E. (2000, March). Small-scale gradients and large-scale diffusion of charged particles in the heliospheric magnetic field. *The Astrophysical Journal Letters 532*: L75–L78. https://doi.org/10.1086/312564.

Goldstein, H. (1983, November). On the field configuration in magnetic clouds. *In Nasa conference publication* (Vol. 228).

Goldstein, M. L., Roberts, D. A., & Matthaeus, W. H. (1995). Magnetohydrodynamic turbulence in the solar wind. *Annual Review of Astronomy and Astrophysics*, *33*, 283–326. doi: 10.1146/annurev.aa .33.090195.001435.

Gosling, J.T. (2005). Magnetic disconnection from the Sun: Observations of a reconnection exhaust in the solar wind at the heliospheric current sheet. *Geophysical Research Letters 32* (5) https://doi.org/10.1029/2005GL022406.

Gosling, J.T. (2012, November). Magnetic reconnection in the solar wind. *Space Science Reviews 172*: 187–200. https://doi.org/10.1007/s11214-011-9747-2.

Gosling, J.T., Borrini, G., Asbridge, J.R. et al. (1981, July). Coronal streamers in the solar wind at 1 AU. *Journal of Geophysical Research 86*: 5438–5448. https://doi.org/10.1029/JA086iA07p05438.

Gosling, J.T., Eriksson, S., and Schwenn, R. (2006, October). Petschek-type magnetic reconnection exhausts in the solar wind well inside 1 AU: Helios. *Journal of Geophysical Research 111* (A10) https://doi.org/10.1029/2006JA011863.

Gosling, J.T., Hundhausen, A.J., and Bame, S.J. (1976, May). Solar wind stream evolution at large heliocentric distances – Experimental demonstration and the test of a model. *Journal of Geophysical Research 81*: 2111–2122. https://doi.org/10.1029/JA081i013p02111.

Gosling, J.T. and Phan, T.D. (2013, January). Magnetic reconnection in the solar wind at current sheets associated with extremely small field shear angles. *The Astrophysical Journal 763* (2): L39. https://doi.org/10.1088/2041-8205/763/2/L39.

Gosling, J.T. and Pizzo, V.J. (1999, July). Formation and evolution of corotating interaction regions and their three dimensional structure. *Space Science Review 89*: 21–52. https://doi.org/10.1023/A:1005291711900.

Gosling, J.T. and Szabo, A. (2008). Bifurcated current sheets produced by magnetic reconnection in the solar wind. *Journal of Geophysical Research: Space Physics 113* (A10).

Gosling, J.T., Skoug, R.M., McComas, D.J., and Smith, C.W. (2005, January). Direct evidence for magnetic reconnection in the solar wind near 1 AU. *Journal of Geophysical Research: Space Physics 110*: A01107. https://doi.org/10.1029/2004JA010809.

Greco, A., Perri, S., Servidio, S. et al. (2016, June). The complex structure of magnetic field discontinuities in the turbulent solar wind. *The Astrophysical Journal Letters 823*: L39. https://doi.org/10.3847/2041-8205/823/2/L39.

Hamilton, K., Smith, C.W., Vasquez, B.J., and Leamon, R.J. (2008, January). Anisotropies and helicities in the solar wind inertial and dissipation ranges at 1 AU. *Journal of Geophysical Research: Space Physics 113*: A01106. https://doi.org/10.1029/2007JA012559.

Harrison, R.A., Davis, C.J., and Davies, J.A. (2009, October). Pre-CME onset fuses – Do the STEREO heliospheric imagers hold the clues to the CME onset process? *Solar Physics 259*: 277–296. https://doi.org/10.1007/s11207-009-9417-7.

Hartinger, M.D., Welling, D., Viall, N.M. et al. (2014, October). The effect of magnetopause motion on fast mode resonance. *Journal of Geophysical Research: Space Physics 119*: 8212–8227. https://doi.org/10.1002/2014JA020401.

Hellinger, P., Matteini, L., Štverák, S., Trávníček, P. M., & Marsch, E. (2011, September). Heating and cooling of protons in the fast solar wind between 0.3 and 1 AU: Helios revisited. *Journal of Geophysical Research: Space Physics*, *116*, 9105. doi: 10.1029/2011JA016674.

Higginson, A.K., Antiochos, S.K., DeVore, C.R. et al. (2017, May). Formation of heliospheric arcs of slow solar wind. *The Astrophysical Journal 840*: L10. https://doi.org/10.3847/2041-8213/aa6d72.

Higginson, A.K. and Lynch, B.J. (2018, May). Structured slow solar wind variability: Streamer-blob flux ropes and torsional Alfvén waves. *The Astrophysical Journal 859*: 6. https://doi.org/10.3847/1538-4357/aabc08.

Hollweg, J.V. (2002). Heating and acceleration of the solar wind in coronal holes: cyclotron resonances. *Advances in Space Research 30*: 469–469. https://doi.org/10.1016/ S0273-1177(02)00324-1.

Horbury, T. S., Forman, M., & Oughton, S. (2008, October). Anisotropic scaling of magnetohydrodynamic turbulence. *Physical Review Letters*, *101* (17), 175005-+. doi: https://doi.org/10.1103/ PhysRevLett.101.175005.

Horbury, T. S., Matteini, L., & Stansby, D. (2018, August). Short, large-amplitude speed enhancements in the near-Sunfast solar wind. *Monthly Notices of the Royal Astronomical Society*, *478*, 1980–1986. doi: 10 .1093/mnras/sty953.

Howes, G.G., Cowley, S.C., Dorland, W. et al. (2006, November). Astrophysical gyrokinetics: Basic equations and linear theory. *The Astrophysical Journal 651*: 590–614. https://doi.org/10.1086/506172.

Howes, G.G., Tenbarge, J.M., Dorland, W. et al. (2011, July). Gyrokinetic simulations of solar wind turbulence from ion to electron scales. *Physical Review Letters 107* (3): 035004. https://doi.org/10.1103/PhysRevLett.107.035004.

Hudson, P.D. (1970, November). Discontinuities in an anisotropic plasma and their identification in the solar wind. *Planetary and Space Science 18*: 1611–1622. https://doi.org/10.1016/0032-0633(70) 90036-X.

Hundhausen, A.J. and Gosling, J.T. (1976, March). Solar wind structure at large heliocentric distances – an interpretation of Pioneer 10 observations. *Journal of Geophysical Research 81*: 1436–1440. https://doi.org/10.1029/JA081i007p01436.

Hyder, C.L. and Lites, B.W. (1970, September). Hα Doppler brightening and Lyman-a Doppler dimming in moving Hα Prominences. *Solar Physics 14*: 147–156. https://doi.org/10.1007/BF00240170.

Isenberg, P.A. (1987, February). Evolution of interstellar pickup ions in the solar wind. *Journal of Geophysical Research 92*: 1067–1073. https://doi.org/10.1029/JA092iA02p01067.

Isenberg, P.A., Lee, M.A., and Hollweg, J.V. (2001, April). The kinetic shell model of coronal heating and acceleration by ion cyclotron waves: 1. *Outward propagating waves*. *Journal of Geophysical Research: Space Physics 106*: 5649–5660. https://doi.org/10.1029/2000JA000099.

Jian, L., Russell, C.T., Luhmann, J.G., and Skoug, R.M. (2006, December). Properties of stream interactions at one AU during 1995 2004. *Solar Physics 239*: 337–392. https://doi.org/10.1007/s11207-006-0132-3.

Jian, L.K., Wei, H.Y., Russell, C.T. et al. (2014, May). Electromagnetic waves near the proton cyclotron frequency: STEREO observations. *The Astrophysical Journal 786*: 123. https://doi.org/10.1088/0004-637X/786/2/123.

Jovanović, D., Alexandrova, O., Maksimović, M., and Belic, M. (2020, June). Fluid Theory of Coherent Magnetic Vortices in High-β Space Plasmas. *The Astrophysical Journal 896* (1):8. https://doi.org/10.3847/1538-4357/ab8a45.

Kahler, S. and Lin, R.P. (1994, July). The determination of interplanetary magnetic field polarities around sector boundaries using E greater than 2 keV electrons. *Geophysical Research Letters 21*: 1575–1578.

https://doi.org/10.1029/94GL01362.

Kahler, S.W., Crooker, N.U., and Gosling, J.T. (1996, November). The topology of intrasector reversals of the interplanetary magnetic field. *Journal of Geophysical Research 101*: 24373–24382. https://doi.org/10.1029/96JA02232.

Kajdič, P., Alexandrova, O., Maksimovic, M. et al. (2016a, December). Suprathermal electron Strahl widths in the presence of narrow-band whistler waves in the solar wind. *The Astrophysical Journal 833*: 172. https://doi.org/10.3847/1538-4357/833/2/172.

Kajdič, P., Alexandrova, O., Maksimovic, M. et al. (2016b, December). Suprathermal electron strahl widths in the presence of narrow-band whistler waves in the solar wind. *The Astrophysical Journal 833*: 172. https://doi.org/10.3847/1538-4357/833/2/172.

Karpen, J.T., DeVore, C.R., Antiochos, S.K., and Pariat, E. (2017, January). Reconnection-driven coronal-hole jets with gravity and solar wind. *The Astrophysical Journal 834*: 62. https://doi.org/10.3847/1538-4357/834/1/62.

Kasper, J.C., Stevens, M.L., Korreck, K.E. et al. (2012, February). Evolution of the relationships between helium abundance, minor ion charge state, and solar wind speed over the solar cycle. *The Astrophysical Journal 745*: 162. https://doi.org/10.1088/0004-637X/745/2/162.

Kennel, C.F. and Engelmann, F. (1966, December). Velocity space diffusion from weak plasma turbulence in a magnetic field. *Physics of Fluids 9*: 2377–2388. https://doi.org/10.1063/1.1761629.

Kepko, L. and Spence, H.E. (2003, June). Observations of discrete, global magnetospheric oscillations directly driven by solar wind density variations. *Journal of Geophysical Research: Space Physics 108*: 1257. https://doi.org/10.1029/2002JA009676.

Kepko, L., Spence, H.E., and Singer, H.J. (2002, April). ULF waves in the solar wind as direct drivers of magnetospheric pulsations. *Geophysical Research Letters 29*: 1197. https://doi.org/10.1029/ 2001GL014405.

Kepko, L., Viall, N.M., Antiochos, S.K. et al. (2016, May). Implications of L1 observations for slow solar wind formation by solar reconnection. *Geophysical Research Letters 43*: 4089–4097. https://doi.org/10.1002/2016GL068607.

Kilpua, E.K.J., Luhmann, J.G., Gosling, J. et al. (2009, May). Small solar wind transients and their connection to the large-scale coronal structure. *Solar Physics 256*: 327–344. https://doi.org/10.1007/s11207-009-9366-1.

Kiyani, K.H., Chapman, S.C., Sahraoui, F. et al. (2013, January). Enhanced magnetic compressibility and isotropic scale invariance at sub-ion Larmor scales in solar wind turbulence. *The Astrophysical Journal 763*: 10. https://doi.org/10.1088/0004-637X/763/1/10.

Kiyani, K. H., Osman, K. T., & Chapman, S. C. (2015). Dissipation and heating in solar wind turbulence: from the macro to the micro and back again. *Philosophical Transactions of the Royal Society A: Mathematical, Physical and Engineering Sciences*, *373*(2041), 20140155. doi: https://doi.org/10.1098/rsta.2014.01550.

Ko, Y.-K., Muglach, K., Wang, Y.-M., Young, P. R., & Lepri, S. T. (2014). Temporal evolution of solar wind ion composition and their source coronal holes during the declining phase of cycle 23. I. Low-latitude extension of polar coronal holes. *The Astrophysical Journal*, *787*(2), 121.

Kohl, J.L., Esser, R., Gardner, L.D. et al. (1995, December). The ultraviolet coronagraph spectrometer for the solar and heliospheric observatory. *Solar Physics 162*: 313–356. https://doi.org/10.1007/BF00733433.

Kohl, J.L., Noci, G., Antonucci, E. et al. (1998, July). UVCS/SOHO empirical determinations of anisotropic velocity distributions in the solar corona. *The Astrophysical Journal 501*: L127–L131. https://doi.org/10.1086/311434.

Kohl, J.L., Noci, G., Antonucci, E. et al. (1997, October). First results from the SOHO ultraviolet coronagraph spectrometer. *Solar Physics 175*: 613–644. https://doi.org/10.1023/A:1004903206467.

Lacombe, C., Alexandrova, O., and Matteini, L. (2017, October). Anisotropies of the magnetic field fluctuations at kinetic scales in the solar wind: cluster observations. *The Astrophysical Journal 848*: 45. https://doi.org/10.3847/1538-4357/aa8c06.

Lacombe, C., Alexandrova, O., Matteini, L. et al. (2014, November). Whistler mode waves and the electron heat flux in the solar wind: Cluster observations. *The Astrophysical Journal 796*: 5. https://doi.org/10.1088/0004-637X/796/1/5.

Laming, J.M. (2009, April). Non-Wkb models of the first ionization potential effect: Implications for solar coronal heating and the coronal helium and neon abundances. *The Astrophysical Journal 695*: 954–969. https://doi.org/10.1088/0004-637X/695/2/954.

Laming, J.M. (2015, September). The FIP and inverse FIP effects in solar and stellar coronae. *Living Reviews in Solar Physics 12*: 2. https://doi.org/10.1007/lrsp-2015 -2.

Lavraud, B., Gosling, J.T., Rouillard, A.P. et al. (2009, May). Observation of a complex solar wind reconnection exhaust from spacecraft separated by over 1800 R E. *Solar Physics 256*: 379–392.

https://doi.org/10.1007/s11207-009-9341-x.

Lavraud, B., Ruffenach, A., Rouillard, A.P. et al. (2014, January). Geo-effectiveness and radial dependence of magnetic cloud erosion by magnetic reconnection. *Journal of Geophysical Research: Space Physics 119*: 26–35. https://doi.org/10.1002/2013JA019154.

Lazar, M., Yoon, P.H., López, R.A., and Moya, P.S. (2018, January). Electromagnetic electron cyclotron instability in the solar wind. *Journal of Geophysical Research: Space Physics 123*: 6–19. https://doi.org/10.1002/2017JA024759.

Leamon, R.J., Smith, C.W., Ness, N.F. et al. (1998, March). Observational constraints on the dynamics of the interplanetary magnetic field dissipation range. *Journal of Geophysical Research Atmospheres 103*: 4775. https://doi.org/10.1029/97JA03394.

Lee, M.A. (2000, May). An analytical theory of the morphology, flows, and shock compressions at corotating interaction regions in the solar wind. *Journal of Geophysical Research 105*: 10491–10500. https://doi.org/10.1029/1999JA000327.

Leubner, M.P. and Vörös, Z. (2005, January). A nonextensive entropy approach to solar wind intermittency. *The Astrophysical Journal 618*: 547–555. https://doi.org/10.1086/425893.

Lin, R.P. (1974, June). Non-relativistic solar electrons. *Space Science Reviews 16*: 189–256. https://doi.org/10.1007/ BF00240886.

Lin, R.P. (1998, July). WIND observations of suprathermal electrons in the interplanetary medium. *Space Science Reviews 86*: 61–78. https://doi.org/10.1023/A:1005048428480.

Linker, J.A., Lionello, R., Mikić, Z. et al. (2011, April). The evolution of open magnetic flux driven by photospheric dynamics. *The Astrophysical Journal 731*: 110. https://doi.org/10.1088/0004-637X/731/2/110.

Lion, S., Alexandrova, O., and Zaslavsky, A. (2016, June). Coherent events and spectral shape at ion kinetic scales in the fast solar wind turbulence. *The Astrophysical Journal 824*: 47. https://doi.org/10.3847/0004-637X/824/1/47.

Lionello, R., Riley, P., Linker, J.A., and Mikić, Z. (2005, May). The effects of differential rotation on the magnetic structure of the solar corona: Magnetohydrodynamic simulations. *The Astrophysical Journal 625*: 463–473. https://doi.org/10.1086/429268.

Lionello, R., Velli, M., Downs, C. et al. (2014, April). Validating a Time-dependent Turbulence-driven Model of the Solar Wind. *The Astrophysical Journal 784*: 120. https://doi.org/10.1088/0004-637X/784/2/120.

Liou, K., Takahashi, K., Newell, P.T., and Yumoto, K. (2008, August). Polar Ultraviolet Imager observations of solar wind-driven ULF auroral pulsations. *Geophysical Research Letters 35*: L16101. https://doi.org/10.1029/2008GL034953.

Liu, Y.C.-M., Huang, J., Wang, C. et al. (2014, November). A statistical analysis of heliospheric plasma sheets, heliospheric current sheets, and sector boundaries observed in situ by STEREO. *Journal of Geophysical Research: Space Physics 119*: 8721–8732. https://doi.org/10.1002/2014JA019956.

Lockwood, M., Owens, M., & Rouillard, A. P. (2009a, November). Excess open solar magnetic flux from satellite data: 1. Analysis of the third perihelion Ulysses pass. *Journal of Geophysical Research: Space Physics*, *114* (A11), A11103. doi: 10.1029/2009JA014449.

Lockwood, M., Owens, M., & Rouillard, A. P. (2009b, November). Excess open solar magnetic flux from satellite data: 2. A survey of kinematic effects. *Journal of Geophysical Research: Space Physics*, *114* (A11), A11104. doi: 10.1029/2009JA014450.

Lopez, R.E., Freeman, J.W., and Roelof, E.C. (1986, July). The relationship between proton temperature and momentum flux density in the solar wind. *Geophysical Research Letters 13*: 640–643. https://doi.org/10.1029/GL013i007p00640.

Maksimovic, M., Gary, S.P., and Skoug, R.M. (2000, August). Solar wind electron suprathermal strength and temperature gradients: Ulysses observations. *Journal of Geophysical Research: Space Physics 105*: 18337–18350. https://doi.org/10.1029/2000JA900039.

Maksimovic, M., Pierrard, V., and Riley, P. (1997). Ulysses electron distributions fitted with Kappa functions. *Geophysical Research Letters 24*: 1151–1154. https://doi.org/10.1029/97GL00992.

Manchester, W.B., Kozyra, J.U., Lepri, S.T., and Lavraud, B. (2014, July). Simulation of magnetic cloud erosion during propagation. *Journal of Geophysical Research: Space Physics 119* (7): 5449–5464. https://doi.org/10.1002/2014JA019882.

Manchester, W.B., van der Holst, B., and Lavraud, B. (2014, March). Flux rope evolution in interplanetary coronal mass ejections: The 13 May 2005 event. *Plasma Physics and Controlled Fusion 56* (6): 064006. https://doi.org/10.1088/0741-3335/56/6/064006.

Marocchi, D., Antonucci, E., and Giordano, S. (2001, February). Oxygen abundance in coronal streamers during solar minimum. *Annales Geophysicae 19*: 135–145. https://doi.org/10.5194/angeo-19-135-2001.

Marsch, E. (2012, November). Helios: Evolution of distribution functions 0.3-1 AU. *Space Science Reviews 172*: 23–39. https://doi.org/10.1007/s11214-010-9734-z.

Marsch, E., Schwenn, R., Rosenbauer, H. et al. (1982, January). Solar wind protons – Three-dimensional velocity distributions and derived plasma parameters measured between 0.3 and 1 AU. *Journal of Geophysical Research: Space Physics 87*: 52–72. https://doi.org/10.1029/JA087iA01p00052.

Marsch, E. and Tu, C.-Y. (1993, December). Modeling results on spatial transport and spectral transfer of solar wind Alfvenic turbulence. *Journal of Geophysical Research: Space Physics 98*: 21. https://doi.org/10.1029/93JA02365.

Matteini, L., Alexandrova, O., Chen, C.H.K., and Lacombe, C. (2017, April). Electric and magnetic spectra from MHD to electron scales in the magnetosheath. *Monthly Notices of the Royal Astronomical Society 466*: 945–951. https://doi.org/10.1093/mnras/stw3163.

Matteini, L., Horbury, T.S., Neugebauer, M., and Goldstein, B.E. (2014). Dependence of solar wind speed on the local magnetic field orientation: Role of Alfvenic fluctuations. *Geophysical Research Letters 41*: 259–265. https://doi.org/10.1002/2013GL058482.

Matteini, L., Horbury, T.S., Pantellini, F. et al. (2015, March). Ion kinetic energy conservation and magnetic field strength constancy in multi-fluid solar wind Alfvénic turbulence. *The Astrophysical Journal 802*: 11. https://doi.org/10.1088/0004-637X/802/1/11.

Matteini, L., Stansby, D., Horbury, T.S., and Chen, C.H.K. (2018). On the 1/f spectrum in the solar wind and its connection with magnetic compressibility. *The Astrophysical Journal Letters 869*: L32.

Matteini, L., Hellinger, P., Landi, S. et al. (2012, November). Ion Kinetics in the solar wind: Coupling global expansion to local microphysics, *Space Science Review 172* (1-4): 373-396. https://doi.org/10.1007/s11214-011-9774-z.

Matthaeus, W. H., & Goldstein, M. L. (1986, July). Low-frequency 1/f noise in the interplanetary magnetic field. *Physical Review Letters*, *57*, 495–498. doi: 10 .1103/PhysRevLett.57.495.

Mazur, J.E., Mason, G.M., Dwyer, J.R. et al. (2000, March). Interplanetary magnetic field line mixing deduced from impulsive solar flare particles. *The Astrophysical Journal Letters 532*: L79–L82. https://doi.org/10.1086/312561.

McComas, D.J., Bame, S.J., Barraclough, B.L. et al. (1998). Ulysses' return to the slow solar wind. *Geophysical Research Letters 25*: 1–4. https://doi.org/10.1029/97GL03444.

McComas, D.J., Ebert, R.W., Elliott, H.A. et al. (2008, September). Weaker solar wind from the polar coronal holes and the whole Sun. *Geophysical Research Letters 35*: L18103. https://doi.org/10.1029/2008GL034896.

McComas, D.J., Gosling, J.T., Winterhalter, D., and Smith, E.J. (1988, April). Interplanetary magnetic field draping about fast coronal mass ejecta in the outer heliosphere. *Journal of Geophysical Research: Space Physics 93* (A4): 2519–2526. https://doi.org/10.1029/JA093iA04p02519.

McComas, D.J., Hoogeveen, G.W., Gosling, J.T. et al. (1996, December). ULYSSES observations of pressure-balance structures in the polar solar wind. *Astronomy and Astrophysics 316*: 368–373.

Moldwin, M.B., Ford, S., Lepping, R. et al. (2000, January). *Small-scale magnetic flux ropes in the solar wind. 27*: 57–60. https://doi.org/10.1029/1999GL010724.

Moldwin, M.B., Phillips, J.L., Gosling, J.T. et al. (1995, October). Ulysses observation of a noncoronal mass ejection flux rope: Evidence of interplanetary magnetic reconnection. *Journal of Geophysical Research: Space Physics 100*: 19903–19910. https://doi.org/10.1029/95JA01123.

Morton, R. J., Tomczyk, S., & Pinto, R. (2015, July). Investigating Alfvenic wave propagation in coronal open-field regions. *Nature Communications*, *6*. Retrieved 2015-07-27, from http://www.nature.com/ncomms/2015/150727/ncomms8813/full/ncomms8813.html doi: https://doi.org/10.1038/ncomms8813.

Morton, R. J., Tomczyk, S., & Pinto, R. F. (2016, September). A global view of velocity fluctuations in the corona below 1.3 R with CoMP. *The Astrophysical Journal*, *828*, 89. Retrieved 2016-09-12, from http://adsabs.harvard.edu/abs/2016ApJ...828...89M doi: https://doi.org/10.3847/0004-637X/828/2/89.

Möstl, C., Miklenic, C., Farrugia, C. J., Temmer, M., Veronig, A., Galvin, A. B., et al. (2008, October). Two-spacecraft reconstruction of a magnetic cloud and comparison to its solar source. *Annales Geophysicae*, *26*(10), 3139–3152. doi: https://doi.org/10.5194/angeo-26-3139-2008.

Neugebauer, M. (2012, May). Evidence for polar X-ray jets as sources of microstream peaks in the solar wind. *The Astrophysical Journal 750*: 50. https://doi.org/10.1088/0004-637X/750/1/50.

Neugebauer, M., Clay, D.R., Goldstein, B.E. et al. (1984, July). A reexamination of rotational and tangential discontinuities in the solar wind. *Journal of Geophysical Research: Space Physics 89*: 5395–5408. https://doi.org/10.1029/JA089iA07p05395.

Neugebauer, M. and Giacalone, J. (2015, October). Energetic particles, tangential discontinuities, and solar flux tubes. *Journal of Geophysical Research: Space Physics 120*: 8281–8287. https://doi.org/10.1002/2015JA021632.

Neugebauer, M., Goldstein, B.E., McComas, D.J. et al. (1995, December). Ulysses observations of microstreams in the solar wind from coronal holes. *Journal of Geophysical Research: Space Physics 100*: 23389–23396. https://doi.org/10.1029/95JA02723.

Neugebauer, M., Ruzmaikin, A., & McComas, D. J. (1997, January). Wavelet analysis of the structure of microstreams in the polar solar wind. In S. R. Habbal (Ed.), *Robotic exploration close to the sun: Scientific basis* (Vol. *385*, p. 41–46). doi: https://doi.org/10.1063/1.51765.

Neugebauer, M. and Snyder, C.W. (1962, December). Solar plasma experiment. *Science 138*: 1095–1097. https://doi.org/10.1126/science.138.3545.1095-a.

Nicol, R.M., Chapman, S.C., and Dendy, R.O. (2009, October). Quantifying the anisotropy and solar cycle dependence of "1/f" solar wind fluctuations observed by advanced composition explorer. *The Astrophysical Journal 703*: 2138–2151. https://doi.org/10.1088/0004-637X/703/2/2138.

Noci, G., Kohl, J.L., and Withbroe, G.L. (1987, April). Solar wind diagnostics from Doppler-enhanced scattering. *The Astrophysical Journal 315*: 706–715. https://doi.org/10.1086/165172.

Ogilvie, K.W., Fitzenreiter, R., and Desch, M. (2000, December). Electrons in the low-density solar wind. *Journal of Geophysical Research: Space Physics 105*: 27277–27288. https://doi.org/10.1029/2000JA000131.

Oran, R., van der Holst, B., Landi, E. et al. (2013, December). A global wave-driven magnetohydrodynamic solar model with a unified treatment of open and closed magnetic field topologies. *The Astrophysical Journal 778*: 176. https://doi.org/10.1088/0004-637X/778/2/176.

Owens, M.J. and Forsyth, R.J. (2013). The heliospheric magnetic field. *Living Reviews in Solar Physics 10*.

Owens, M.J., Crooker, N.U., and Lockwood, M. (2013, May). Solar origin of heliospheric magnetic field inversions: Evidence for coronal loop opening within pseudostreamers. *Journal of Geophysical Research: Space Physics 118*: 1868–1879. https://doi.org/10.1002/jgra.50259.

Owens, M. J., Wicks, R. T., & Horbury, T. S. (2011, April). Magnetic discontinuities in the near-earth solar wind: Evidence of in-transit turbulence or remnants of coronal structure?, 269, 411-420. doi: https://doi.org/10.1007/s11207-010-9695-0.

Parker, E.N. (1958, November). Dynamics of the interplanetary gas and magnetic fields. *The Astrophysical Journal 128*: 664. https://doi.org/10.1086/146579.

Perri, S., Goldstein, M.L., Dorelli, J.C., and Sahraoui, F. (2012, November). Detection of small-scale structures in the dissipation regime of solar-wind turbulence. *Physical Review Letters 109* (19): 191101. https://doi.org/10.1103/PhysRevLett.109.191101.

Perrone, D., Alexandrova, O., Mangeney, A. et al. (2016, August). Compressive coherent structures at ion scales in the slow solar wind. *The Astrophysical Journal 826*: 196. https://doi.org/10.3847/0004-637X/826/2/196.

Perrone, D., Alexandrova, O., Roberts, O.W. et al. (2017, November). Coherent structures at ion scales in fast solar wind: Cluster observations. *The Astrophysical Journal 849*: 49. https://doi.org/10.3847/1538-4357/aa9022.

Phan, T.D., Gosling, J.T., Davis, M.S. et al. (2006, January). A magnetic reconnection X-line extending more than 390 Earth radii in the solar wind. *Nature 439* (7073): 175–178. https://doi.org/10.1038/nature04393.

Pierrard, V. (2011, February). *Solar wind electron transport: Interplanetary electric field and heat conduction. 172*: 315–324. https://doi.org/10.1007/s11214-011-9743-6.

Pierrard, V., & Lamy, H. (2003, September). The effects of the velocity filtration mechanism on the minor ions of the corona. *Solar Physics*, *216*, 47–58. doi: 10.1023/ A:1026157306754.

Pierrard, V. and Lazar, M. (2010, November). Kappa distributions: Theory and applications in space plasmas. *Solar Physics 267*: 153–174. https://doi.org/10.1007/s11207-010-9640-2.

Pierrard, V., Lazar, M., Poedts, S. et al. (2016, August). The electron temperature and anisotropy in the solar wind. comparison of the core and halo populations. *Solar Physics 291*: 2165–2179. https://doi.org/10.1007/s11207-016-0961-7.

Pierrard, V., Lazar, M., and Schlickeiser, R. (2011, April). Evolution of the electron distribution function in the whistler wave turbulence of the solar wind. *Solar Physics 269*: 421–438. https://doi.org/10.1007/s11207-010-9700-7.

Pierrard, V., Maksimovic, M., and Lemaire, J. (1999, August). Electron velocity distribution functions from the solar

wind to the corona. *Journal of Geophysical Research: Space Physics 104*: 17021–17032. https://doi.org/10.1029/1999JA900169.

Pierrard, V. and Pieters, M. (2014, December). Coronal heating and solar wind acceleration for electrons, protons, and minor ions obtained from kinetic models based on kappa distributions. *Journal of Geophysical Research: Space Physics 119*: 9441–9455. https://doi.org/10.1002/2014JA020678.

Pilipp, W.G., Miggenrieder, H., Montgomery, M.D. et al. (1987, February). Characteristics of electron velocity distribution functions in the solar wind derived from the HELIOS plasma experiment. *Journal of Geophysical Research: Space Physics 92*: 1075–1092. https://doi.org/10.1029/JA092iA02p01075.

Pilipp, W.G., Muehlhaeuser, K.-H., Miggenrieder, H. et al. (1990, May). Large-scale variations of thermal electron parameters in the solar wind between 0.3 and 1 AU. *Journal of Geophysical Research: Space Physics 95*: 6305–6329. https://doi.org/10.1029/JA095iA05p06305.

Pinto, R.F., Brun, A.S., Jouve, L., and Grappin, R. (2011, August). Coupling the solar dynamo and the corona: Wind properties, mass, and momentum losses during an activity cycle. *The Astrophysical Journal 737*: 72. https://doi.org/10.1088/0004-637X/737/2/72.

Pinto, R. F., Brun, A. S., & Rouillard, A. P. (2016, August). Flux-tube geometry and solar wind speed during an activity cycle. *Astronomy & Astrophysics*, *592*, A65. Retrieved 2019-03-04, from https://www.aanda.org/articles/ `aa/abs/2016/08/aa28599-16/aa28599-16.html` doi: https://doi.org/10.1051/0004-6361/ 201628599.

Pinto, R.F. and Rouillard, A.P. (2017, April). A multiple flux-tube solar wind model. *The Astrophysical Journal 838*: 89. https://doi.org/10.3847/1538-4357/aa6398.

Pizzo, V.J. (1982, June). A three-dimensional model of corotating streams in the solar wind. *III - Magnetohydrodynamic streams. Journal of Geophysical Research: Space Physics 87*: 4374–4394. https://doi.org/10.1029/ JA087iA06p04374.

Podesta, J. J., Roberts, D. A., & Goldstein, M. L. (2006, October). Power spectrum of small-scale turbulent velocity fluctuations in the solar wind. *Journal of Geophysical Research: Space Physics*, *111* (A10), 10109-+. doi: 10.1029/2006JA011834.

Poletto, G. (2015, December). Solar coronal plumes. *Living Reviews in Solar Physics 12*: 7. https://doi.org/10.1007/lrsp-2015-7.

Pylaev, O.S., Zaqarashvili, T.V., Brazhenko, A.I. et al. (2017, May). Oscillation of solar radio emission at coronal acoustic cut-off frequency. *Astronomy and Astrophysics 601*: A42. https://doi.org/10.1051/0004-6361/201629218.

Rakowski, C.E. and Laming, J.M. (2012). On the origin of the slow speed solar wind: helium abundance variations. *The Astrophysical Journal 754* (1): 65.

Raouafi, N.E., Patsourakos, S., Pariat, E. et al. (2016, November). Solar coronal jets: Observations, theory, and modeling. *Space Science Reviews 201*: 1–53. https://doi.org/10.1007/s11214-016-0260-5.

Reisenfeld, D.B., McComas, D.J., and Steinberg, J.T. (1999). Evidence of a solar origin for pressure balance structures in the high-latitude solar wind. *Geophysical Research Letters 26*: 1805–1808. https://doi.org/10.1029/1999GL900368.

Riley, P., Linker, J., Lionello, R. et al. (2004, October). Fitting flux ropes to a global MHD solution: A comparison of techniques. *Journal of Atmospheric and Solar-Terrestrial Physics 66* (15–16): 1321–1331. https://doi.org/10.1016/j.jastp.2004.03.019.

Roberts, M.A., Uritsky, V.M., DeVore, C.R., and Karpen, J.T. (2018, October). Simulated encounters of the parker solar probe with a coronal-hole jet. *The Astrophysical Journal 866*: 14. https://doi.org/10.3847/1538-4357/aadb41.

Roberts, O.W., Alexandrova, O., Kajdič, P. et al. (2017, December). Variability of the magnetic field power spectrum in the solar wind at electron scales. *The Astrophysical Journal 850*: 120. https://doi.org/10.3847/1538-4357/aa93e5.

Rouillard, A. P., Davies, J. A., Lavraud, B., Forsyth, R. J., Savani, N. P., Bewsher, D., et al. (2010, April). Intermittent release of transients in the slow solar wind: 1. Remote sensing observations. *Journal of Geophysical Research: Space Physics*, *115*, A04103. doi: 10.1029/2009JA014471.

Rouillard, A. P., Lavraud, B., Davies, J. A., Savani, N. P., Burlaga, L. F., Forsyth, R. J., et al. (2010, April). Intermittent release of transients in the slow solar wind: 2. In situ evidence. *Journal of Geophysical Research: Space Physics*, *115*, A04104. doi: 10.1029/2009JA014472.

Rouillard, A. P., Savani, N. P., Davies, J. A., Lavraud, B., Forsyth, R. J., Morley, S. K., et al. (2009, May 01). A multispacecraft analysis of a small-scale transient entrained by solar wind streams. *Solar Physics*, *256*(1), 307–326. Retrieved from https://doi.org/10.1007/s11207-009-9329-6 doi: 10.1007/s11207-009-9329-6.

Rouillard, A.P., Sheeley, N.R. Jr., Cooper, T.J. et al. (2011, June). The solar origin of small interplanetary transients. *The Astrophysical Journal 734*: 7. https://doi.org/10.1088/0004-637X/734/1/7.

Ruffenach, A., Lavraud, B., Farrugia, C.J. et al. (2015, January). Statistical study of magnetic cloud erosion by magnetic reconnection. *Journal of Geophysical Research: Space Physics 120*: 43–60. https://doi.org/10.1002/2014JA020628.

Ruffenach, A., Lavraud, B., Owens, M. J., Sauvaud, J.-A., Savani, N. P., Rouillard, A. P., et al. (2012, September). Multispacecraft observation of magnetic cloud erosion by magnetic reconnection during propagation: Magnetic Cloud Erosion. *Journal of Geophysical Research: Space Physics*, *117*(A09101), 1-16. doi: 10.1029/2012JA017624.

Sahraoui, F., Huang, S.Y., Belmont, G. et al. (2013, November). Scaling of the electron dissipation range of solar wind turbulence. *The Astrophysical Journal 777*: 15. https://doi.org/10.1088/0004-637X/777/1/15.

Salem, C., Hubert, D., Lacombe, C. et al. (2003, March). Electron properties and Coulomb collisions in the solar wind at 1 AU: Wind observations. *The Astrophysical Journal 585*: 1147–1157. https://doi.org/10.1086/346185.

Salem, C., Mangeney, A., Bale, S.D., and Veltri, P. (2009, September). Solar wind magnetohydrodynamics turbulence: Anomalous scaling and role of intermittency. *The Astrophysical Journal 702*: 537–553. https://doi.org/10.1088/0004-637X/702/1/537.

Salem, C.S., Howes, G.G., Sundkvist, D. et al. (2012, January). Identification of kinetic Alfven wave turbulence in the solar wind. *The Astrophysical Journal Letters 745*: L9. https://doi.org/10.1088/2041-8205/745/1/ L9.

Sanchez-Diaz, E., Rouillard, A.P., Davies, J.A. et al. (2017, January). Observational evidence for the associated formation of blobs and raining inflows in the solar corona. *The Astrophysical Journal Letters 835*: L7. https://doi.org/10.3847/2041-8213/835/1/L7.

Sanchez-Diaz, E., Rouillard, A.P., Lavraud, B. et al. (2016, April). The very slow solar wind: Properties, origin and variability. *Journal of Geophysical Research: Space Physics 121*: 2830–2841. https://doi.org/10.1002/2016JA022433.

Saur, J. and Bieber, J.W. (1999, May). Geometry of low-frequency solar wind magnetic turbulence: Evidence for radially aligned Alfénic fluctuations. *Journal of Geophysical Research 104*: 9975–9988. https://doi.org/10.1029/1998JA900077.

Schekochihin, A.A., Cowley, S.C., Dorland, W. et al. (2009, May). Astrophysical Gyrokinetics: Kinetic and fluid turbulent cascades in magnetized weakly collisional plasmas. *The Astrophysical Journal 182*: 310–377. https://doi.org/10.1088/0067-0049/182/1/310.

Schreiner, A. and Saur, J. (2017, February). A model for dissipation of solar wind magnetic turbulence by kinetic Alfven waves at electron scales: Comparison with observations. *The Astrophysical Journal 835*: 133. https://doi.org/10.3847/1538-4357/835/2/133.

Schrijver, C.J., Sandman, A.W., Aschwanden, M.J., and De Rosa, M.L. (2004, November). The coronal heating mechanism as identified by full-sun visualizations. *The Astrophysical Journal 615*: 512–525. https://doi.org/10.1086/424028.

Schwadron, N.A., Fisk, L.A., and Zurbuchen, T.H. (1999, August). Elemental fractionation in the slow solar wind. *The Astrophysical Journal 521*: 859–867. https://doi.org/10.1086/307575.

Schwenn, R. (1990). Large-scale structure of the interplanetary medium. *Physics of the Inner Heliosphere I*: 99–181.

Sheeley, N.R. and Rouillard, A.P. (2010, May). Tracking streamer blobs into the heliosphere. *The Astrophysical Journal 715*: 300–309. https://doi.org/10.1088/0004 -637X/715/1/300.

Sheeley, N.R., Wang, Y.-M., Hawley, S.H. et al. (1997, July). Measurements of flow speeds in the corona between 2 and 30 R. *The Astrophysical Journal 484*: 472–478. https://doi.org/10.1086/304338.

Sheeley, N.R., Warren, H.P., and Wang, Y.-M. (2007, December). A streamer ejection with reconnection close to the Sun. *The Astrophysical Journal 671*: 926–935. https://doi.org/10.1086/522940.

Smith, C.W., Hamilton, K., Vasquez, B.J., and Leamon, R.J. (2006, July). Dependence of the dissipation range spectrum of interplanetary magnetic fluctuations on the rate of energy cascade. *The Astrophysical Journal Letters 645*: L85–L88. https://doi.org/10.1086/506151.

Smith, E.J. and Wolfe, J.H. (1976, March). Observations of interaction regions and corotating shocks between one and five AU – Pioneers 10 and 11. *Geophysical Research Letters 3*: 137–140. https://doi.org/10.1029/GL003i003p00137.

Sorriso-Valvo, L., Marino, R., Carbone, V. et al. (2007, September). Observation of inertial energy cascade in interplanetary space plasma. *Physical Review Letters 99* (11): 115001. https://doi.org/10.1103/PhysRevLett.99.115001.

Stansby, D. and Horbury, T.S. (2018, June). Number density structures in the inner heliosphere. *Astronomy & Astrophysics (A&A) 613*: A62. https://doi.org/10.1051/0004-6361/201732567.

Stansby, D., Horbury, T.S., Chen, C.H.K., and Matteini, L. (2016, September). Experimental determination of whistler wave dispersion relation in the solar wind. *The Astrophysical Journal Letters 829*: L16. https://doi.org/10.3847/2041-8205/829/1/L16.

Stansby, D., Horbury, T.S., and Matteini, L. (2019, January). Diagnosing solar wind origins using in situ measurements in the inner heliosphere. *Monthly Notices of the Royal Astronomical Society 482*: 1706–1714. https://doi.org/10.1093/mnras/sty2814.

Stephenson, J.A.E. and Walker, A.D.M. (2002, May). HF radar observations of Pc5 ULF pulsations driven by the solar wind. *Geophysical Research Letters 29*: 1297. https://doi.org/10.1029/2001GL014291.

Strachan, L., Kohl, J.L., Weiser, H. et al. (1993, July). A Doppler dimming determination of coronal outflow velocity. *The Astrophysical Journal 412*: 410–420. https://doi.org/10.1086/172930.

Strachan, L., Panasyuk, A.V., Dobrzycka, D. et al. (2000, February). Latitudinal dependence of outflow velocities from O VI Doppler dimming observations during the Whole Sun Month. *Journal of Geophysical Research: Space Physics 105*: 2345–2356. https://doi.org/10.1029/1999JA900459.

Štverák, S., Travnicek, P., Maksimovic, M. et al. (2008, March). Electron temperature anisotropy constraints in the solar wind. *Journal of Geophysical Research: Space Physics 113*: A03103. https://doi.org/10.1029/2007JA012733.

Susino, R., Ventura, R., Spadaro, D. et al. (2008, September). Physical parameters along the boundaries of a mid-latitude streamer and in its adjacent regions. *Astronomy & Astrophysics (A&A) 488*: 303–310. https://doi.org/10.1051/0004-6361:200809713.

Telloni, D., Antonucci, E., & Dodero, M. A. (2007, September). Outflow velocity of the O^{+5} ions in polar coronal holes out to 5 R. *Astronomy & Astrophysics (A&A), 472*, 299–307. doi: 10.1051/ 0004-6361:20077083.

Teriaca, L., Poletto, G., Romoli, M., and Biesecker, D.A. (2003, May). The nascent solar wind: Origin and acceleration. *The Astrophysical Journal 588*: 566–577. https://doi.org/10.1086/368409.

Thieme, K.M., Marsch, E., and Schwenn, R. (1990, November). Spatial structures in high-speed streams as signatures of fine structures in coronal holes. *Annales Geophysicae 8*: 713–723.

Thieme, K.M., Schwenn, R., and Marsch, E. (1989). Are structures in high-speed streams signatures of coronal fine structures? *Advances in Space Research 9*: 127–130. https://doi.org/10.1016/0273-1177(89)90105-1.

Tian, H., Yao, S., Zong, Q. et al. (2010, September). Signatures of magnetic reconnection at boundaries of interplanetary small-scale magnetic flux ropes. *The Astrophysical Journal 720*: 454–464. https://doi.org/10.1088/0004-637X/720/1/454.

Titov, V.S., Forbes, T.G., Priest, E.R. et al. (2009, March). Slip-squashing factors as a measure of three-dimensional magnetic reconnection. *The Astrophysical Journal 693*: 1029–1044. https://doi.org/10.1088/0004-637X/693/1/1029.

Titov, V.S., Mikić, Z., Linker, J.A. et al. (2011, April). Magnetic topology of coronal hole linkages. *The Astrophysical Journal 731*: 111. https://doi.org/10.1088/0004-637X/731/2/111.

Tomczyk, S., Landi, E., Burkepile, J.T. et al. (2016, August). Scientific objectives and capabilities of the Coronal Solar Magnetism Observatory. *Journal of Geophysical Research: Space Physics 121*: 7470–7487. https://doi.org/10.1002/2016JA022871.

Török, T., Aulanier, G., Schmieder, B. et al. (2009, October). Fan-spine topology formation through two-step reconnection driven by twisted flux emergence. *The Astrophysical Journal 704*: 485–495. https://doi.org/10.1088/0004-637X/704/1/485.

Tu, C.-Y., & Marsch, E. (1995, July). Comment on “Evolution of energy-containing turbulent eddies in the solar wind” by W. H. Matthaeus, S. Oughton, D. H. Pontius, Jr., and Y. Zhou. *Journal of Geophysical Research*, *100*, 12323–12328. doi: https://doi.org/10.1029/95JA01103.

Tu, C.-Y. and Marsch, E. (1997, April). Two-fluid model for heating of the solar corona and acceleration of the solar wind by high-frequency Alfven waves. *Solar Physics 171*: 363–391. https://doi.org/10.1023/A:1004968327196.

Turner, A.J., Gogoberidze, G., Chapman, S.C. et al. (2011, August). Nonaxisymmetric anisotropy of solar wind turbulence. *Physical Review Letters 107* (9): 095002. https://doi.org/10.1103/PhysRevLett.107.095002.

van der Holst, B., Sokolov, I.V., Meng, X. et al. (2014, February). Alfvén Wave Solar Model (AWSoM): coronal heating. *The Astrophysical Journal 782*: 81. https://doi.org/10.1088/0004-637X/782/2/81.

Vasyliunas, V.M. and Siscoe, G.L. (1976, March). On the flux and the energy spectrum of interstellar ions in the solar system. *Journal of Geophysical Research 81*: 1247–1252. https://doi.org/10.1029/JA081i007p01247.

Velli, M., Grappin, R., and Mangeney, A. (1989, October). Turbulent cascade of incompressible unidirectional Alfven waves in the interplanetary medium. *Physical Review Letters 63*: 1807–1810. https://doi.org/10.1103/PhysRevLett.63.1807.

Velli, M., Lionello, R., Linker, J.A., and Mikić, Z. (2011, July). Coronal plumes in the fast solar wind. *The Astrophysical Journal 736*: 32. https://doi.org/10.1088/0004-637X/736/1/32.

Verdini, A., Grappin, R., Pinto, R., and Velli, M. (2012, May). On the origin of the 1/f spectrum in the solar wind magnetic field. *The Astrophysical Journal Letters 750*: L33. https://doi.org/10.1088/2041 -8205/750/2/L33.

Viall, N.M., Kepko, L., and Spence, H.E. (2008, July). Inherent length-scales of periodic solar wind number density structures. *Journal of Geophysical Research: Space Physics 113*: A07101. https://doi.org/10.1029/2007JA012881.

Viall, N.M., Kepko, L., and Spence, H.E. (2009, January). Relative occurrence rates and connection of discrete frequency oscillations in the solar wind density and dayside magnetosphere. *Journal of Geophysical Research: Space Physics 114*: A01201. https://doi.org/10.1029/2008JA013334.

Viall, N.M., Spence, H.E., and Kasper, J. (2009, December). Are periodic solar wind number density structures formed in the solar corona? *Geophysical Research Letters 36*: L23102. https://doi.org/10.1029/2009GL041191.

Viall, N.M., Spence, H.E., Vourlidas, A., and Howard, R. (2010, November). Examining periodic solar-wind density structures observed in the SECCHI heliospheric imagers. *Solar Physics 267*: 175–202. https://doi.org/10.1007/s11207-010-9633-1.

Viall, N. M., & Vourlidas, A. (2015, July). Periodic density structures and the origin of the slow solar wind. *The Astrophysical Journal*, *807*, 176. doi: 10 .1088/0004-637X/807/2/176.

Villante, U., Del Corpo, A., and Francia, P. (2013, January). Geomagnetic and solar wind fluctuations at discrete frequencies: A case study. *Journal of Geophysical Research: Space Physics 118*: 218–231. https://doi.org/10.1029/2012JA017971.

Villante, U., Di Matteo, S., and Piersanti, M. (2016, January). On the transmission of waves at discrete frequencies from the solar wind to the magnetosphere and ground: A case study. *Journal of Geophysical Research: Space Physics 121*: 380–396. https://doi.org/10.1002/2015JA021628.

Vocks, C. (2012, November). Kinetic models for whistler wave scattering of electrons in the solar corona and wind. *Space Science Reviews 172*: 303–314. https://doi.org/10.1007/s11214-011-9749-0.

Vocks, C. and Mann, G. (2003, August). Generation of suprathermal electrons by resonant wave-particle interaction in the solar corona and wind. *The Astrophysical Journal 593*: 1134–1145. https://doi.org/10.1086/376682.

Vocks, C., Mann, G., and Rausche, G. (2008, March). Formation of suprathermal electron distributions in the quiet solar corona. *Astronomy & Astrophysics (A&A) 480*: 527–536. https://doi.org/10.1051/0004-6361:20078826.

Vocks, C., Salem, C., Lin, R.P., and Mann, G. (2005, July). Electron Halo and Strahl formation in the solar wind by resonant interaction with whistler waves. *The Astrophysical Journal 627*: 540–549. https://doi.org/10.1086/430119.

von Rosenvinge, T.T., Richardson, I.G., Reames, D.V. et al. (2009, May). The solar energetic particle event of 14 December 2006. *Solar Physics 256*: 443–462. https://doi.org/10.1007/s11207-009-9353-6.

von Steiger, R., Schwadron, N.A., Fisk, L.A. et al. (2000, December). Composition of quasi-stationary solar wind flows from Ulysses/Solar Wind Ion Composition Spectrometer. *Journal of Geophysical Research: Space Physics 105*: 27217–27238. https://doi.org/10.1029/1999JA000358.

Wang, Y., Wei, F.S., Feng, X.S. et al. (2012, March). Variations of solar electron and proton flux in magnetic cloud boundary layers and comparisons with those across the shocks and in the reconnection exhausts. *The Astrophysical Journal 749* (1): 82. https://doi.org/10.1088/0004-637X/749/1/82.

Wang, Y.-M., Ko, Y.-K., and Grappin, R. (2009, January). Slow solar wind from open regions with strong low-coronal heating. *The Astrophysical Journal 691*: 760–769. https://doi.org/10.1088/0004-637X/691/1/760.

Wang, Y.M., Sheeley, J., and N. R., & Rouillard, A. P. (2006, Jun). Role of the Sun's nonaxisymmetric open flux in cosmic-ray modulation. *The Astrophysical Journal 644* (1): 638–645. https://doi.org/10.1086/503523.

Wang, Y.-M., Sheeley, N.R., Socker, D.G. et al. (1998, December). Observations of correlated white-light and extreme-ultraviolet jets from polar coronal holes. *The Astrophysical Journal 508*: 899–907. https://doi.org/10.1086/306450.

Wang, Y.-M., Sheeley, N.R., Socker, D.G. et al. (2000, November). The dynamical nature of coronal streamers. *Journal of Geophysical Research 105*: 25133–25142. https://doi.org/10.1029/2000JA000149.

Wang, Y.-M., Sheeley, N.R. Jr., Nash, A.G., and Shampine, L.R. (1988, April). The quasi-rigid rotation of coronal magnetic fields. *The Astrophysical Journal, Part 1* (327): 427–450. https://doi.org/10.1086/166205.

Wei, F., Liu, R., Fan, Q., and Feng, X. (2003, June). Identification of the magnetic cloud boundary layers. *Journal of Geophysical Research: Space Physics 108* (A6) https://doi.org/10.1029/2002JA009511.

Whang, Y.C. and Burlaga, L.F. (1990, December). Simulation of period doubling of recurrent solar wind structures. *Journal of Geophysical Research: Space Physics 95*: 20663–20671. https://doi.org/10.1029/JA095iA12p20663.

Wicks, R.T., Horbury, T.S., Chen, C.H.K., and Schekochihin, A.A. (2010). Power and spectral index anisotropy of the entire inertial range of turbulence in the fast solar wind. *Monthly Notices of the Royal Astronomical Society: Letters 407*: L31–L35. https://doi.org/10.1111/j.1745-3933.2010.00898.x.

Widing, K.G. and Feldman, U. (2001, July). On the rate of abundance modifications versus time in active region plasmas. *The Astrophysical Journal 555*: 426–434. https://doi.org/10.1086/ 321482.

Winterhalter, D., Smith, E.J., Burton, M.E. et al. (1994, April). The heliospheric plasma sheet. *Journal of Geophysical Research: Space Physics 99*: 6667–6680. https://doi.org/10.1029/93JA03481.

Withbroe, G.L., Kohl, J.L., Weiser, H., and Munro, R.H. (1982, March). Probing the solar wind acceleration region using spectroscopic techniques. *Space Science Reviews 33*: 17–52. https://doi.org/10.1007/BF00213247.

Yoon, P.H., Kim, S., and Choe, G.S. (2015, October). Steady-state model of solar wind electrons revisited. *The Astrophysical Journal 812*: 169. https://doi.org/10.1088/0004-637X/812/2/169.

Zangrilli, L. and Poletto, G. (2016, October). Evolution of active region outflows throughout an active region lifetime. *Astronomy & Astrophysics (A&A) 594*: A40. https://doi.org/10.1051/0004-6361/ 201628421.

Zank, G.P. (1999, July). Interaction of the solar wind with the local interstellar medium: A theoretical perspective. *Space Science Reviews 89*: 413–688. https://doi.org/10.1023/A:1005155601277.

Zurbuchen, T.H., Hefti, S., Fisk, L.A. et al. (1999, January). The transition between fast and slow solar wind from composition data. *Space Science Reviews 87*: 353–356. https://doi.org/10.1023/A:1005126718714.